

**Coordinated Jacobian Transpose Control
and its Application to a Climbing Machine**

by

Craig Daniel Sunada

Bachelor of Science in Mechanical Engineering
University of Colorado, Boulder (1992)

Submitted to the
Department of Mechanical Engineering
in partial fulfillment of the requirements for the degree of

Master of Science in Mechanical Engineering

at the

Massachusetts Institute of Technology

August 1994

© 1994 Massachusetts Institute of Technology

Signature of Author _____
Department of Mechanical Engineering
August 21, 1994

Certified by _____
Steven Dubowsky
Thesis Supervisor

Accepted by _____
Ain A. Sonin
Chairman, Departmental Graduate Committee

Barker Eng

MASSACHUSETTS INSTITUTE
OF TECHNOLOGY

OCT 24 1994

LIBRARIES

Coordinated Jacobian Transpose Control and its Application to a Climbing Machine

Submitted to the
Department of Mechanical Engineering
in partial fulfillment of the requirements for the degree of
Master of Science in Mechanical Engineering

by

Craig Daniel Sunada

Abstract

This thesis proposes a control algorithm based on Jacobian Transpose Control for coordinated position and force control of autonomous multilimbed mobile robotic systems performing both mobility and manipulation. The technique is called Coordinated Jacobian Transpose Control, or CJTC. CJTC has advantages over other techniques used to control multilimbed mobile robots, including being computationally inexpensive and providing a simple and unified interface with higher level planners. It can also control functions other than positions and orientations of the system. A methodology called the Extended Mobility Analysis is presented to choose a set of control variables that does not overconstrain the system. The effectiveness of CJTC is demonstrated in laboratory experiments on a climbing system.

Thesis Supervisor : Dr. Steven Dubowsky

Title : Professor of Mechanical Engineering

Acknowledgments

Betsy, my love, thank you for your love, your support, and your understanding. I never dreamed that love could be so overwhelming before we met. Alex, even though you are still too young to understand what I say, thank you for being such a wonderful son. I am ever so grateful that you are much better behaved than I was at your age. Thank you also for reminding me just how small my work is compared to the miracles that surround me every day.

To my parents, who provided the guidance and inspiration that led me to MIT, this thesis is proof of your accomplishments as parents and teachers of me. I hope that I can do as well for my son. To my brother Wade: our rivalry helped spur me to greater heights than I would have achieved alone.

To the rest of my family: Glen, Aunt Dorothy, Aunt Grace, Granny, Aunt Tania, and all the others, thank you for your support. The strong foundation of the love that my family shares allowed me to reach these levels.

Rick and Lucy, thank you for your support. Even though I have only known you for two years, you are already family in my heart. Hopey, even though you will never comprehend anything, you still give me your unconditional love.

Bob and Fran, thank you for your hospitality. You have made me feel welcome in this strange, hostile city. Sophie and Hannah, I hope that you also strive for educational excellence, and that in some small way I helped inspire you.

Dr. Dubowsky, thank you for providing me with insight and guidance in much more than just academics and research. Someday I will tell my students your stories (or stories about you).

Tom, thank you for your friendship, as well as your technical help. I would like to thank Dalila Arguez for her contribution to my work: she started it all! I would like to thank my fellow students for their assistance during my research: Jeff Cole, Nathan Rutman, Richard Wang, Michelle Tescuiba, and Pengyun (Perry) Gu. I hope to see you all at my next barbeque! Joe Deck, thanks for imparting upon me some of your perspective on life at MIT.

The support of this work by NASA (Langley Research Center, Automation Branch) under Grant NAG-1-801 is acknowledged.

Table of Contents

Abstract	2
Acknowledgments	3
Table of Contents	4
List of Figures	5
Nomenclature:	6
1: Introduction	7
1.1: Purpose and Contributions	7
1.2: Motivation	8
1.3: Background	10
1.3.1: Existing Multilimbed Mobile Robots	10
1.3.2: Control algorithms	12
1.4: Assumptions	16
2: Control Scheme Development	19
2.1: Jacobian Transpose Control	19
2.1.1: Derivation of Jacobian Transpose Control	21
2.2: Coordinated Jacobian Transpose Control	22
2.2.1: Derivation of Coordinated Jacobian Transpose Control	23
3: Control Vector Selection	26
3.1: Control Variables	26
3.2: Control Vector Selection	27
3.2.1: Gruebler's Mobility Analysis	28
3.2.2: Extended Mobility Analysis	31
4: Application of CJTC to a laboratory climbing robot	39
4.1: System description	39
4.1.1: Climbing Machine	40
4.1.2: Power Amplifiers	43
4.1.3: Control Computers	43
4.2: Climbing Gait	44
4.3: Control Vector Selection	45
4.4: Control equations	51
4.5: Control gain selection	53
4.5.1: Dynamic Model	53
4.6: Experimental performance	57
4.6.1: Data from climbing stage one	57
4.6.2: Data from a full climbing cycle	61
5: Summary and Conclusions	67
6: References	68
Appendix A: LIBRA Jacobian Equations	73
Appendix B: Power Amplifiers	77
Appendix C: Gain Selection	84
Appendices References	98

List of Figures

Fig. 1: A Schematic of the LIBRA climbing system	8
Fig. 2: A multilimbed mobile robot	9
Fig. 3: A representative multilimbed mobile robot.....	18
Fig. 4: Block Diagram of Jacobian Transpose Control.....	20
Fig. 5: 2-link manipulator controlled through JTC	20
Fig. 6: Multilimbed Mobile Robotic system controlled through CJTC.	23
Fig. 7: Block Diagram of CJTC	24
Fig. 8: Common Planar Constraints	30
Fig. 9: Stage One of the Extended Mobility Analysis	33
Fig. 10: Stage two of the Extended Mobility Analysis	35
Fig. 11: Over actuated system.....	36
Fig. 12: Over actuated system with environmental and internal constraints relaxed.....	36
Fig. 13: The LIBRA climbing system.....	39
Fig. 14: LIBRA system block diagram	40
Fig. 15: A Schematic of the LIBRA	41
Fig. 16: Climbing Gait used by the LIBRA	44
Fig. 17: LIBRA under full environmental constraints	45
Fig. 18: Constraining x of the Center Body	46
Fig. 19: Constraining x,y of the Center Body	46
Fig. 20: Constraining x,y,θ of the Center Body	47
Fig. 21: Constraining x,y of Foot 3	47
Fig. 22: Relaxing the x environmental constraint	48
Fig. 23: LIBRA with control vector 1	49
Fig. 24: LIBRA with control vector 2	50
Fig. 25: LIBRA with control vector 3	51
Fig. 26: Model of the LIBRA top kinematic chain	54
Fig. 27: Dominant poles of the LIBRA for y_{body} from $-0.20m \rightarrow 0.14 m$	56
Fig. 28: Desired motion for the climbing robot	58
Fig. 29: x_b, y_b position for a pushup maneuver	59
Fig. 30: θ_b for a pushup maneuver.....	59
Fig. 31: x_2 Force for a pushup maneuver.....	60
Fig. 32: x_3 location for a pushup maneuver	60
Fig. 33: Desired Cartesian movements for one gait cycle	61
Fig. 34: Actual Cartesian movements for one gait cycle	62
Fig. 35: Body movements for one gait cycle	63
Fig. 36: Body orientations for one gait cycle	63
Fig. 37: x positions for all the feet for one gait cycle	64
Fig. 38: y positions for all the feet for one gait cycle	64
Fig. 39: Foot 1 position vs. time for one gait cycle	65
Fig. 40: Foot 2 position vs. time for one gait cycle	65
Fig. 41: Foot 3 position vs. time for one gait cycle	66
Fig. B1: Power amplifier schematic	78
Fig. B2: Power Amplifier Card Layout	79
Fig. C1: Model of the LIBRA	84
Fig. C2: Poles of the LIBRA for y_{body} from $-0.20m \rightarrow 0.14m$	93
Fig. C3: Dominant poles of the LIBRA for y_{body} from $-0.20m \rightarrow 0.14 m$	94
Fig. C4: Bode plot for the x_{body} position variable.....	95
Fig. C5: Bode plot for the y_{body} position variable.....	96
Fig. C6: Bode plot for the q_{body} position variable.....	97

Nomenclature:

a	=	number of DOF of a system under full environmental constraints
b	=	number of uncontrolled DOF of a system under the current constraints
F	=	number of DOF of a system using Gruebler's mobility analysis
\underline{F}	=	vector of desired forces
f_1	=	number of slider or pin joints
f_2	=	number of roll-slide joints
f_i	=	number of DOF of joint i
$\underline{G}(q)$	=	gravity compensation vector
j	=	number of joints of a system
j_i	=	joint i
\mathbf{K}_p	=	proportional gain matrix
\mathbf{K}_d	=	derivative gain matrix
l	=	number of links of a system
m_i	=	number of active joints in limb i
n	=	number of limbs
r	=	number of control variables in the control vector
s	=	total number of active joints
$\underline{\tau}$	=	input vector of joint efforts
\underline{u}	=	control vector
\underline{u}_{cmd}	=	commanded position of the control vector
x,y,z	=	Cartesian coordinates
α,β,γ	=	Cartesian orientations

1: Introduction

1.1: Purpose and Contributions

The purpose of this thesis is to develop a control technique that can control both mobility and manipulation of a multilimbed mobile robot while being computationally feasible for small on-board computers. Mobility refers to the locomotion of the robot, whether through walking, climbing, sliding, or other forms of limbed locomotion, and manipulation refers to the interaction forces exerted on a task and the manipulation of an object in the environment. Here, an approach called Coordinated Jacobian Transpose Control, or CJTC, is proposed for the control of multilimbed, multi-degree of freedom mobile robotic systems. An extension of classical Jacobian Transpose Control, CJTC uses the simplest form of impedance control and an extended Jacobian matrix to control the entire system's forces and motions in a consistent and coordinated manner while being computationally feasible for small on-board computers. The effectiveness of CJTC is demonstrated in laboratory experiments on a three-limbed climbing system called the Limbed Intelligent Basic Robotic Ascender, or LIBRA, shown schematically in Figure 1. This system was designed and built by Dalila Argaez, and she first proposes the concept of CJTC ¹. This thesis develops her concept into a working control scheme and demonstrates its effectiveness. This first chapter presents the motivation for studying multilimbed mobile robots, and the need for new control algorithms to control simultaneously their movements and interaction forces with the environment.

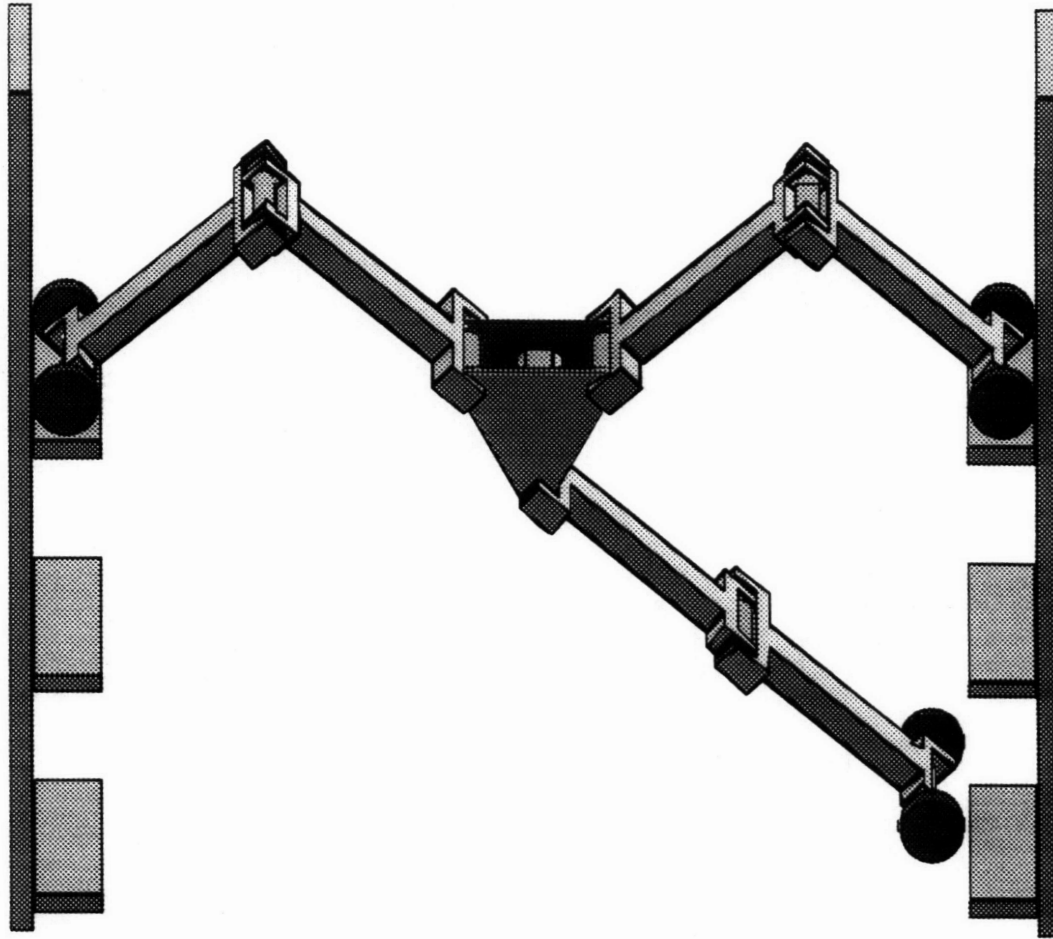


Fig. 1: A Schematic of the LIBRA climbing system

1.2: Motivation

The area of multilimbed mobile robots is an expanding field, with many important applications. It is becoming increasingly clear that multilimbed mobile robots are going to be important for performing tasks in areas that are either inaccessible to humans or undesirable or unsafe for humans to work. Such applications include toxic waste handling and work at nuclear sites ^{2, 3, 4, 5, 6, 7}. Multilimbed mobile robots are virtually the only feasible solution for planetary exploration ^{8, 9, 10}. These tasks take place in partially structured environments, where the general characteristics and layout of the terrain and tasks are known, but the specific details are not. Most of these tasks require

the robot to interact with the environment -- taking measurements and manipulating objects. Manipulation tasks may require carefully controlled forces to be applied. Often, the manipulation tasks will have to be performed while also moving the robot. For instance, a mechanical monkey might scurry into a toxic waste area and carefully take some measurements. Another part of its task might be to then shut off a valve, and then pick up a waste drum and carry it out. An example of a multilimbed robotics system is shown schematically in Figure 2, with limbs that are capable of both mobility and manipulation. As discussed in the next section, no multilimbed mobile robotic system in existence today is capable of performing tasks requiring both mobility and manipulation simultaneously, and that new control algorithms need to be developed to perform such tasks.

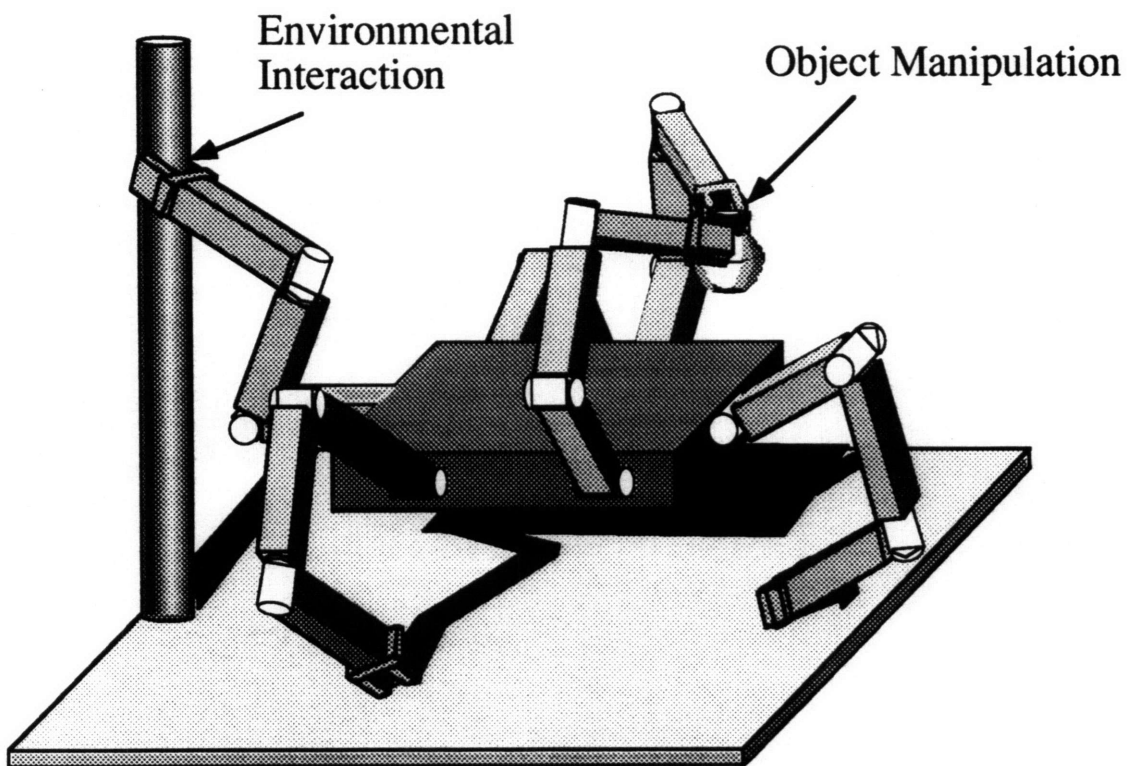


Fig. 2: A multilimbed mobile robot

1.3: Background

1.3.1: Existing Multilimbed Mobile Robots

Multilimbed mobile robots in existence today are a wonderfully diverse set of machines, ranging from pogo-stick like hopping machines ¹¹ to mouse-like miniature walking machines ¹² to massive walking vehicles ¹³. The types of mobility displayed by these robots can be classified into two separate categories: dynamically and statically stable. Dynamic movement relies on the dynamics of the system for mobility and stability. Raibert's hopping machines ¹¹ and Fukuda's brachiation machine ¹⁴ are examples of this type of movement. While effective and potentially faster over smooth or well-known terrain, these machines are generally not suitable for the rough, partially structured terrains that would be found in the tasks described above. Statically stable machines are more effective for these tasks, and are the focus of this thesis.

Statically stable movement refers to the notion that if the robot were to freeze at any point in its movement, then it would not fall over. The number of robots that use this type of movement is quite large. Dante and Ambler are two well-known walking machines used to study potential systems for planetary exploration ^{15, 16}. Planetary exploration requires legged locomotion to handle the extreme terrains that are encountered. The A d a p t i v e S u s p e n s i o n V e h i c l e, or ASV, built at Ohio State University as a proof-of-concept vehicle is a massive 5.8 m long six-legged walking vehicle ^{13, 17}. It has demonstrated the feasibility of walking as a viable form of locomotion on a large scale. Many smaller hexapod walking machines have been built, including the Moscow State Hexapod ¹⁸, the OSU Hexapod ¹⁹, and the CMU Hexapod ²⁰, as well as some very small hexapods such as Genghis and Atilla built by Brooks ^{12, 21}. These have mainly been used to research the control and planning issues involved in walking. Other forms of walking machines have also been built, such as the NCTU Quadruped²². Hirose ²³

built Titan III, a quadruped that is capable of both statically stable and dynamic walking. Multilimbed mobile robotic systems used for climbing include the Portsmouth Polytechnic Robug II, which uses vacuum grippers to climb walls ²⁴. Neubauer ²⁵ built a 6 legged climbing machine that uses friction to climb between two walls. Gradetsky et. al. ²⁶ discuss a climbing robot using vacuum grippers for actuation. Hirose ²⁷ has also built a climbing machine with vacuum grippers, capable of both statically stable and dynamic walking. While these walking and climbing machines have demonstrated substantial capabilities, none of these systems are capable of manipulation.

While mobility is certainly the first step in field robotic systems, manipulation must also be addressed. Even the field robots such as Dante aren't capable of manipulation, but rather are used simply to position sensors. The ability to collect ground samples, move obstacles, and probe the environment would all enhance the utility of Dante as a terrestrial exploration robot. One robot that is capable of both mobility and manipulation is the Savannah River Nuclear Mobile Robot -- a hexapod robot with a manipulator mounted on top ²⁸. However, during manipulation tasks the base is usually stationary and it is not capable of controlling both mobility and manipulation simultaneously. Despite this significant drawback, it has been found to be useful enough to warrant a second generation of the design. There are also a number of mobile robots that use tracks or wheels for mobility rather than limbs have been built and used that are capable of manipulation and have proven to be quite useful. HAZBOT, for instance, is used for hazardous materials handling ⁷, and the Foster Miller *Ferret* has proven to be very effective in explosives handling ²⁹.

While the current designs of multilimbed mobile robots largely ignore manipulation or treat manipulation separately from mobility, given the usefulness of other systems capable of both mobility and manipulation, new multilimbed mobile robots are sure to be

developed that will be capable of simultaneous mobility and manipulation. In order to control these future systems, new control schemes will need to be developed.

1.3.2: Control algorithms

Control algorithms that would allow the control of manipulation forces and motions while simultaneously controlling the trajectory of the rest of the system have yet to be developed for multilimbed mobile robots. The Savannah River Nuclear Robot, a current experimental multilimbed mobile robotic system capable of both mobility and manipulation, treats mobility and manipulation separately -- performing only one or the other at a time. It also does not control the forces exerted on the environment ²⁸. In order to increase the utility of robots, new control approaches must be developed to control simultaneously the motions of such articulated multilimbed mobile robotic systems and the forces that they exert on their environment or tasks. One way to develop new approaches is to attempt to extend the current methods used for mobility to also include manipulation, or to attempt to extend current methods used for manipulation to also include mobility.

A significant amount of work has been done in the area of the control of walking machines. A common form of control currently used is simple joint space position control. However, this form of control cannot directly control the forces being applied to the environment, and therefore isn't applicable for the control of forces during manipulation. Joint space position control also produces rough, jerky motion of the body of the robot in Cartesian space, and is difficult to adapt for rough terrain and changes in the environment ³⁰. A form of force control is therefore required.

A common form of control used that controls the forces being applied to the environment is called coordinated walking. Coordinated walking is an inverse plant controller, and like other forms of inverse plant controllers, coordinated walking is

computationally expensive, requires a detailed model of the system, and is sensitive to modeling errors ³¹. One form of coordinated walking treats the legs as force servos and resolves the desired motions and a force distribution algorithm into forces to be applied by the legs ^{32, 33}. This type of controller has demonstrated problems associated with practical difficulties in getting the legs to act like high-performance force servos ³⁰. Also, the system performance is low because the bandwidth of the overall trajectory controller must be substantially less than the bandwidth of the legs' controllers ³¹. Designing this type of coordinated walking is difficult because of the sensitivity to modeling errors. Without incorporating the often difficult to model actuator dynamics in the controller or analysis, the control gains must be chosen by trial and error ³¹. Another form of coordinated walking includes a simple model of the actuator dynamics in its model of the system, and directly reflects the desired trajectory and limb forces to the limb actuators ³¹. While this controller offers several advantages, such as the ability to decouple the system and linearize the control, it is also very computationally expensive. The ASV, which uses this control scheme, has 16 dedicated processors for the control alone ¹³. Coordinated walking does not address the issue of manipulation. Although it might be possible to extend coordinated walking to include manipulation, the computational burden would be large. While this is acceptable on large systems such as the ASV that can carry powerful computers, for small self-contained systems with small capability processors, this would not be feasible. Also, the sensitivity to modeling errors would pose a problem when manipulating an object in a partially known field environment where a detailed model of the object is not available. Given the limitations of that this controller would have, another approach for controlling mobility and manipulation is desired.

Looking for another way to develop a control algorithm to control both mobility and manipulation, control techniques that are currently used for manipulation are examined to see if they could be extended to also control mobility. There are two primary forms of

force control used to control fixed base serial manipulators -- hybrid control and impedance control. Khatib shows how generalized joint torques are reflected at the end-effector for redundant manipulators, an important understanding for either form of force control of redundant manipulators³⁴. Raibert and Craig propose a hybrid control scheme to control manipulator motions to satisfy position and force constraints simultaneously, and have demonstrated this approach through controlling the end-effector of a two link fixed-based manipulator³⁵. Hybrid control can also be extended to systems other than simple serial manipulators. For instance, Yoshikawa and Zheng extend hybrid position/force control to multiple robot manipulators working in well-known environments³⁶. However, hybrid control techniques require detailed knowledge of the environment for effective force control, including a good estimate of the environmental stiffness³⁷. Since such an estimate probably would not be available in a partially known environment, hybrid control is not suitable for this research.

Impedance control is the other primary form of force control. Hogan introduced impedance control, which controls a relationship between force and displacement, as a unified method for controlling the force and the position of a manipulator's end-effector^{38, 39}. Hogan also asserts that it is possible to superimpose impedances, which is necessary if multiple degrees of freedom are to be controlled. Schneider and Cannon use Hogan's impedance control approach to arrive at an object impedance controller for cooperative manipulation, which gives a straightforward interface for supervisory control by directly controlling the object being manipulated^{40, 41}. Impedance control has demonstrated good stability in contact transitions -- a quality that many other force control schemes lack⁴². It also does not require precise knowledge of the environment, in contrast to hybrid control. Some simple forms of impedance control don't even require a dynamic model of the system. Given these characteristics, impedance control is promising as a possible controller for both mobility and manipulation.

Current control techniques that deal with mobility and manipulation are investigated for possible methods to extend impedance control to control simultaneous mobility and manipulation. A number of control algorithms have been developed for motion control of manipulators mounted on simple vehicles, such as on spacecraft and trucks ^{43, 44}. Hootsmans and Dubowsky use an extended Jacobian matrix to compensate for base dynamics while using Jacobian Transpose Control to control a manipulator mounted on a mobile base ⁴⁵. However, these algorithms only look at manipulation while compensating for base movements and do not actively control the base. Seraji, on the other hand, proposes an extended Jacobian matrix to actively control the motions of a system composed of a manipulator mounted on a track or otherwise mobile base through inverse Jacobian control ^{46, 47}. His control algorithm was demonstrated experimentally on a 7 DOF robot arm mounted on a motorized track ⁴⁸. The use of an extended Jacobian matrix might allow impedance control to control both mobility and manipulation.

While there currently is no control algorithm reported in the literature that controls both the mobility and manipulation of a multilimbed mobile robot, several promising avenues exist. As discussed before, coordinated walking could be extendible to control manipulation, but would probably be too computationally expensive for this problem. Impedance control, currently used for manipulation with serial arms, is promising for both the ability to control the position of the end-effector while it is free and the forces it exerts while constrained, and for stability during contact transition. The use of an extended Jacobian matrix, similar to Seraji ^{46, 47} or Hootsmans ⁴⁵ might enable impedance control to control multiple points on a robot in order to control both manipulation and mobility, and this is the approach pursued in this research.

1.4: Assumptions

The need for developing a new control algorithm that controls both mobility and manipulation has been discussed, but the exact problem domain remains to be defined. The range of systems and tasks that could be covered by the terms 'multilimbed mobile robot' is too large to be covered by any single control scheme, and specific assumptions need to be made to limit that range. Assumptions are made about the nature and requirements of the environments and tasks, the computational capability and the kinematics of the class of robots to be controlled.

It is assumed that the robot is operating in a partially known environment. This implies that the general nature of the environment is known, and perhaps even the general layout of the environment and task, but the precision to which these things are known beforehand is not great, perhaps to within 5% or 10% of the limb span of the robot. The order of magnitude of the environmental stiffness might be known, and an approximate mass of an object to be manipulated, but detailed models will not be available. This assumption is representative of robots working in field environments, and prevents the use of control schemes that require good knowledge of the environment, such as hybrid control. It also prevents the use of control schemes that require a detailed dynamic model of the task and environment.

It is assumed that the task will require the forces being applied to the task to be controlled, but not to great precision. This assumption is made to allow a control scheme without force feedback. It is also assumed that for all tasks, all degrees of freedom of the system under the full kinematic constraints imposed by the environment must be controlled. This is generally required for acceptable system performance ⁴⁹.

It is assumed that the computational capability will be from a single processor of medium capability -- approximately the capability of an Intel 80386 processor or a

Motorola 68020. This represents an accessible amount of processing capability for almost any size except for very small systems.

These assumptions are not suitable for every multilimbed mobile robotic system, and limit the applicability of the control scheme developed in this thesis. Also, many of these assumptions are qualitative, and are meant as guidelines. As technology changes and additional sensors, actuators, and computational capability become readily available, many of the assumptions made may be relaxed. For instance, if much more processing capability is readily available, then it might be desirable to develop other control techniques that take advantage of that fact and subsequently give better performance.

The following is a description of the kinematics of the class of robots to be treated in this thesis. Figure 3 shows an n-limbed mobile robotic system representative of the class of robots dealt with herein. The system contains one main body with the n limbs attached and a base, which represents the ground. Some of the limbs position the main body with respect to ground for mobility purposes, while the remaining limbs may perform manipulation tasks or be free. It is assumed that the i^{th} limb is a j_i joint serial chain where m_i of the joints are active and $(j_i - m_i)$ joints are passive. Among the $(j_i - m_i)$ passive joints, some are passive due to the physical contact of the limb with the ground or a manipulated object; the others are mechanical non-actuated joints. The total number of active joints for the system is given by:

$$s = \sum_1^n m_i. \quad (1)$$

The kinematic variables q_i of the s active joints form a set that is referred to as the *joint vector* \mathbf{q} . The effort variables of the system's actuators, a torque for a revolute joint or a force for a prismatic joint, are the inputs to the system; they form the s by 1 input vector $\mathbf{\tau}$. It is assumed that the actuators are backdrivable.

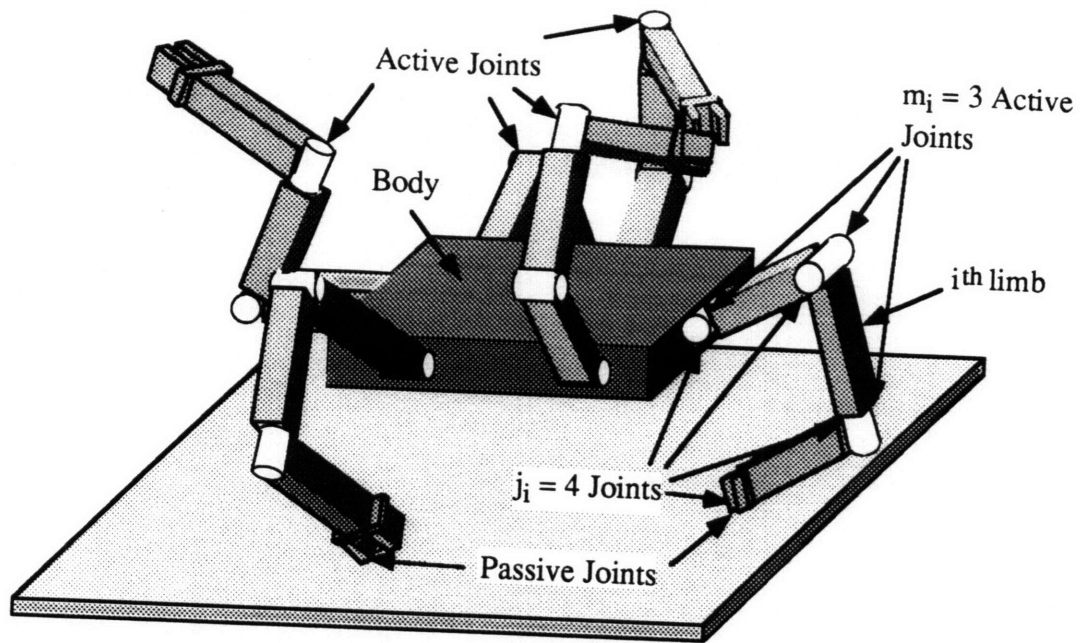


Fig. 3: A representative multilimbed mobile robot

2: Control Scheme Development

Looking at existing control techniques and given the assumptions made, a form of impedance control is chosen to be extended to control both mobility and manipulation for the following reasons. Given the need to actively control forces, either impedance control or hybrid control could be used. Given the assumption of partially known environments, hybrid control would have been difficult to implement. Impedance control does not require exact knowledge of the environment. Given the restriction on computational capability, the simplest form of impedance control, Jacobian Transpose Control^{37???} is used. This control does not require the use of force sensors for feedback, which might be advantageous for some systems. Controlling forces without force feedback is only possible with the use of backdrivable actuators, which is assumed in the previous section.

2.1: Jacobian Transpose Control

Since Coordinated Jacobian Transpose Control is based on Jacobian Transpose Control, this section first gives the derivation for classical Jacobian Transpose Control (JTC). A complete analysis of Jacobian Transpose Control, including a Lyapunov stability analysis, can be found in³⁷. Conceptually, Jacobian Transpose Control is proportional-derivative control of the position of the end-effector (\underline{x}) of a serial manipulator in Cartesian space. JTC controls the dynamic relationship between force and position, or the *mechanical impedance* of the end-effector. The end-effector is pulled towards the commanded end-effector position by a set of virtual springs and dampers. After calculating the vector of desired forces (\underline{F}) from these virtual springs and dampers, JTC directly transforms them into desired efforts at the actuators ($\underline{\tau}$) through the transpose of the Jacobian matrix \mathbf{J} . A block diagram of the controller is shown in Figure

4. Figure 5 shows this concept applied to a simple two link serial manipulator, where the end-effector Cartesian x and y positions are controlled.

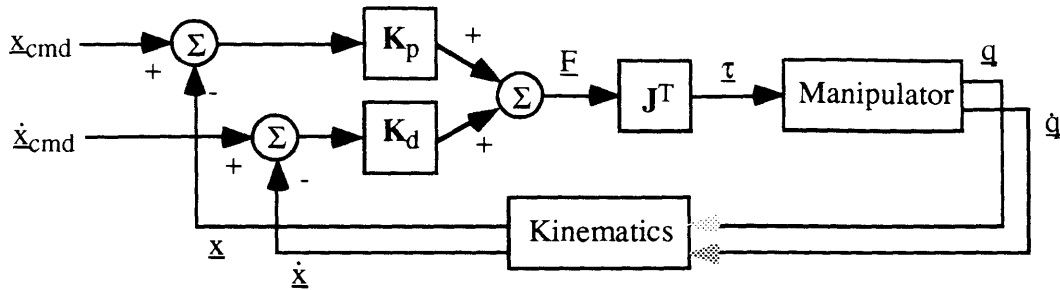


Fig. 4: Block Diagram of Jacobian Transpose Control

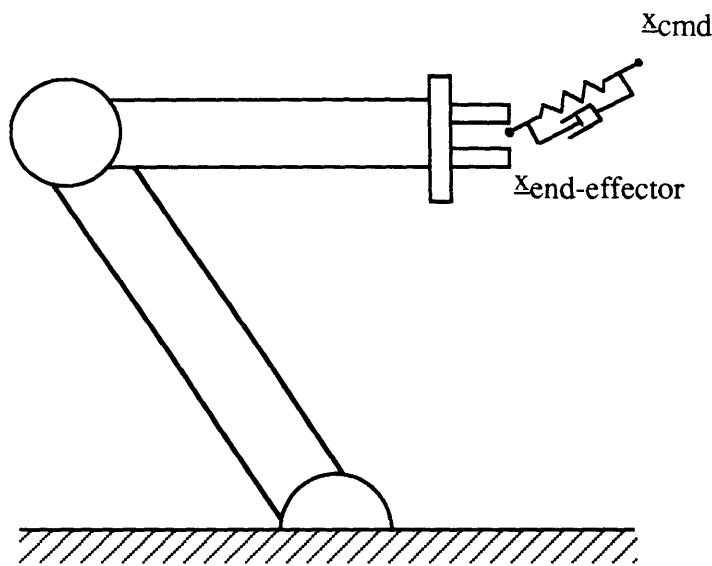


Fig. 5: 2-link manipulator controlled through JTC

As with other impedance control approaches, when the end-effector is constrained in a direction, a force is applied in that direction, and when the end-effector is unconstrained in a direction, a motion results. A compliant constraint results in both a force and displacement. Impedance control eliminates the need for switching between control structures to control both the position when unconstrained and force when constrained. This allows simple, intuitive control of the system. Jacobian Transpose Control is also robust to parametric uncertainty both in the manipulator itself and in the environment, and does not require a mass model of the manipulator. Although both position and force

control with Jacobian Transpose Control is not as high performance as some other control schemes, it is quite acceptable and demonstrates good contact stability.

2.1.1: Derivation of Jacobian Transpose Control

The vector of Cartesian coordinates \underline{x} of the end-effector is defined as:

$$\underline{x} = \begin{bmatrix} x \\ y \\ z \\ \alpha \\ \beta \\ \gamma \end{bmatrix} \quad (2)$$

or a subset thereof, depending on the degrees of freedom the manipulator has.

The desired force vector \underline{F} is defined to be:

$$\underline{F} = \mathbf{K}_p \cdot [\underline{x}_{cmd} - \underline{x}] + \mathbf{K}_d \cdot [\dot{\underline{x}}_{cmd} - \dot{\underline{x}}] \quad (3)$$

The gain matrices \mathbf{K}_p and \mathbf{K}_d determine the response of the system, and are chosen to satisfy the controller design requirements. The gain matrices are generally chosen to be diagonal, but can be non-diagonal if coupling between end-effector Cartesian coordinates is desired.

The Jacobian is defined as the transformation between joint space velocities and Cartesian velocities:

$$\mathbf{J}(\mathbf{q}) = \begin{bmatrix} \frac{\partial x}{\partial q_1} & \dots & \frac{\partial x}{\partial q_s} \\ \vdots & & \vdots \\ \frac{\partial \gamma}{\partial q_1} & \dots & \frac{\partial \gamma}{\partial q_s} \end{bmatrix} \quad (4)$$

The end-effector velocities are given by:

$$\delta \underline{u} = \mathbf{J}(\underline{q}) \cdot \delta \underline{q} \quad (5)$$

Applying the principle of virtual work, which relates infinitesimally small amounts of work performed in control space to infinitesimally small amounts of work performed in joint space, the following basic equation is derived:

$$\underline{\tau} = \mathbf{J}^T(\mathbf{q}) \cdot \underline{\mathbf{F}} \quad (6)$$

Using the principle of control partitioning ⁵⁰, a term can be added to compensate for the gravity forces acting on the robot; $\underline{\mathbf{G}}(\mathbf{q})$. The torque command then becomes:

$$\underline{\tau} = \mathbf{J}^T(\mathbf{q}) \cdot \underline{\mathbf{F}} + \underline{\mathbf{G}}(\mathbf{q}) \quad (7)$$

Combining (3) and (7), the control algorithm becomes:

$$\underline{\tau} = \mathbf{J}^T(\mathbf{q}) \cdot \left(\mathbf{K}_p \cdot [\underline{\mathbf{x}}_{\text{cmd}} - \underline{\mathbf{x}}] + \mathbf{K}_d \cdot [\dot{\underline{\mathbf{x}}}_{\text{cmd}} - \dot{\underline{\mathbf{x}}}] \right) + \underline{\mathbf{G}}(\mathbf{q}) \quad (8)$$

2.2: Coordinated Jacobian Transpose Control

Coordinated Jacobian Transpose Control extends Jacobian Transpose Control, given in the last section, by using an extended control vector and an extended Jacobian matrix. Rather than just controlling the vector of end-effector positions $\underline{\mathbf{x}}$, CJTC controls the positions and orientations of multiple points on the system, plus other differential functions of the joints vector \mathbf{q} . The possible positions and other functions to be controlled are the *control variables* of the system, and the vector of the control variables chosen to be controlled through CJTC is the *control vector* $\underline{\mathbf{u}}$. The control vector can be given as:

$$\underline{\mathbf{u}} = \begin{bmatrix} \underline{\mathbf{x}}(\mathbf{q}) \\ \underline{\boldsymbol{\alpha}}(\mathbf{q}) \\ \underline{\Gamma}(\mathbf{q}) \end{bmatrix} \quad (9)$$

where:

$\underline{\mathbf{x}}(\mathbf{q})$ = position of a point on the system

$\underline{\boldsymbol{\alpha}}(\mathbf{q})$ = orientations of points on the system, and

$\underline{\Gamma}(\mathbf{q})$ = other functions of the joint vector, such as the potential energy

The control vector is chosen based on what is desirable and possible to control, and Section 3 describes a method for choosing an admissible control vector.

Conceptually, Coordinated Jacobian Transpose Control is proportional-derivative control in control space. Each element of the control vector is forced to move towards its corresponding element of a desired or commanded control vector (\underline{u}_{cmd}) by a set of virtual springs and dampers in the classical Jacobian Transpose Control approach. Figure 6 shows a multilimbed mobile robot under CJTC with the virtual spring-dampers applied to the control vector.

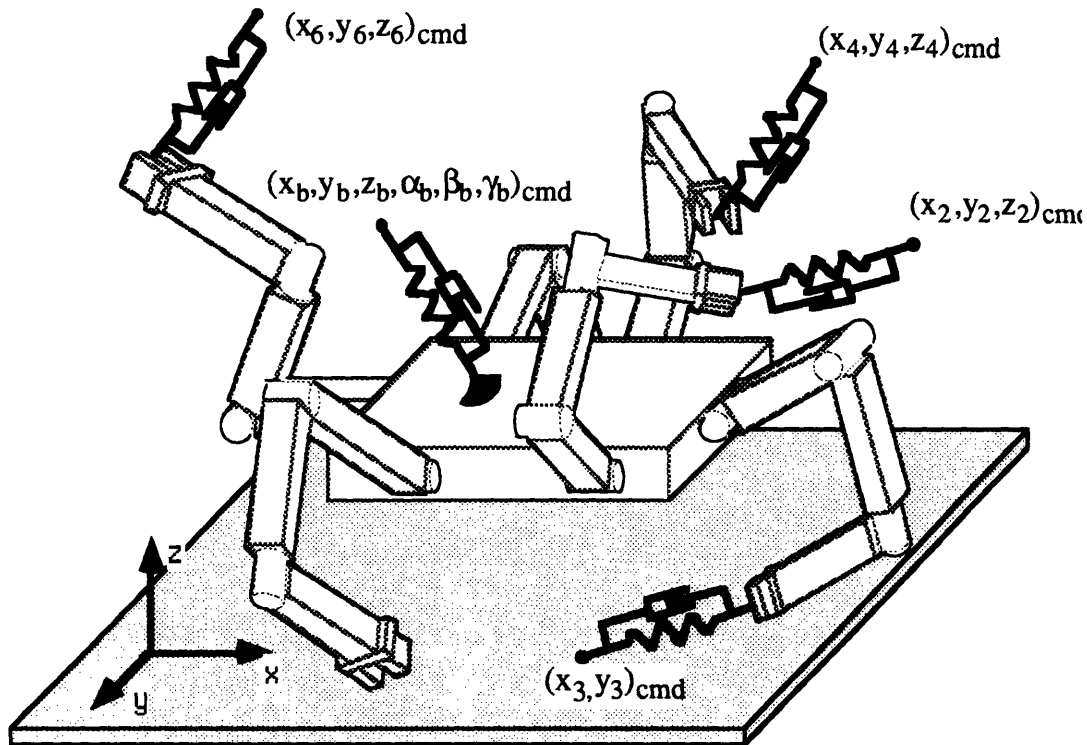


Fig. 6: Multilimbed Mobile Robotic system controlled through CJTC.

2.2.1: Derivation of Coordinated Jacobian Transpose Control

The derivation for CJTC closely follows that of Jacobian Transpose Control, and some of the same equations will be referenced. A block diagram of the control scheme is given in Figure 7. The additional block for sensors is required if one or more of the control variables are functions of other variables in addition to the joint vector q . In this case, sensors are required that can measure these other variables.

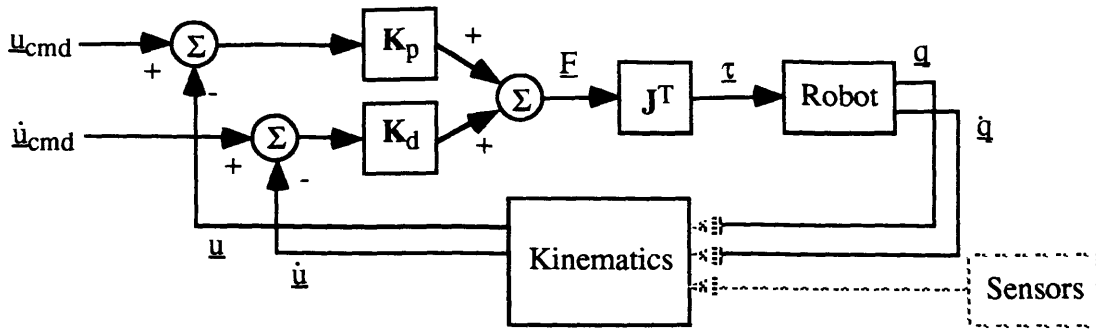


Fig. 7: Block Diagram of CJTC

The (rx1) desired force vector \underline{F} is defined to be:

$$\underline{F} = \mathbf{K}_p \cdot [\underline{u}_{cmd} - \underline{u}] + \mathbf{K}_d \cdot [\dot{\underline{u}}_{cmd} - \dot{\underline{u}}] \quad (10)$$

where r is the number of control variables in the control vector

Again, the gain matrices \mathbf{K}_p and \mathbf{K}_d are generally chosen to be diagonal, and are chosen to satisfy the controller design requirements. Each element of the force vector (\underline{F}) results in an acceleration of the system if the corresponding element of the control vector (\underline{u}) is unconstrained or in a force applied to the environment if the corresponding element of the control vector is constrained.

The extended Jacobian is defined as the transformation between joint space velocities and control space velocities:

$$\mathbf{J}(q) = \begin{bmatrix} \frac{\partial u_1}{\partial q_1} & \dots & \frac{\partial u_1}{\partial q_s} \\ \vdots & & \vdots \\ \frac{\partial u_r}{\partial q_1} & \dots & \frac{\partial u_r}{\partial q_s} \end{bmatrix} = \begin{bmatrix} \frac{\partial x_1}{\partial q_1} & \dots & \frac{\partial x_1}{\partial q_s} \\ \vdots & & \vdots \\ \frac{\partial \alpha_i}{\partial q_1} & \dots & \frac{\partial \alpha_i}{\partial q_s} \\ \vdots & & \vdots \\ \frac{\partial \Gamma_r}{\partial q_1} & \dots & \frac{\partial \Gamma_r}{\partial q_s} \end{bmatrix} \quad (11)$$

The Jacobian is r by s , where $r \leq s$ is the number of control variables and s is the total number of active joints. The Jacobian does not need to be square, and some redundancies

can be left uncontrolled if they are not important for the system performance. Combining (7), (10) and (11), the control algorithm becomes:

$$\underline{\tau} = \mathbf{J}^T(\mathbf{q}) \cdot (\mathbf{K}_p \cdot [\underline{\mathbf{u}}_{\text{cmd}} - \underline{\mathbf{u}}] + \mathbf{K}_d \cdot [\dot{\underline{\mathbf{u}}}_{\text{cmd}} - \dot{\underline{\mathbf{u}}}] + \underline{\mathbf{G}}(\mathbf{q})) \quad (12)$$

Coordinated Jacobian Transpose Control for multilimbed systems has the same advantages that Jacobian Transpose Control offers for serial manipulators. Namely, only the forward kinematics and their derivatives are required, implying a relatively small number of computations. No inertial model of the robot is required. Also, the Jacobian matrix can be rectangular, which is of great importance for redundant systems. CJTC is also robust to parametric uncertainties in both the robot itself and in the environment. Finally, this control scheme provides an intuitively simple interface for controlling endpoint positions and forces of a multilimbed system. By moving the commanded endpoints through space or into an object, the limb moves or pushes accordingly. By controlling all the control variables in this fashion, straightforward integration is achieved with higher level planning algorithms.

However, CJTC does not compensate for the changing dynamics of the system, and as a result the performance is configuration dependent. The extent of the configuration dependence is a function of the mass distribution of the robot. When selecting the gain matrices, the controller must be designed for the worst-case configuration⁵¹. If the dynamic response varies dramatically, then performance will be sacrificed significantly over the majority of the workspace. If this is the case, gain scheduling or other forms of adaptation might be required. Also, no attempt is made to decouple the system, and significant coupling between control variables can occur. This can be compensated for by using a non-diagonal gain matrix, but the degree of coupling is configuration dependent and adaptive control or gains scheduling might be required. Despite these characteristics, it will be demonstrated that the control system performance is quite acceptable for the LIBRA climbing robot.

3: Control Vector Selection

The control algorithm derived in the previous section operates on the control vector \underline{u} , and the method for choosing the control vector is presented in this section. The control vector is chosen by the designer, based on the task and the environmental constraints. CJTC allows considerable freedom in choosing the control vector, and this allows the designer to directly control the control variables of interest. The points made in this section are based on general control theory, but are tailored specifically for the CJTC, with all the assumptions and restrictions given in Section 1.4.

3.1: Control Variables

Any differentiable mathematical function of \underline{q} with non-zero first partial derivatives with respect to \underline{q} that describes a physical property of the system is defined to be a *control variable*. For instance, the Cartesian coordinates x , y and z of a point on the system are functions of \underline{q} and are three possible control variables. The Cartesian orientations α , β , and γ of a point on the system are also possible control variables. The most basic control variables are the joint displacements. More abstract control variables might include the system's potential energy or a static stability function to prevent the robot from tipping over. For any given system, there are an infinite number of possible control variables. Of these possible control variables, an admissible set must be chosen to control. A methodology called the Extended Mobility Analysis for choosing an admissible set of control variables is described below. The set of chosen control variables is called the *control vector* \underline{u} . The space of control vectors corresponding to all possible configurations of the system is called the control space.

In order to reflect the control errors to the actuators through the Jacobian matrix, the control variables must be written in terms of the joint vector \underline{q} . In order to do so, the control variables will generally be written using the assumed environmental constraints both implicitly and explicitly. Since the control variables are functions of the joint vector \underline{q} , joint position sensors are needed for joint vector feedback. If the control variables are also functions of other variables, then sensors that can measure those variables are also required. Additional sensors might be required to obtain the initial position, to check the position during the movement and correct for errors caused by unexpected slipping, but are not required by the control scheme.

3.2: Control Vector Selection

Choosing the control vector \underline{u} is not trivial. While the joint vector \underline{q} is imposed on the system by the mechanical design, the control vector \underline{u} is chosen by the designer. The designer must choose an admissible set from the infinite number of possible control variables, based on the tasks a specific system must perform, the environmental constraints placed on the system, and desirable performance characteristics. Since the range of possible control variables is so diverse, it is often possible to directly control the points or functions of interest. For instance, if visual feedback from a camera mounted on the robot is important, then good choices for control variables would be the positions and orientations of the camera. If the location of the center of mass of the body is more important, then it is possible to directly control that as well. As stated in the problem definition, all the degrees of freedom of a system under the full kinematic constraints imposed by the environment must be controlled. The environmental interaction forces or other control variables do not have to be controlled, but it often is desirable to do so.

It is important to note that the control vector will change during a robot's mission, based on the changing constraints and desired tasks that the robot will perform. For mobility, it is necessary to lift and maneuver a foot at certain times in the gait, and use that foot to support the body at others. So, for the different tasks and constraints, different control vectors must be chosen. Given the constraints that the system will be subject to, an Extended Mobility Analysis can be performed to determine admissible control vectors.

For the s active joints of the system, s control variables are possible to control. At the lowest level, the s individual active joint positions can be controlled. However, it is not necessary to control all s possible control variables. Sometimes, after choosing a number of important control variables to control, the only control variables admissible to complete the control vector are unimportant for the system. In such cases, it might be wise not to waste the computing resources needed to control these unimportant control variables. When deciding whether to control these unimportant control variables, the designer should consider just how important the control variables are to the system, and how much computing capability is available.

3.2.1: Gruebler's Mobility Analysis

A brief summary of Gruebler's Mobility analysis is given here for review, since it is heavily relied upon in the Extended Mobility Analysis. In this thesis, the term 'mobility analysis' refers to Gruebler's Mobility Analysis. This review is not complete, and a more complete description of Gruebler's Mobility Analysis is given in ⁵².

An unconstrained rigid body in spatial motion has six degrees of freedom, the x , y , z translations and the α , β and γ rotations. A mechanism constructed of l rigid links will

have 6·l degrees of freedom before they are connected to form a system of links. The connections constrain the system and result in losses of degrees of freedom of the system. Different forms of connectors constrain various numbers of degrees of freedom. A pin joint, one type of lower-pair connector, constrains the three translational degrees of freedom and permits only rotation in one direction. For instance, a link connected to ground through a pin joint has but one degree of freedom, and therefore lost five of the six degrees of freedom it had when unconstrained. A slider joint, another type of lower-pair connector, also constrains five degrees of freedom, as it only allows movement in one translational direction. Another type of constraint is referred to as the roll-slide contact. Two bodies are in contact, but can translate across each others' surfaces and also rotate with respect to each other. Only one degree of freedom -- translation in the normal direction to the surfaces -- is constrained.

Gruebler's equation is now given as:

$$F = 6 \cdot (l - j - 1) + \sum f_i \quad (13)$$

where:

F = the number of degrees of freedom of the system

l = the number of links, including the ground

j = the number of joints, including ground contacts

f_i = the number of degrees of freedom allowed by joint i

In planar motion, there are only three degrees of freedom -- the x and y translations and the single rotation θ . Gruebler's equation in planar motion is given as:

$$F = 3 \cdot (l - 1) - 2 \cdot f_1 - f_2 \quad (14)$$

where:

f_1 = the number of slider or pin joints

f_2 = the number of roll-slide contacts

Figure 8, adapted from Sandor and Erdman⁵³, gives some common planar kinematic joints and their appropriate degrees of freedom.

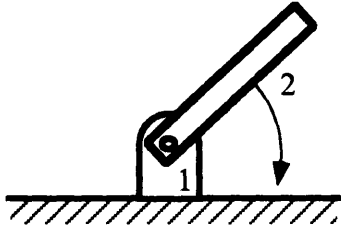
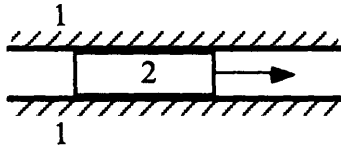
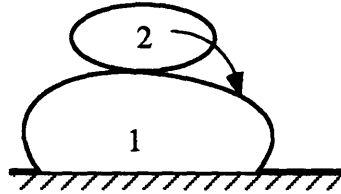
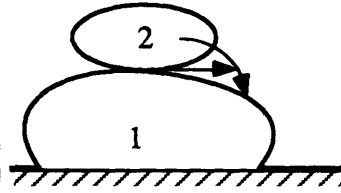
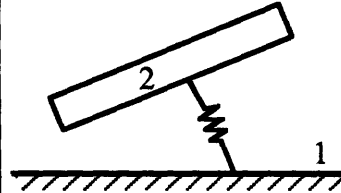
Joint	Diagram	Characteristic Variables
Pin (revolute)		$l = 2$ $f_1 = 1$ $f_2 = 0$ $f_i = 1$ degree of freedom
Slider (prismatic)		$l = 2$ $f_1 = 1$ $f_2 = 0$ $f_i = 1$ degree of freedom
Rolling Contact		$l = 2$ $f_1 = 1$ $f_2 = 0$ $f_i = 1$ degree of freedom
Roll-Slide Contact		$l = 2$ $f_1 = 0$ $f_2 = 1$ $f_i = 2$ degrees of freedom
Spring		$l = 2$ $f_1 = 0$ $f_2 = 0$ $f_i = 3$ degrees of freedom

Fig. 8: Common Planar Constraints

3.2.2: Extended Mobility Analysis

The Extended Mobility Analysis is based on Gruebler's mobility analysis. It addresses which sets of control variables can be controlled for a system subject to a given set of environmental constraints. It also insures that the control variables chosen are independent, and that the system does not become overconstrained. The basic procedure is to repeatedly perform Gruebler's mobility analysis, adding constraints for the control variables chosen and relaxing environmental constraints to test if an interaction force or moment can be controlled. A flow graph of the Extended Mobility Analysis is given in Figures 9 and 10. The nomenclature used is:

a = number of DOF of the system under the full environmental constraints

b = number of uncontrolled DOF

r = number of control variables selected

s = number of active joints

The first stage of the Extended Mobility Analysis, shown in Figure 9, deals with choosing control variables to control the available degrees of freedom under the full environmental constraints. Performing a mobility analysis on a multilimbed mobile robot under the full constraints of the environment will yield (a) degrees of freedom ($b=a$). It is assumed all of these degrees of freedom must be controlled for acceptable system performance. If there are less active joints than degrees of freedom ($s < a$), then the system is under actuated and cannot be controlled using this control scheme. To test if a control variable is admissible, a constraint must be placed on it and another mobility analysis run. If the mobility analysis yields the loss of one degree of freedom ($b=b-1$), then the control variable does not overconstrain the system and is admissible. If the mobility analysis does not yield the loss of one degree of freedom ($b=b$), then the control variable cannot be controlled because it is already constrained by the given environmental constraints or the constraints from the previous control variables chosen. If it is highly desirable to control that control variable, then it is still possible to do so either by choosing it later in

the analysis as a controlled environmental interaction force, if an environmental constraint is constraining it, or by eliminating one or more previously selected control variables, if the control variable constraints are constraining it. If the control variable is inadmissible and it is not highly desirable to control it, then the constraint is removed and another control variable tested. After (a) admissible control variables are chosen and constrained, then the system shouldn't have any degrees of freedom ($b=0$). If it does, then the set of a control variables chosen are not independent of each other and cannot be controlled simultaneously. If the number of active joints is greater than the number of degrees of freedom ($s>a$), then it is possible to control a number ($s-a$) of interaction forces with the environment, internal forces, or other control variables. The second stage of the Extended Mobility Analysis must then be performed.

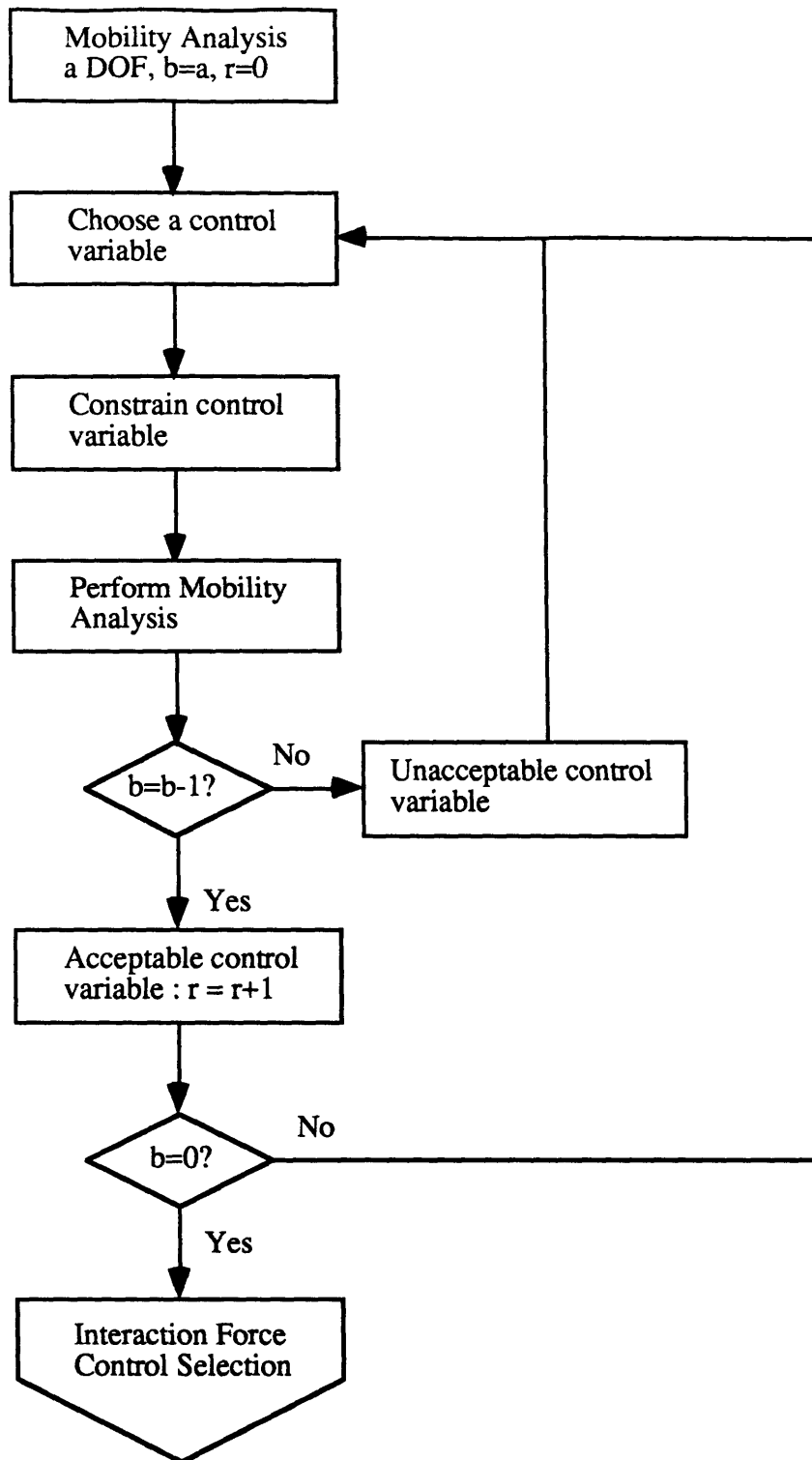


Fig. 9: Stage One of the Extended Mobility Analysis

The second stage of the Extended Mobility Analysis, shown in Figure 10, deals with controlling environmental interaction forces and internal forces. At the start of the second stage, all degrees of freedom of the system are controlled, and $b=0$. To test if a desired interaction or internal force or moment is controllable, a control variable is chosen as the desired interaction force with the environment or internal force, and the environmental position constraint or internal displacement constraint on that control variable is relaxed. With all the other control variables constrained, the system should then have one additional degree of freedom ($b=b+1$). If so, then that force or moment is controllable. To mark that the force or moment is controlled, replace the corresponding constraint with a spring. Note that a spring does not act as a link or constraint for purposes of a mobility analysis and it is merely there to indicate visually that the corresponding interaction force is being controlled. If the system does not have an additional degree of freedom ($b=b$), then that interaction or internal force is not controllable, perhaps due to the other control variables chosen or because the mechanism cannot apply forces in that direction. In this case, restore the original constraint. If there are still more actuators than control variables chosen ($s>r$), then additional control variables can be controlled, if desired.

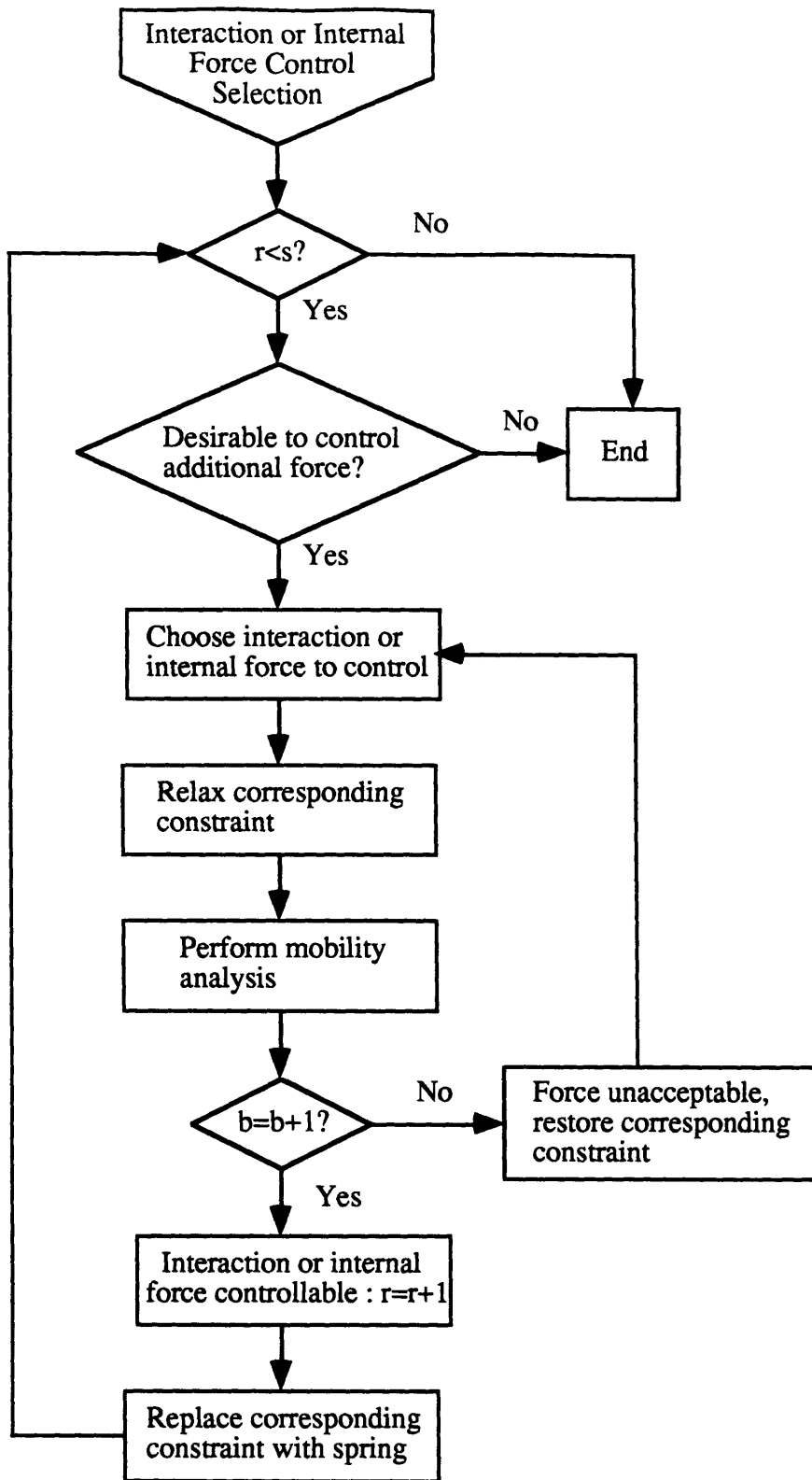


Fig. 10: Stage two of the Extended Mobility Analysis

It is possible that all controllable environmental interaction forces are controlled before $r=s$, and the only additional control variables that can be controlled are the internal forces. Such a system is shown in Figure 11. The system has zero degrees of freedom with all environmental constraints in place. After relaxing an environmental constraint in the x direction, the system has one degree of freedom, and therefore the environmental interaction force can be controlled. However, $r = 1$, $s = 2$, therefore $r < s$, so an additional control variable can be selected. Relaxing an internal constraint on prismatic actuator 2 yields an additional degree of freedom, and thus an internal force can be controlled as well as the environmental interaction force, as shown in Figure 12. However, this force might not be important and the designer might very well elect not to control it and save on computational resources.

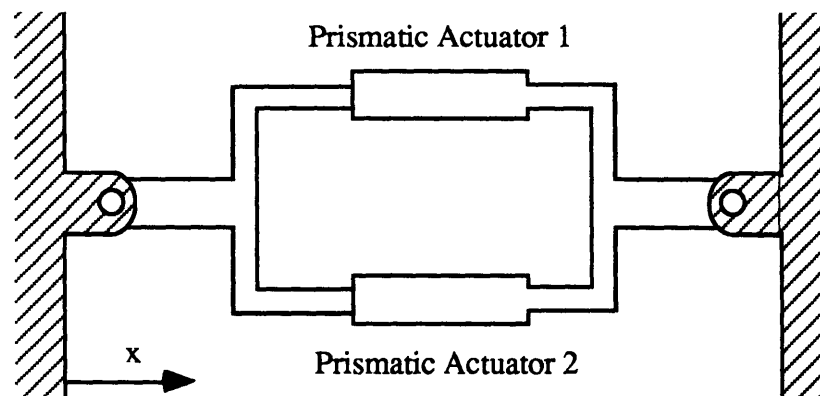


Fig. 11: Over actuated system

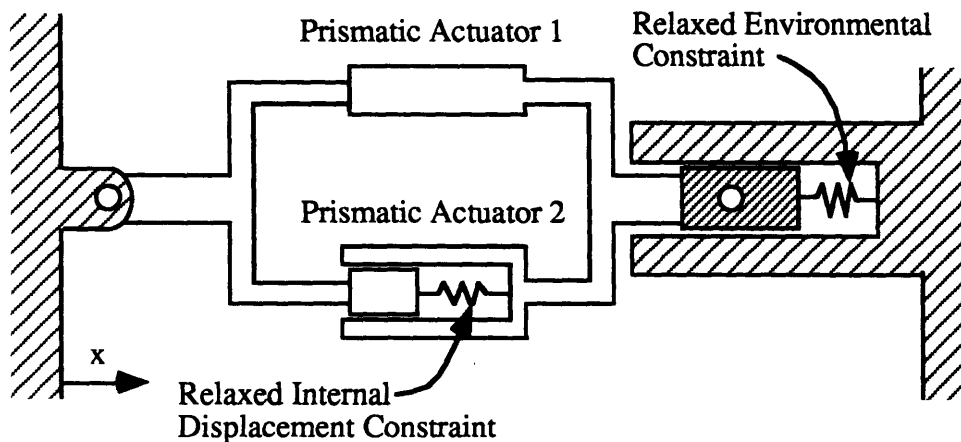


Fig. 12: Over actuated system with environmental and internal constraints relaxed

In some instances, the environment might actually be a spring. While all environments have some compliance, often they are rigid enough to be treated as rigid bodies. If the deflection of the environment under expected loads is small, under 10% of the limb span of the robot, then it can be treated as rigid. In those instances where the environment is too compliant to be treated as rigid, the designer may treat the environment as a spring. Remember that a spring is a joint with six degrees of freedom in a mobility analysis. This prevents the use of CJTC for walking solely on loose springs: the mobility analysis will always yield an under actuated system. CJTC also cannot be used to control free-floating spacecraft, as the mobility analysis will yield an under actuated system. If a control variable is chosen as the positions or orientations of the contact with the compliant environment, the designer has two options: treat it as no constraint, or treat it as a rigid constraint. If the first option is chosen, treating the spring as no constraint at all, then disturbance forces introduced by the environment will cause position and velocity errors in the movement of the control variables. If the environment is treated as rigid, then the control variable will move into the environment due to its compliance, reducing the effective force. The equilibrium position reached by the control variable is given in ³⁷ as:

$$\mathbf{x} = (\mathbf{K}_p + \mathbf{K}_e)^{-1} \cdot (\mathbf{K}_p \cdot \mathbf{x}_{cmd} + \mathbf{K}_e \cdot \mathbf{x}_e) \quad (15)$$

where \mathbf{x}_e is the undeformed position of the environment.

From this equation and the force equation (3), the equilibrium force that will be reached is given as:

$$\mathbf{F} = \mathbf{K}_p \cdot (\mathbf{K}_p + \mathbf{K}_e)^{-1} \cdot \mathbf{K}_e \cdot (\mathbf{x}_{cmd} - \mathbf{x}_e) \quad (16)$$

However, by moving the end of the virtual spring deeper still, the desired force can still be achieved.

The Extended Mobility Analysis is limited in use to simple control variables, such as positions and forces of various locations on the robotic system. More abstract functions are difficult to deal with, because it is not obvious what a constraint on the potential energy would look like or how to perform a mobility analysis with such a constraint in place. However, a simple test to insure that the selected set of control variables is acceptable is that the Jacobian matrix must be of rank = r . If not, then the system is overconstrained and the control variables cannot be simultaneously controlled using CJTC. When dealing with abstract functions, it might be easier to apply this test after selecting each control variable.

Obviously, the procedure does not have to be rigidly followed for simple or intuitively obvious cases. Often, it is possible to choose simultaneously control variables for all the degrees of freedom of the system subject to the full environmental constraints. Testing the choice by constraining the control variables and performing another mobility analysis is advised, however. The methodology is applied to the LIBRA climbing system in section 4.3.

Care must be taken to test for the singularities of the control vector. In general, the control vector will have singularities caused both by kinematic constraints and by environmental constraints, if interaction forces are being controlled. For instance, in specific configurations it might not be possible to control an interaction force chosen, even though it is possible in general. A simple method for testing for singularities is to test for configurations where the rank of the Jacobian matrix is reduced by one or more.

4: Application of CJTC to a laboratory climbing robot

CJTC was applied to an experimental laboratory climbing machine, called the Limbed Intelligent Basic Robotic Ascender, or LIBRA¹. As shown in Figure 13, it is a planar three limbed system is designed to climb between two ladders, with the eventual goal of climbing between two solid walls using friction to support its weight.

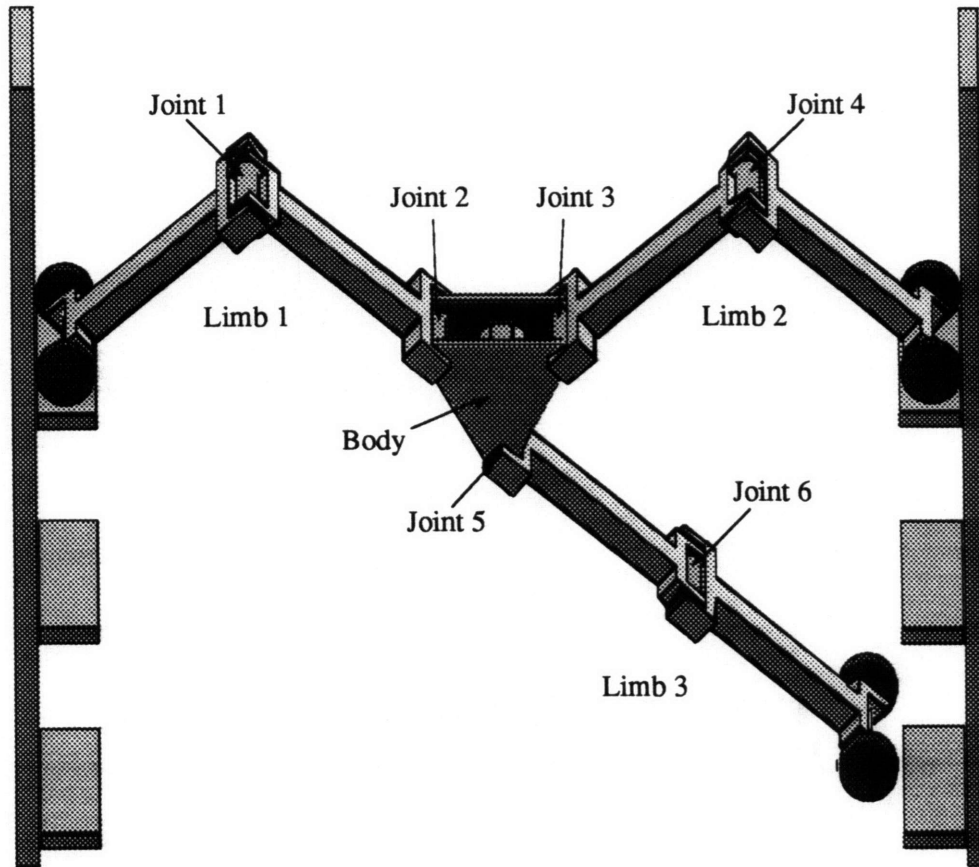


Fig. 13: The LIBRA climbing system

4.1: System description

A block diagram of the experimental setup is shown in Figure 14. It consists of the mechanical LIBRA climbing machine, the power amplifiers, and the control computers. Each part of the system is described in the following sections.

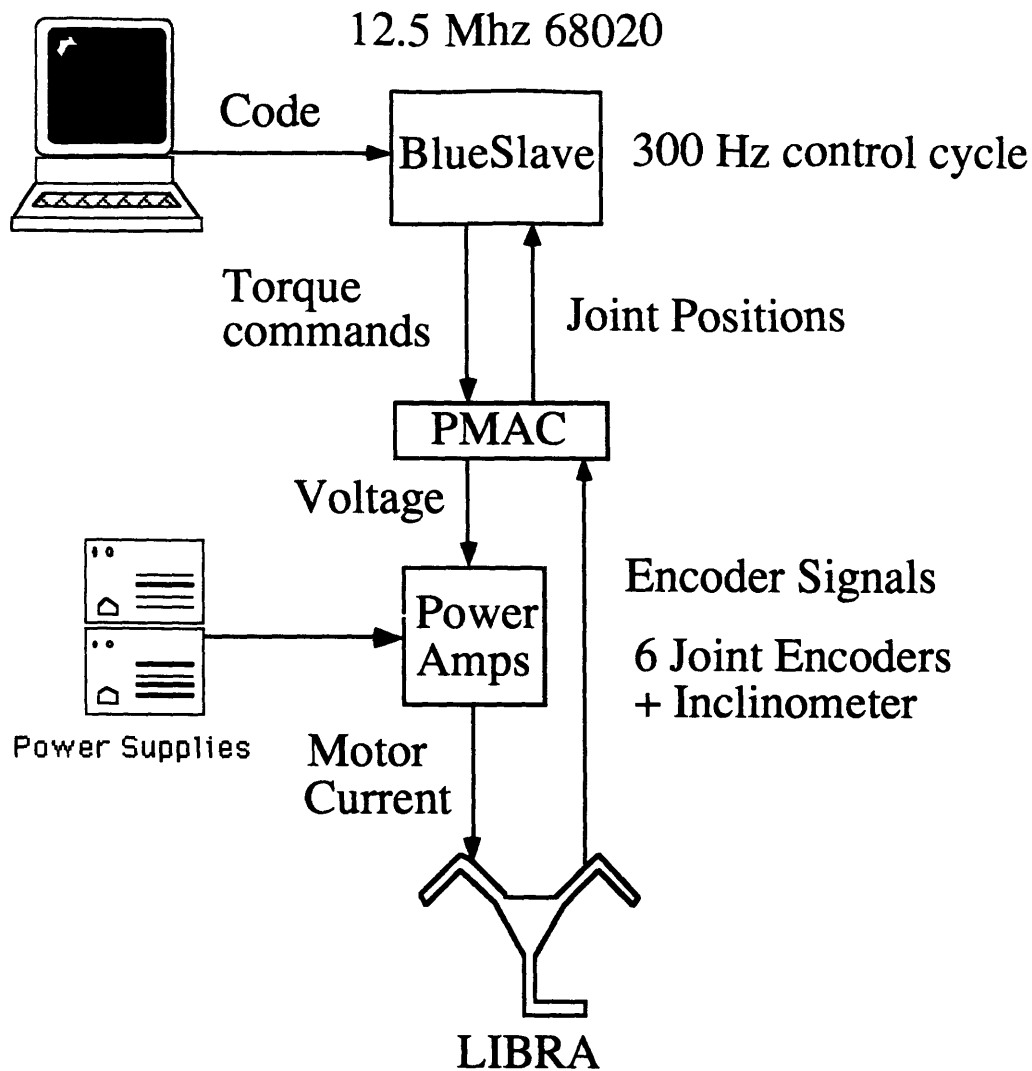


Fig. 14: LIBRA system block diagram

4.1.1: Climbing Machine

The mechanical configuration of the LIBRA is shown in Figure 15. It consists of a main body with three limbs (legs), each with two links and two actuated joints. The angles θ_1 through θ_6 are the joint angles of the actuated joints. The angles θ_2 and θ_3 are measured with respect to the line passing through joint 2 and joint 3. The angle θ_5 is measured with respect to the normal of this line passing through joint five. All angles are measured in a counterclockwise direction. The angle ϕ is a reference angle between the inertial coordinate frame and limb 1. The angle ϕ is not measured directly, but is calculated using the constraint equation for the y location of limb 2.

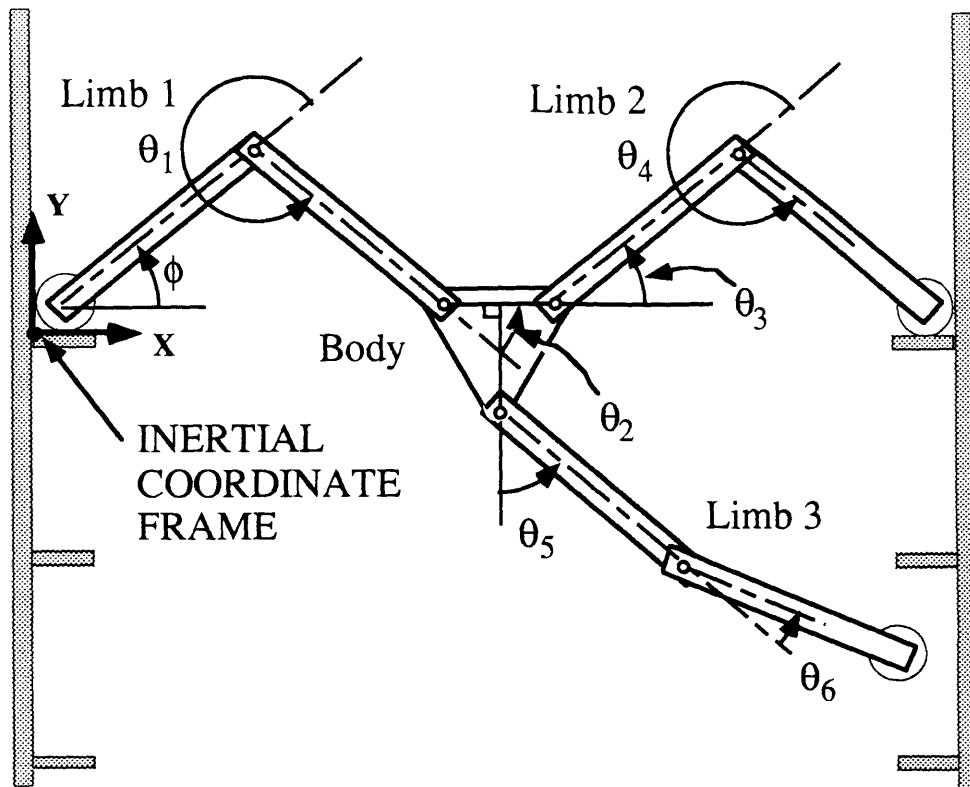


Fig. 15: A Schematic of the LIBRA

The joint vector, consisting of the angles θ of the actuated joints, is defined as:

$$\underline{q} = [\theta_1, \theta_2, \theta_3, \theta_4, \theta_5, \theta_6]^T$$

The actuated joints are driven by Escap 23DT12 -216E electric motors with a 792:1 gear ratio transmission. The large gear ratio was required to produce relatively large torques using small motors. The large gear ratio has several drawbacks, including large transmission friction, poor back-drivability, and significant backlash in the output shaft of two degrees. The motor and gearhead specifications are ⁵⁴:

Torque Constant	=	23.3 mNm/A
Back EMF Constant	=	0.0024 V/rpm
No-Load Current	=	20 mA
Maximum Continuous Current	=	0.9 A
Armature Resistance (R_m)	=	9.7 Ω
Armature Inductance (L_m)	=	0.8 mH
Maximum Dynamic Torque	=	4.5 Nm @ 20 rpm
Maximum Static Torque	=	20 Nm @ 0 rpm
Gearhead Efficiency (η)	=	0.55
Max. input speed	=	3000 rpm
Max. Backlash	=	2°

The ranges of the joint angles are limited by the mounting hardware off the actuators.

The joint limits are given as:

Joint 1 = $\pm 117^\circ$

Joint 2 = $+ 132^\circ, -69^\circ$

Joint 3 = $+ 132^\circ, -69^\circ$

Joint 4 = $\pm 117^\circ$

Joint 5 = $\pm 110^\circ$

Joint 6 = $\pm 117^\circ$

The on-board sensors consist of encoders measuring the joint angles and a pendulum-based inclinometer used to measure the angle of the center body (θ_B). The inclinometer is necessary to obtain the initial orientation, and it is also used to confirm the position of the system as it climbs. The encoders on the motor have a resolution of 2000 counts per revolution of the motor shaft, after utilizing quadrature decoding to enhance the resolution. The gearhead increases this to 1,584,000 counts per revolution of the output shaft. However, the accuracy of the encoder is still limited by the backlash in the output shaft. The inclinometer has a resolution of 0.35 degrees, but stiction limits its sensing accuracy to ± 1 degree. A force sensor was mounted on a ladder step to measure the horizontal force applied by foot 2, but the sensor was only used for collecting data and did not provide feedback to the control loop.

The LIBRA has a limb span of 0.7 meters, and weighs 8 kg. Rubber model airplane wheels 8.3 cm in diameter are used as the end-effectors. Several advantages to using the compliant wheels are: limited impact force, good contact stability, easy seating of the wheels in the steps, and simplicity of building. Hooks are being considered to allow climbing on one ladder and a variety of other climbing gaits. Details of the construction of the LIBRA can be found in ¹. Modifications performed on the LIBRA not documented in Argaez ¹ are minor: some material was removed from the components to reduce weight, and the motor shaft clamps were rebuilt using a friction clamp design, rather than a set screw.

The ladders that are climbed by the LIBRA are constructed of angle iron, providing adjustable step height and L shaped steps. The configuration used for the LIBRA experiments discussed in this thesis are a ladder separation of 0.18 m, and a uniform step height of 0.134 m.

4.1.2: Power Amplifiers

The power amplifiers are voltage to current amplifiers, acting as variable current sources. Their schematics and other details can be found in Appendix B. The amplifier-motor system has a time constant of 1.52 microseconds, resulting in a bandwidth of 656 Hz. Since this far exceeds the bandwidth of the controller, we can treat the amplifier-motor systems as torque servos. However, this does not include the damping resulting from the large friction found in the gearheads. This will result in additional damping added to the system.

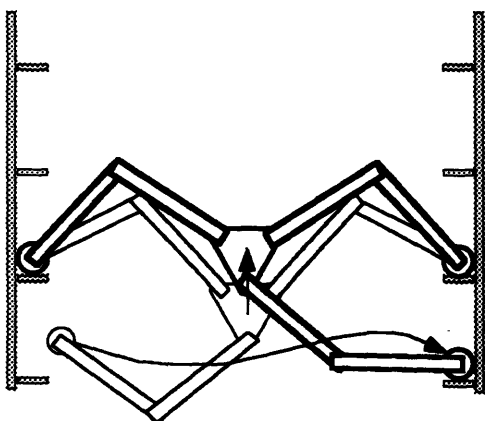
4.1.3: Control Computers

A VME bus computer system running VxWorks is used to control the LIBRA. A Sun 3/80 workstation is used to program, debug, and compile the control code, and for data storage. The compiled control software is then downloaded to run on a 68020, 12.5 MHz processor. The control cycle closes at a rate of 300 Hz. A multi-axis control board mounted on the VME bus, called the Programmable Multi Axis Controller (PMAC)⁵⁵, is used to decode and count the encoder signals and as D/A converters to output the control signals. The PMAC was able to perform these tasks at a rate of 1000 Hz.

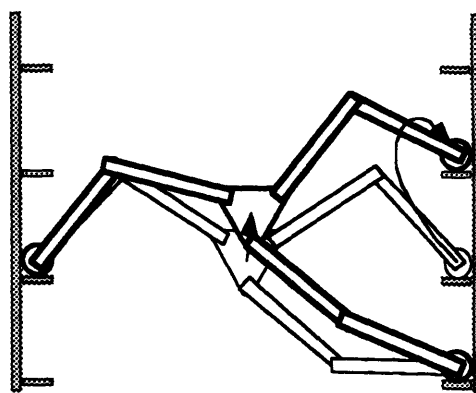
Work is currently being done to implement the control software on a custom-made computer board designed to mount on the LIBRA itself. The board consists of 6 motor control chips and one 8031 processor. This board is representative of the computing capability available for many small robots.

4.2: Climbing Gait

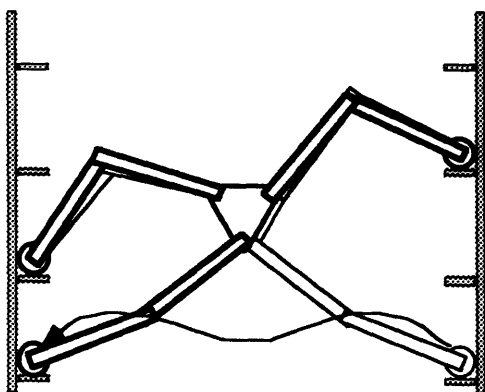
The LIBRA is designed to climb between two ladders. Currently only one climbing gait is used. It is a four stage gait, shown in Figure 16. Stage one starts with a pushup maneuver to get its body level with the next set of rungs, and then places its third foot on the right hand ladder. In stage two, the LIBRA lifts the second foot off of the rung and lets foot 3 support the body. Foot 2 then lifts up one rung, and transfers back to the support of the body at the start of stage three. Foot 3 then swings over to the left hand rung. In stage four, foot 1 lifts up one rung. The cycle then repeats itself, continuing the climb.



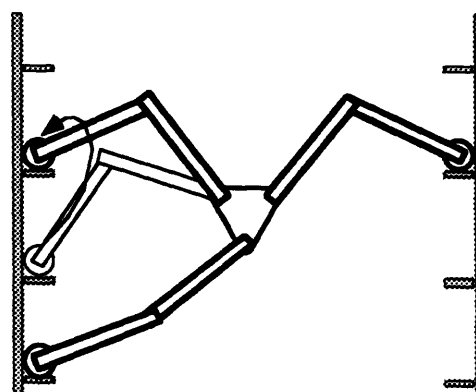
Stage 1 : Foot 3 swings to right step



Stage 2 : Foot 2 lifts one step



Stage 3 : Foot 3 swings to left step



Stage 4 : Foot 1 lifts one step

Fig. 16: Climbing Gait used by the LIBRA

4.3: Control Vector Selection

As can be seen from the above description of the climbing gait, in stages one and three it is desirable for the task of climbing to control the x , y , and θ positions of the center body and the x and y positions of foot 3. A detailed Extended Mobility Analysis is performed to test if this is an acceptable set of control variables. A Gruebler's mobility analysis performed on the LIBRA system with pin joints at two of the feet as shown in Figure 17 reveals that the system has five DOF ($F=a=b=5$).

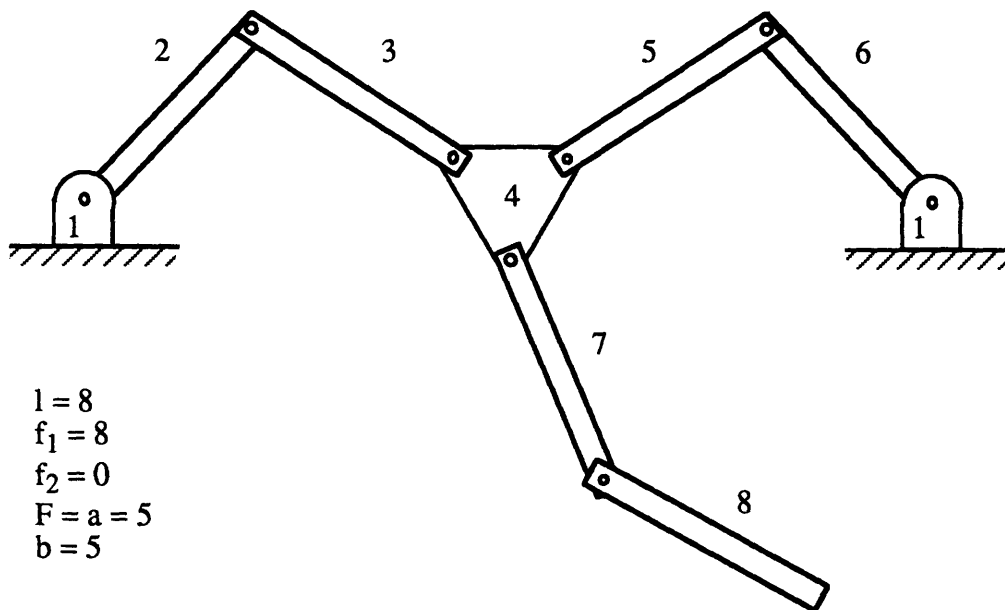


Fig. 17: LIBRA under full environmental constraints

Constraining the x position (placing a vertical slider on the center body as shown in Figure 18) and performing another mobility analysis gives only four DOF ($b=4$), so the x position of the center body is an acceptable control variable.

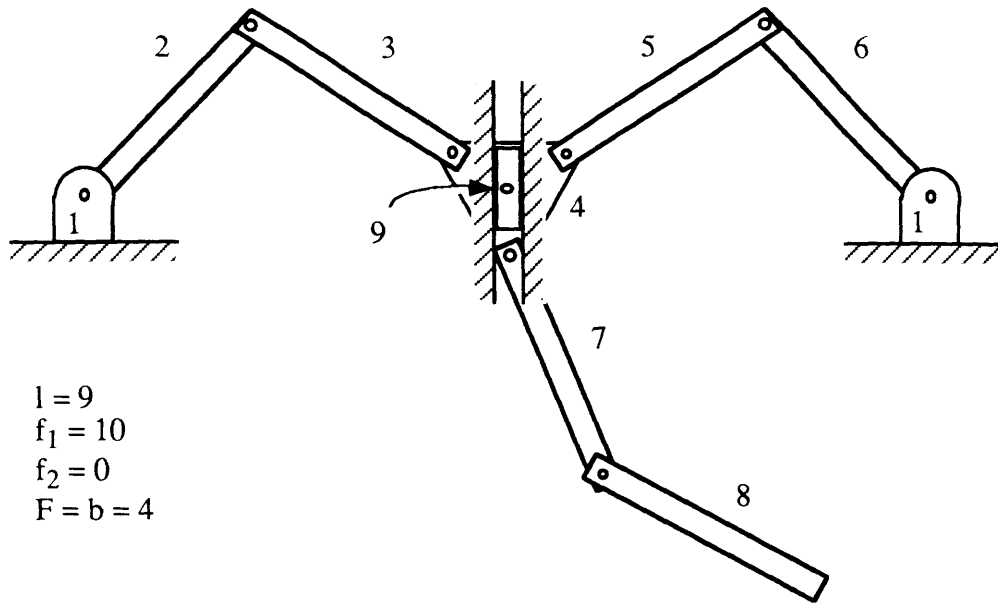


Fig. 18: Constraining x of the Center Body

Adding a constraint on the y position of the center body also results in the loss of a degree of freedom, as shown in Figure 19 (b=3).

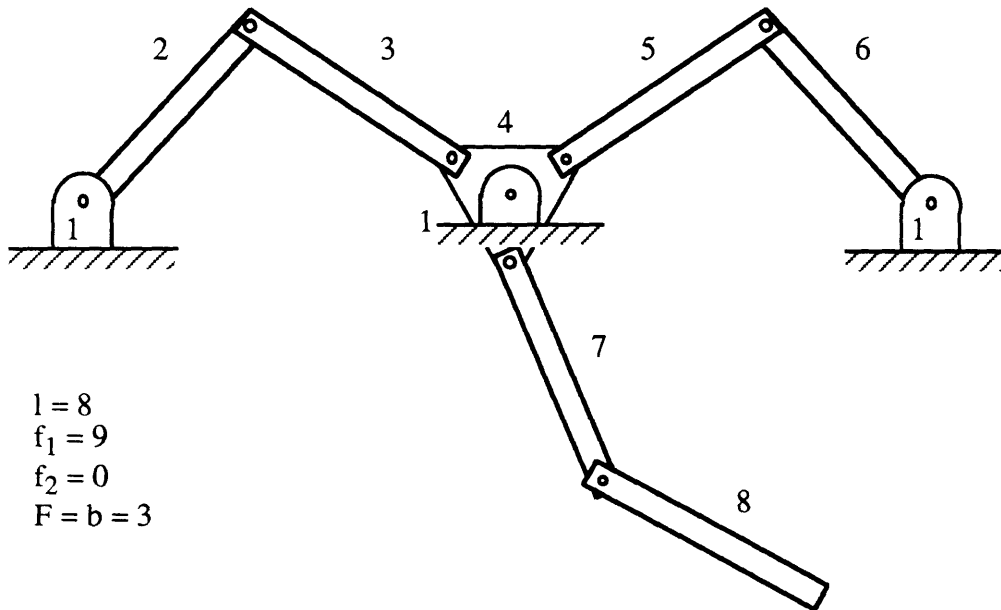


Fig. 19: Constraining x,y of the Center Body

Immobilizing the center body by adding a θ constraint also reduces the degrees of freedom (b=2).

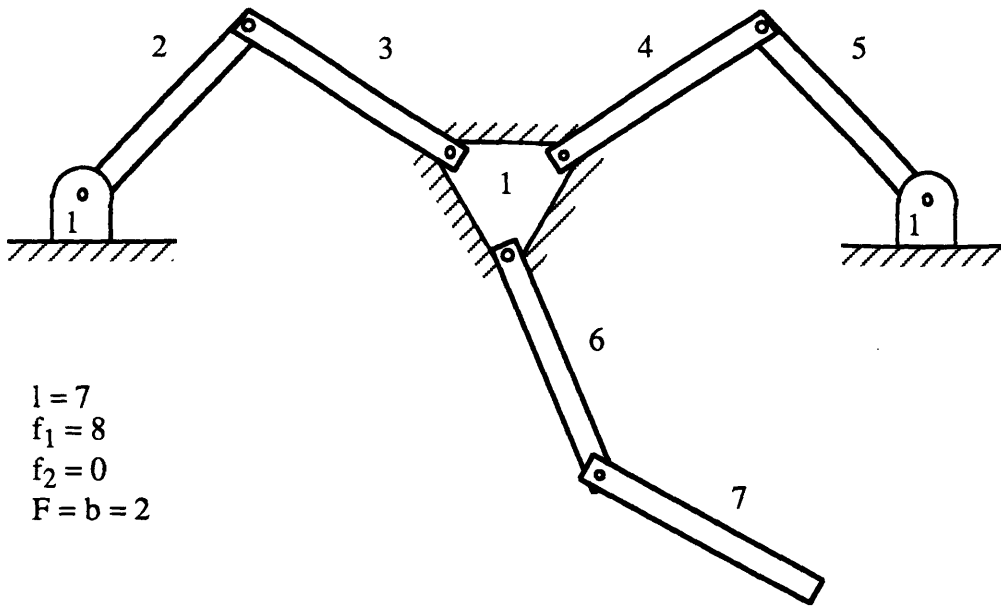


Fig. 20: Constraining x, y, θ of the Center Body

It is obvious that constraining the x and y of the free foot will completely constrain the system, as shown in Figure 21.

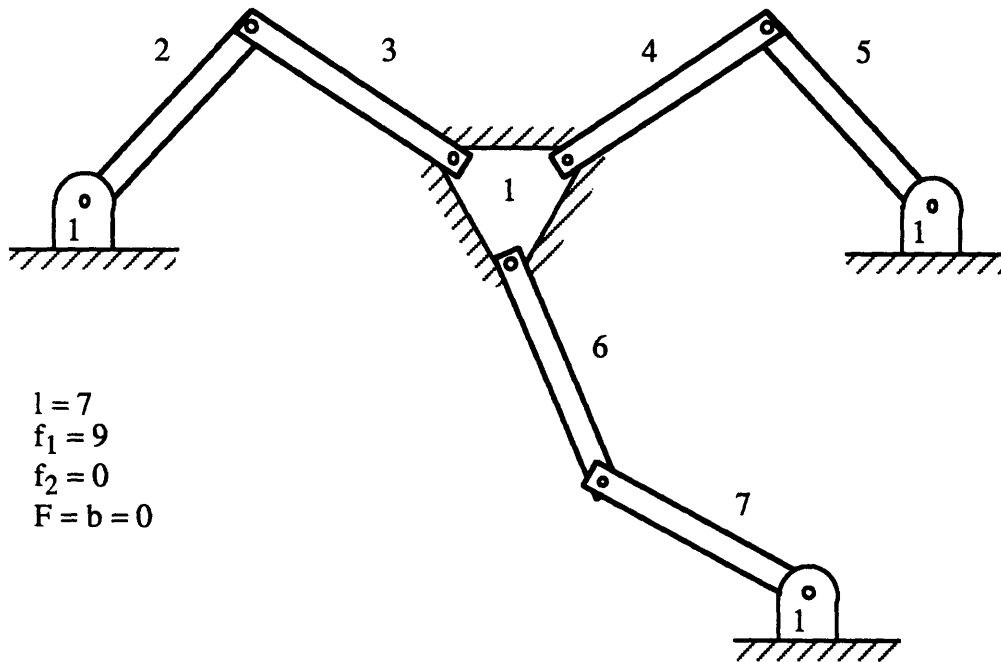


Fig. 21: Constraining x, y of Foot 3

So, after constraining the x , y , and θ of the center body, and the x and y of foot 3, the system has no degrees of freedom ($b=0$, $r=5$). This concludes stage one of the Extended Mobility Analysis.

There are six actuators and only five control variables so far ($r = 5$, $s = 6$, so $r < s$). This implies that an environmental interaction force or internal force can be controlled, and so we go on to the second stage of the Extended Mobility Analysis. For climbing between walls using friction to support its weight, as is the ultimate goal of the LIBRA, it is desirable to control the horizontal force being applied at the wall by the second foot. Relaxing the x constraint on foot 2 as shown in Figure 22, the system has one degree of freedom, and therefore the x force of foot 2 can be controlled.

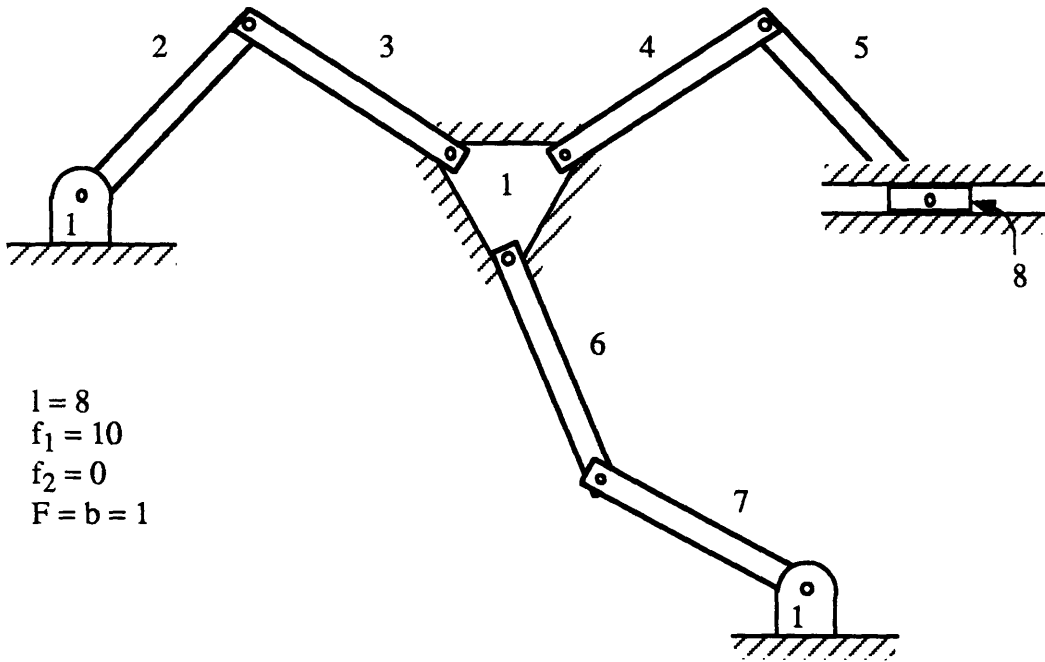


Fig. 22: Relaxing the x environmental constraint

The system now has six actuators and six control variables. The control vector \underline{u} looks like:

$$\underline{u}_1 = [x_b, y_b, \theta_b, x_2, x_3, y_3]^T$$

The LIBRA system with virtual spring-dampers attached to control vector one is shown in Figure 23. The virtual spring-damper attached to foot 2 is used to control the force being applied to the ladder in the x direction.

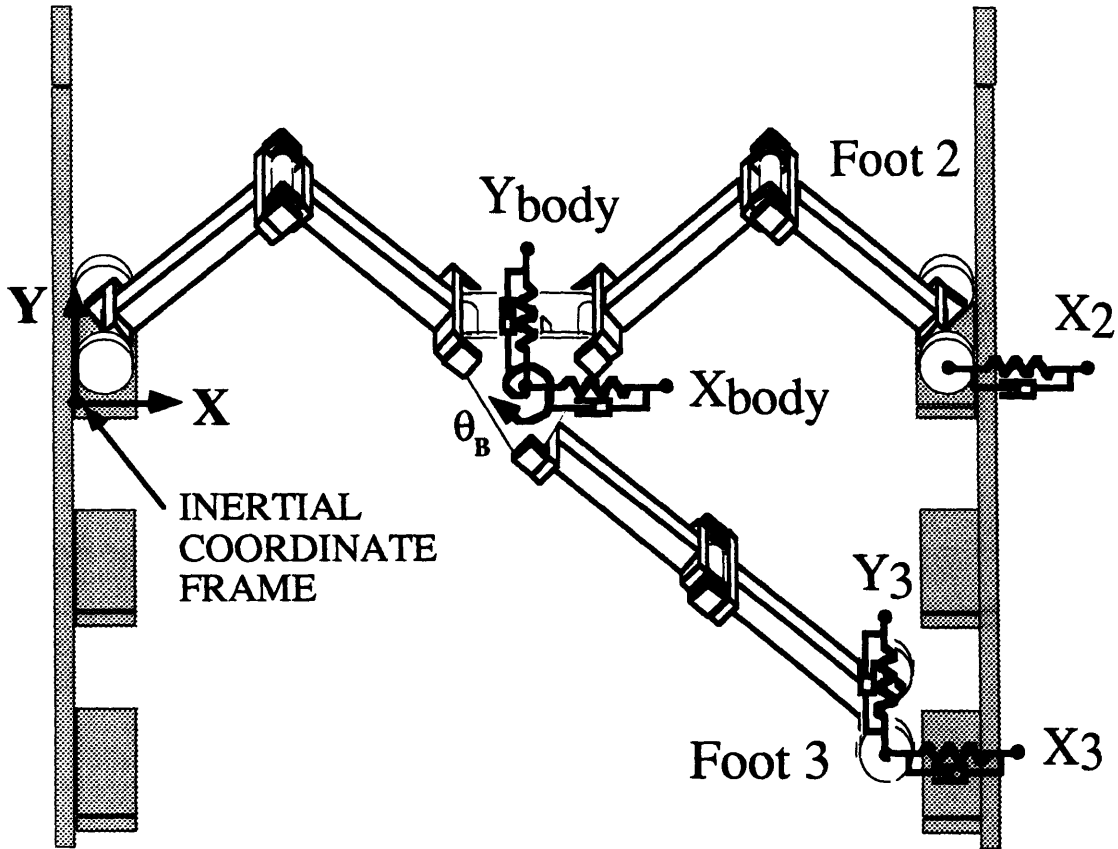


Fig. 23: LIBRA with control vector 1

For the different stages in climbing, different control vectors need to be used. This is because of the different tasks that the system needs to perform. Control vector one is used during stages one and three. During stage two, foot 3 is used to support the body, and foot 2 is lifted and controlled in free space. Control vector two is then used, as given by:

$$\underline{u}_2 = [x_b, y_b, \theta_b, x_2, y_2, x_3]^T$$

The LIBRA with virtual spring-dampers attached to control vector two is shown in Figure 24.

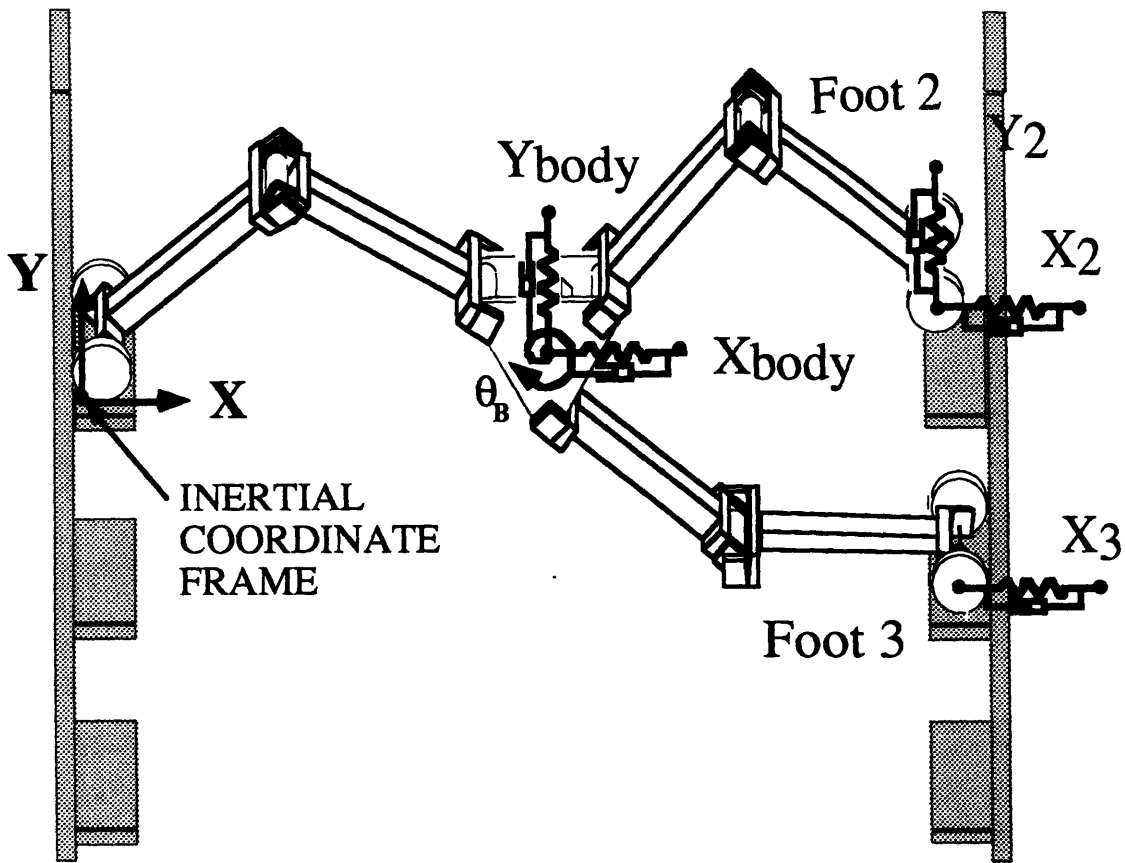


Fig. 24: LIBRA with control vector 2

Stage four requires foot 3 to support the body, and foot 1 is lifted and moved in free space. The LIBRA then uses control vector three:

$$\underline{u}_3 = [x_1, y_1, x_b, y_b, \theta_b, x_2]^T$$

The LIBRA with spring-dampers attached to control vector three is shown in Figure 25. Extended Mobility Analyses can be performed on control vectors two and three to verify that the control vectors are valid. From symmetry, however, it is obvious that they are.

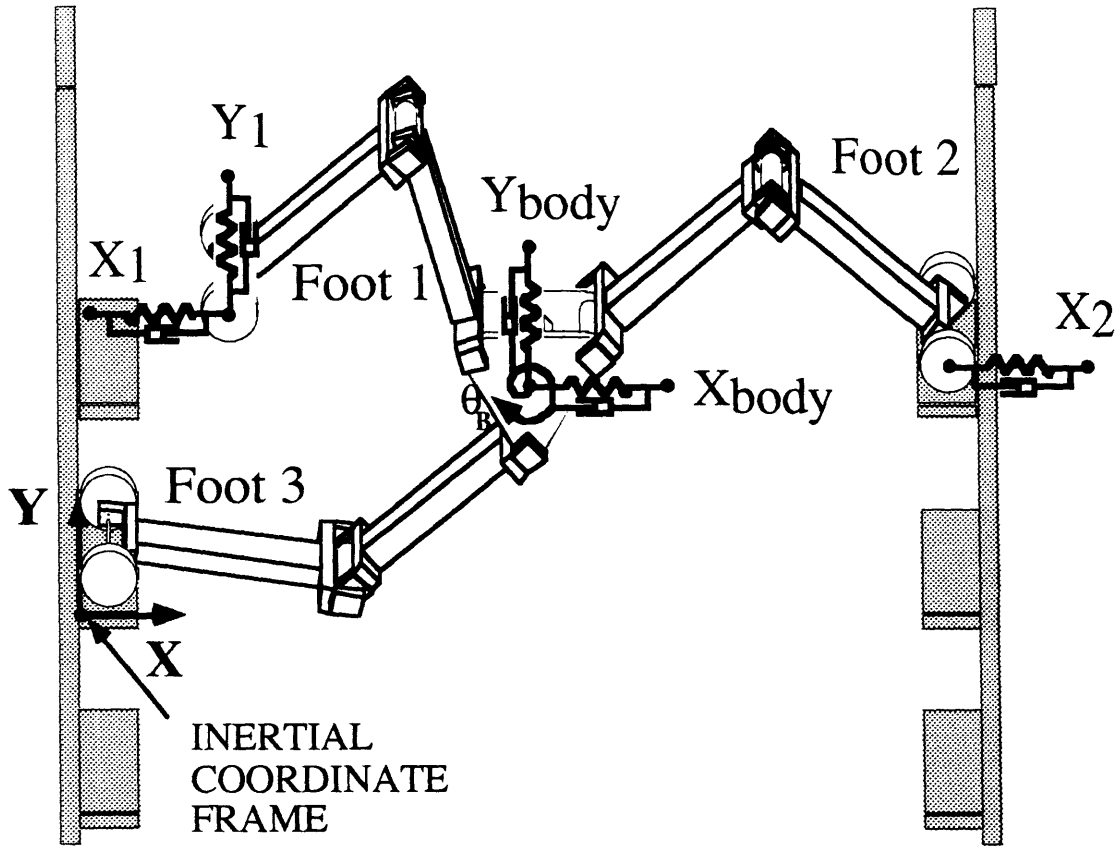


Fig. 25: LIBRA with control vector 3

4.4: Control equations

The control equations in this section are only derived for control vector one. Similar analysis will lead to the control equations for the other two control vectors. The six control variables chosen for control vector one are:

$$\underline{u}_1 = [x_b, y_b, \theta_b, x_2, x_3, y_3]^T$$

The Jacobian matrix, as given by equation (11), is derived in Appendix A for control vector one. To write the Jacobian explicitly in terms of the joint vector q , the position constraint on the y direction of foot 2 is solved algebraically and substituted into the Jacobian.

$$\mathbf{J}(\mathbf{q}) = \begin{bmatrix} \frac{\partial x_b}{\partial \theta_1} & \dots & \frac{\partial x_b}{\partial \theta_6} \\ \frac{\partial y_b}{\partial \theta_1} & \dots & \frac{\partial y_b}{\partial \theta_6} \\ \frac{\partial \theta_b}{\partial \theta_1} & \dots & \frac{\partial \theta_b}{\partial \theta_6} \\ \frac{\partial x_2}{\partial \theta_1} & \dots & \frac{\partial x_2}{\partial \theta_6} \\ \frac{\partial x_3}{\partial \theta_1} & \dots & \frac{\partial x_3}{\partial \theta_6} \\ \frac{\partial y_3}{\partial \theta_1} & \dots & \frac{\partial y_3}{\partial \theta_6} \end{bmatrix} \quad (17)$$

Since the x_2 variable is constrained by the ladder, the force of the foot in the x -direction is controlled by implanting the commanded control variable into the ladder.

The force equation, as given by (10) is

$$\mathbf{F} = \mathbf{K}_p \begin{bmatrix} x_b(\text{cmd}) - x_b \\ y_b(\text{cmd}) - y_b \\ \theta_b(\text{cmd}) - \theta_b \\ x_2(\text{cmd}) - x_2 \\ x_3(\text{cmd}) - x_3 \\ y_3(\text{cmd}) - y_3 \end{bmatrix} + \mathbf{K}_d \begin{bmatrix} \dot{x}_b(\text{cmd}) - \dot{x}_b \\ \dot{y}_b(\text{cmd}) - \dot{y}_b \\ \dot{\theta}_b(\text{cmd}) - \dot{\theta}_b \\ \dot{x}_2(\text{cmd}) - \dot{x}_2 \\ \dot{x}_3(\text{cmd}) - \dot{x}_3 \\ \dot{y}_3(\text{cmd}) - \dot{y}_3 \end{bmatrix} \quad (18)$$

\mathbf{K}_p and \mathbf{K}_d were chosen to be diagonal, with terms of:

$$k_p = (k_{pb}, k_{pb}, k_{p\theta}, k_{p2}, k_{p3}, k_{p3})$$

corresponding to the spring constants for each control variable and a similar form for k_d .

For the purpose of deriving a gravity compensation term, the mass of the system was assumed to be at a point at the main body. Although a more detailed gravity compensation term certainly is possible, computational capability constraints made this simplifying assumption attractive. This resulted in good experimental results and was

computationally inexpensive. The gravity force due to this lumped mass model is transformed into joint torques using the transpose of the system's Jacobian matrix. The gravity term in (12) then becomes:

$$\underline{G}(q) = \mathbf{J}^T[0, M \cdot g, 0, 0, 0, 0]^T \quad (19)$$

Combining (12), (17), (18) and (19), the input vector becomes:

$$\underline{\tau} = \begin{bmatrix} \tau_1 \\ \tau_2 \\ \tau_3 \\ \tau_4 \\ \tau_5 \\ \tau_6 \end{bmatrix} = \mathbf{J}^T \cdot \left(\mathbf{K}_p \begin{bmatrix} x_b^{(cmd)} - x_b \\ y_b^{(cmd)} - y_b \\ \theta_b^{(cmd)} - \theta_b \\ x_2^{(cmd)} - x_2 \\ x_3^{(cmd)} - x_3 \\ y_3^{(cmd)} - y_3 \end{bmatrix} + \mathbf{K}_d \begin{bmatrix} \dot{x}_b^{(cmd)} - \dot{x}_b \\ \dot{y}_b^{(cmd)} - \dot{y}_b \\ \dot{\theta}_b^{(cmd)} - \dot{\theta}_b \\ \dot{x}_2^{(cmd)} - \dot{x}_2 \\ \dot{x}_3^{(cmd)} - \dot{x}_3 \\ \dot{y}_3^{(cmd)} - \dot{y}_3 \end{bmatrix} + \begin{bmatrix} 0 \\ M \cdot g \\ 0 \\ 0 \\ 0 \\ 0 \end{bmatrix} \right) \quad (20)$$

4.5: Control gain selection

A combination of experimental trial and error and an analysis of a dynamic model of the LIBRA system was used to select the control gain matrices \mathbf{K}_p and \mathbf{K}_d . The ranges of the desired \mathbf{K}_p control gains were chosen based on the desired stiffness of the different virtual spring-damper systems attached to the control variables. The position of the body is important to control tightly, so the stiffness of the virtual springs on the body is desired to be high. The feet come in contact with the environment and the forces that they exert are important to control. By having low stiffness virtual springs, small changes in the position of the feet due to compliance or sensor error will only have a small effect on the force being exerted. Therefore the gains on the feet are desired to be fairly low.

4.5.1: Dynamic Model

An analysis of a dynamic model of the LIBRA system assists in selecting the control gain matrices \mathbf{K}_p and \mathbf{K}_d . Only the top chain of the LIBRA was modeled, as it is assumed that the free foot can be analyzed separately. To simplify the model of the LIBRA, point masses m_i are assumed to be located at the positions shown in Figure 26.

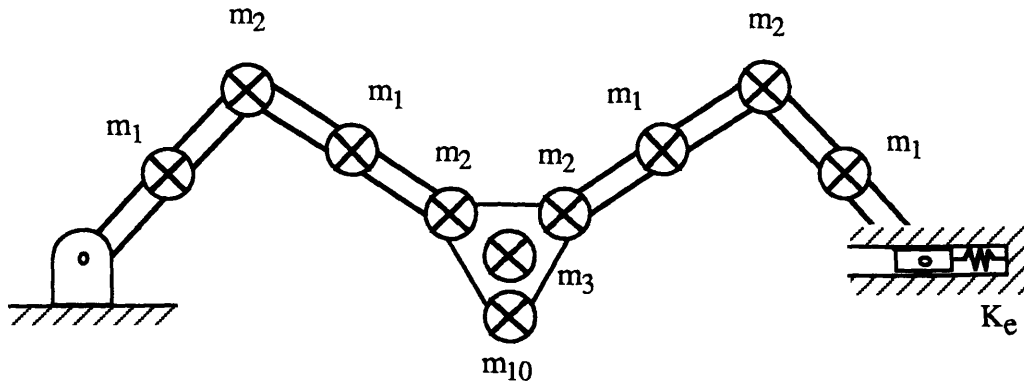


Fig. 26: Model of the LIBRA top kinematic chain

where:

- m_1 = mass of limb link
- m_2 = motor mass
- m_3 = mass of body
- m_{10} = mass of limb three
- K_e = environmental stiffness

The limb link masses, which are identical for all links, are assumed to be lumped halfway along the links. The motor masses are placed at the joints. The body mass is located at the geometric center of the body. As an approximation, the mass of limb three is assumed to be at the first joint of the third limb. The actuators are also modeled as frictionless torque supplies, ignoring the internal friction and actuator dynamics. While the actuator dynamics are sufficiently fast that they shouldn't affect the dynamics of the overall system, the friction in the actuators will add a significant amount of damping. The dynamic equations are derived using Lagrange's equation:

$$\left[\frac{d}{dt} \frac{\partial T}{\partial \dot{\underline{q}}} - \frac{\partial T}{\partial \underline{q}} - \frac{\partial V}{\partial \underline{q}} - \underline{\tau} \right] \cdot \delta \underline{q} = 0 \quad (21)$$

where

- T = the kinetic energy of the system
- V = the potential energy of the system

To further simplify the equations, it is assumed that the gravity compensation term of the controller is exact. The equations are linearized about $\dot{\mathbf{q}} = 0$. Appendix C contains the linearized dynamic equations derived using these assumptions. In state space form, using the control vector as the state space, these equations can be represented as:

$$\begin{bmatrix} \ddot{\mathbf{u}} \\ \dots \\ \dot{\mathbf{u}} \end{bmatrix} = \begin{bmatrix} \mathbf{J}(\mathbf{q}) \cdot \mathbf{H}^{-1}(\mathbf{q}) \cdot \mathbf{J}^T(\mathbf{q}) \cdot \mathbf{K}_d & : & \mathbf{J}(\mathbf{q}) \cdot \mathbf{H}^{-1}(\mathbf{q}) \cdot \mathbf{J}^T(\mathbf{q}) \cdot \mathbf{K}_p \\ \dots & : & \dots \\ \mathbf{I} & : & \mathbf{0} \end{bmatrix} \begin{bmatrix} \ddot{\mathbf{u}} \\ \dots \\ \dot{\mathbf{u}} \end{bmatrix} + \begin{bmatrix} \mathbf{J}(\mathbf{q}) \cdot \mathbf{H}^{-1}(\mathbf{q}) \cdot \mathbf{J}^T(\mathbf{q}) \cdot \mathbf{K}_d & : & \mathbf{J}(\mathbf{q}) \cdot \mathbf{H}^{-1}(\mathbf{q}) \cdot \mathbf{J}^T(\mathbf{q}) \cdot \mathbf{K}_p \\ \dots & : & \dots \end{bmatrix} \begin{bmatrix} \dot{\mathbf{u}}_{cmd} \\ \dots \\ \mathbf{u}_{cmd} \end{bmatrix} \quad (22)$$

$$[y] = [\mathbf{0} : \mathbf{I}] \begin{bmatrix} \dot{\mathbf{u}} \\ \dots \\ \mathbf{u} \end{bmatrix}$$

where \mathbf{H} is the configuration dependent inertia matrix

Since the terms of the matrices are not constant, but are instead very configuration dependent, the system response changes as a function of the configuration.

Equation (22) is linearized around 18 representative configurations of the system. These points were chosen to reflect the range of motion found in the climbing maneuver. The x_{body} position was chosen to be at one half the wall separation of 0.18 m. The θ_{body} is chosen to be zero, which is the commanded position during the entire climbing gait. The x_2 position of foot 2 is chosen to be at the wall. The only control variable in the top kinematic chain that really varies during the climbing gait is the y_{body} , which was chosen to vary from -0.22 m through 0.05 m. This represents the fullest possible vertical movement of the LIBRA in the current climbing setup. Classical root locus methods and bode plots were used to study the stability of the system. The system gains were chosen to meet the design specification of a bandwidth of 6 Hz and steady state positioning errors of the center body of less than 2 mm under a 10 N disturbance. The gains suggested through this analysis were:

$$k_p = [1000, 1000, 22, 500]$$

$$k_d = [160, 160, 4, 120]$$

After experimental tests, the gains were tuned to:

$$k_p = [1000, 500, 8, 100]$$

$$k_d = [200, 100, 2, 20]$$

The dominant poles for these gains, sampled at different configurations, are given in Figure 27. Appendix C shows the entire pole diagram for these configurations, and the bode plots of the dominant control variable loops. While it might appear in these diagrams that the system is under damped and the bandwidth is larger than desired, it is important to note that the analysis did not include the damping effects of the friction in the motor gearheads.

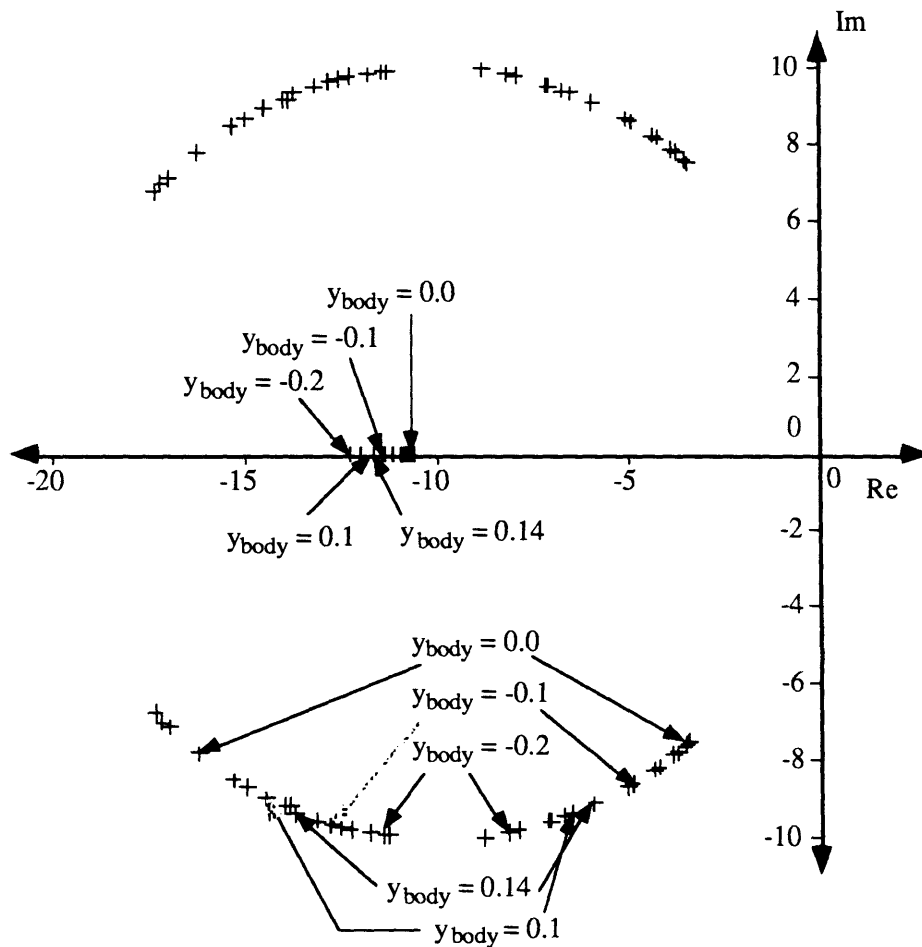


Fig. 27: Dominant poles of the LIBRA for y_{body} from -0.20m to 0.14 m

The last limb, limb three, was chosen separately to have gains of $k_p = [100, 100]$ and $k_d = [10 \ 10]$. This selection was strictly based on experimental trial and error. It was found that the gains for the third foot have little effect the performance of the upper kinematic chain. Also, the third foot performance is not sensitive to the gains chosen, and a wide range of gains could be chosen based on the desired performance of the third foot. Gains of up to $k_p = [1000, 1000]$ and $k_d = [150 \ 150]$ were used for closer trajectory tracking.

4.6: Experimental performance

Data from two experiments are presented in the following sections. First, data are presented for the first stage of the climbing gait including force data gathered from a force sensor mounted on one of the rungs. Secondly, data are presented for a full climbing cycle, but no force data was collected. These data are representative of the performance of the LIBRA under CJTC, and demonstrate the effectiveness of CJTC.

4.6.1: Data from climbing stage one

Figure 28 shows the desired motion for the climbing robot. This is the first stage of the four stage climbing gait. The trajectory consists mainly of the body's vertical motion while swinging the third foot over and placing it on a step. Although θ_b is not shown in Figure 28, it is always commanded to be equal to zero. The second foot is pressing against the step with a commanded horizontal force of 10 Newtons. This force is specified by moving the commanded control variable $x_2(\text{cmd})$ into the wall, at distance of $10\text{N} / 100\text{N/m} = 0.1 \text{ m}$. Although some compliance exists within the foot and the wall, the commanded force remains constant by commanding a constant offset distance from the actual position.

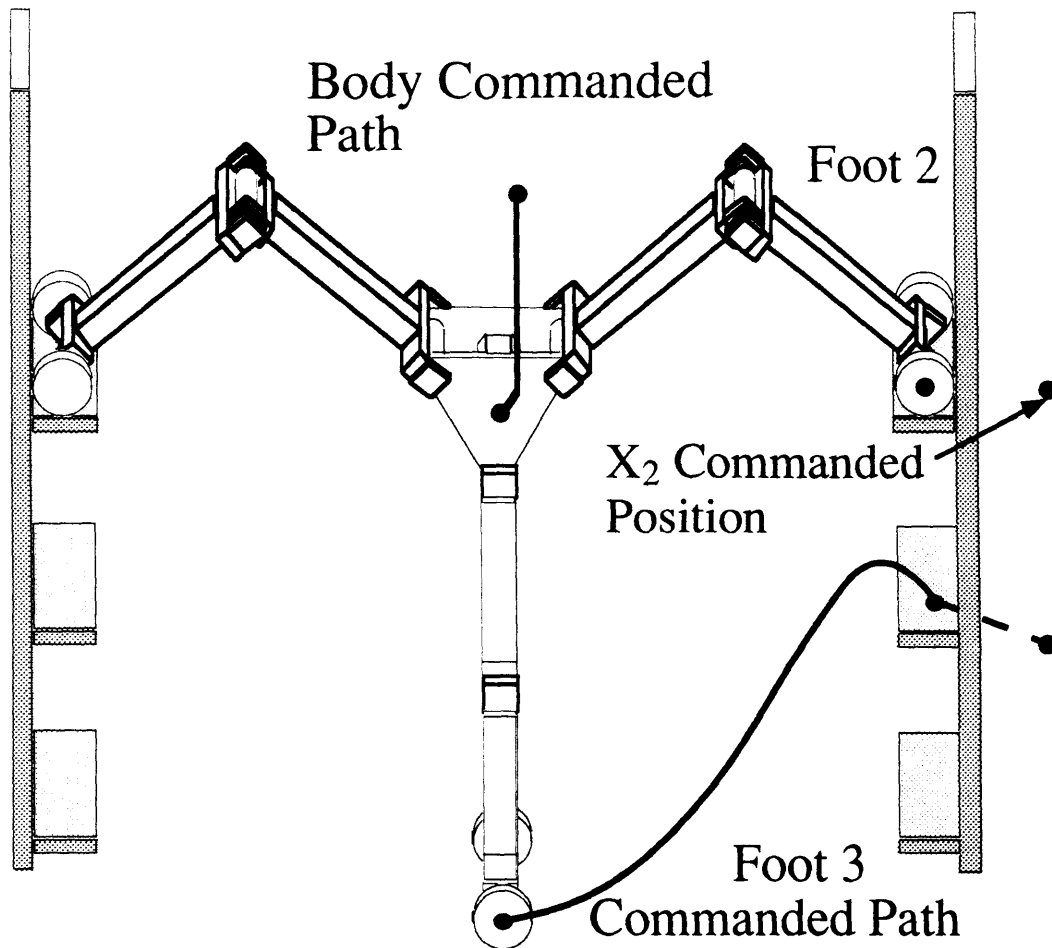


Fig. 28: Desired motion for the climbing robot

Figures 29 and 30 show the trajectory of the main body x_b , y_b and θ_b positions. The main body reaches its steady-state position in approximately 4.5 seconds. During the vertical movement, the x_{body} (x_b) position varies by as much as 5 mm, but remains within 2 mm once the steady-state position is reached. The y_{body} (y_b) control variable followed the desired vertical motion very accurately as shown in Figure 29, and the steady state error is almost 0.00 m. After 5 seconds, the third foot has contacted the ladder and is seating itself, applying forces of up to ten Newtons to the ladder. The center body location stays close to the commanded position despite this force, which demonstrates the capability to control manipulation forces and mobility simultaneously. The θ_{body} shows very small errors, and remains within 3×10^{-2} radians, or 1.7 degrees, at all times. The plateaus seen in Figure 30 are caused by stiction in the inclinometer.

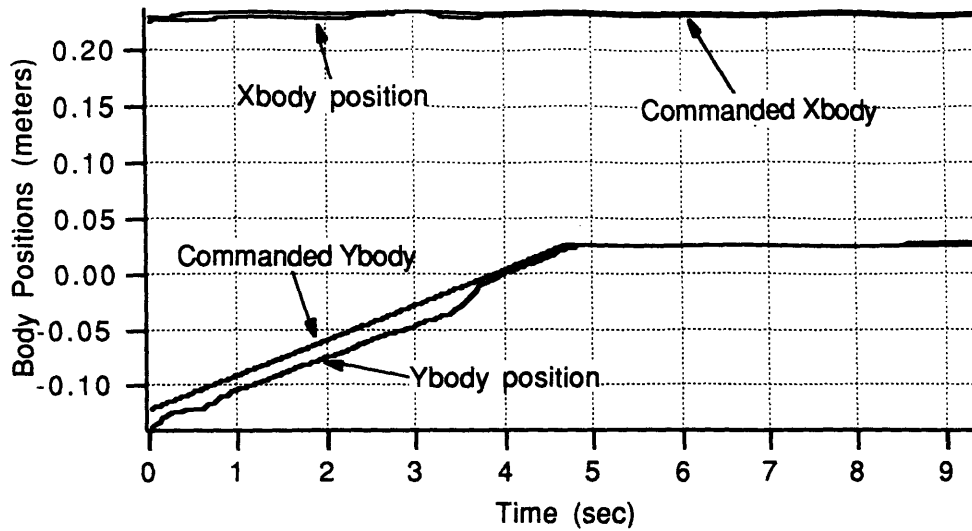


Fig. 29: x_b , y_b position for a pushup maneuver

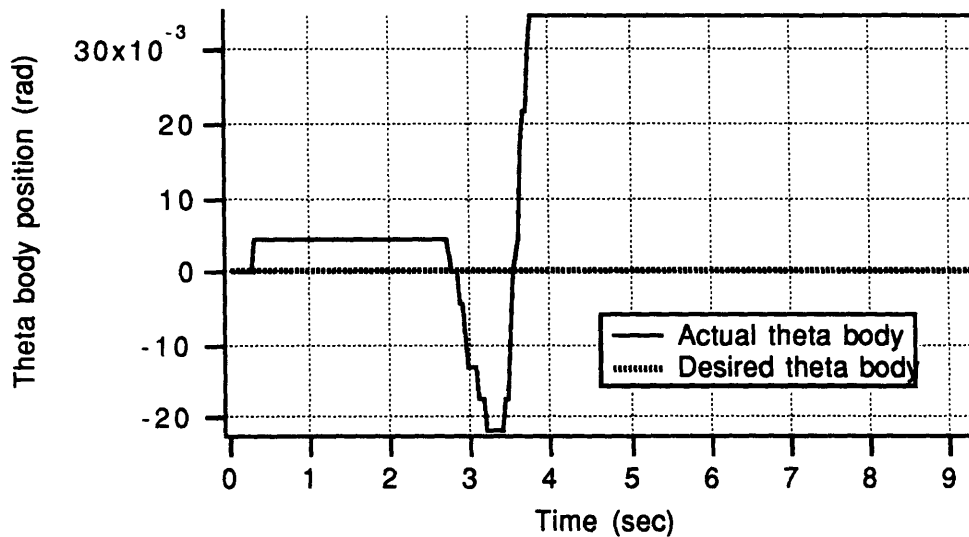


Fig. 30: θ_b for a pushup maneuver

The horizontal foot force of foot 2, shown in Figure 31, stayed within four Newtons of the commanded force of ten Newtons, even though there is no force feedback. The foot force varies, as with the x_{body} , during the vertical motion, but steadies once the movement is finished. Even when foot 3 is exerting a horizontal force against the ladder, as occurs after five seconds, the horizontal force from foot 2 stays very close to the desired force. This demonstrates the capability to control two environmental interaction forces simultaneously. The force response exceeded the design goals.

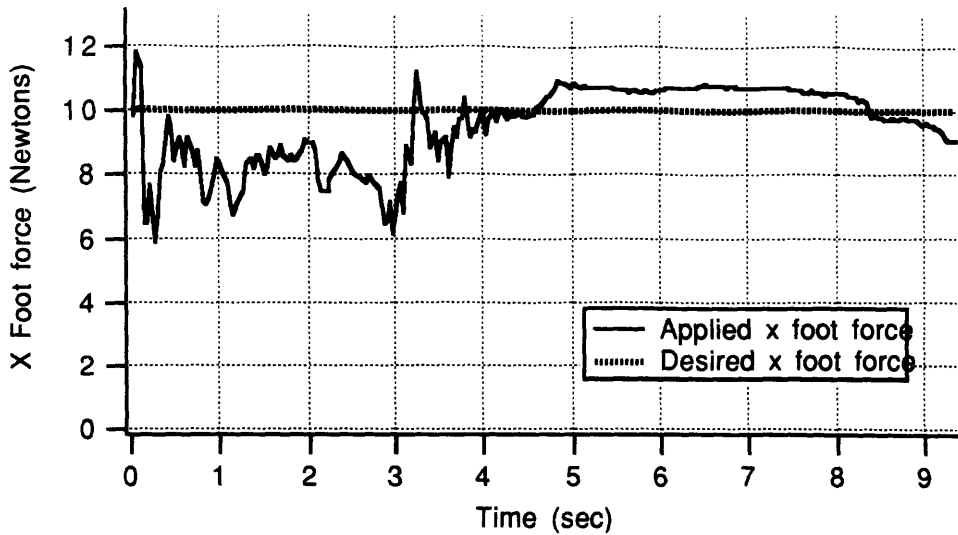


Fig. 31: x_2 Force for a pushup maneuver

The third foot contacts the ladder at nearly 4 seconds, and the growing error in x_3 shown in Figure 32 is actually a force being applied against the step corresponding to (error/k_{p3}) . The foot is commanded to apply this force on the step to insure a smooth transition to the next phase of the climbing gait. The y_3 positions, not shown here, are well behaved.

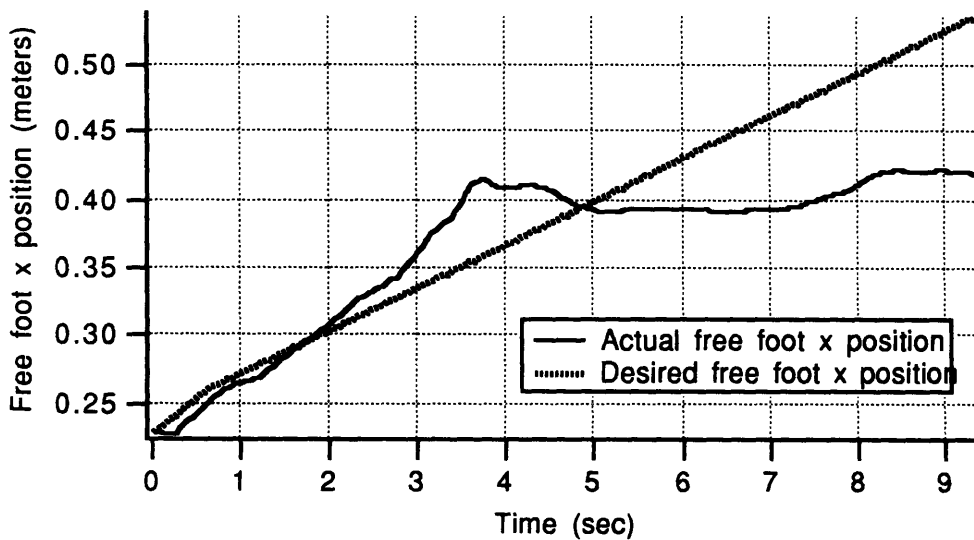


Fig. 32: x_3 location for a pushup maneuver

4.6.2: Data from a full climbing cycle

Figures 33 through 41 present the position data for one complete cycle of the climbing gait. The force data for the various feet was not collected. Figure 33 shows the commanded trajectory of all the control variables in Cartesian space, except for the rotation of the center body. This is intended to give a qualitative understanding of the gross movement performed, and the detailed data for the individual control variables is given later. When the commanded control variable for foot 2 or foot 3 is imbedded in the wall, a controlled force is being exerted on the environment.

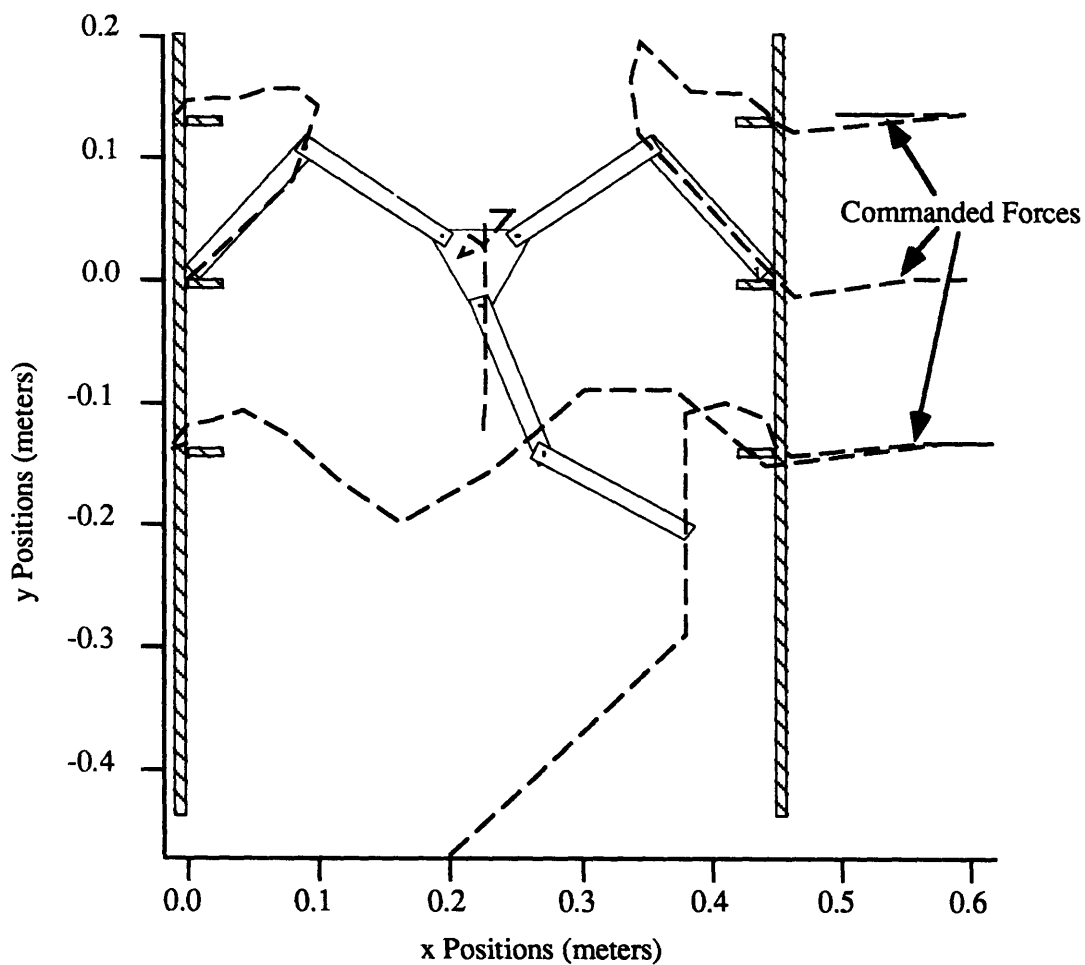


Fig. 33: Desired Cartesian movements for one gait cycle

Figure 34 shows the actual trajectory of all the control variables in Cartesian space, except for the rotation of the center body. Two important areas to note are the areas

where the joint limits were reached. Joint 1 for limb 1 and joint 4 for limb 4 hit hardware limits during the movement, and the feet were therefore unable to follow the commanded trajectory. However, the controller continued to function and completed the movement, demonstrating the robustness of CJTC.

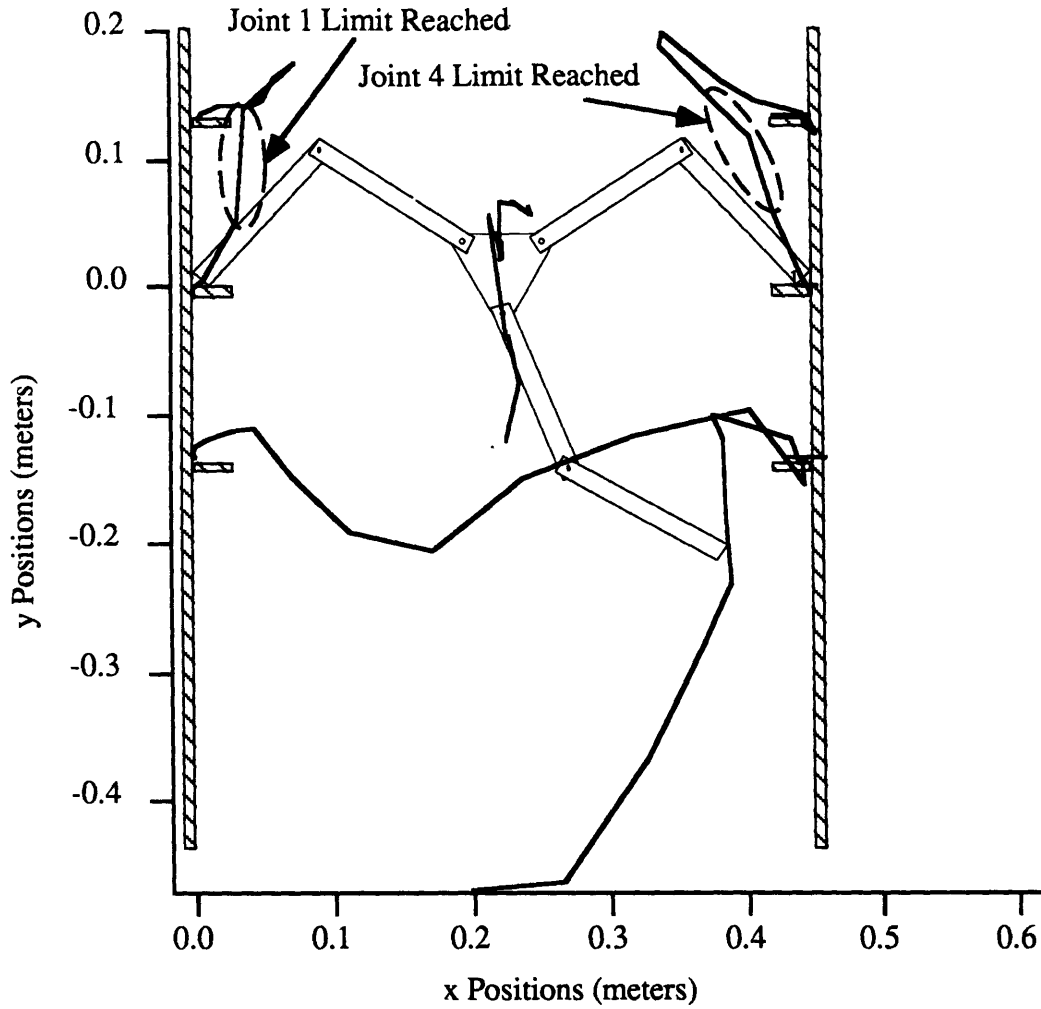


Fig. 34: Actual Cartesian movements for one gait cycle

Figure 35 shows the desired and actual positions of the main body for the climb. The errors are relatively small, and indicate good performance of the system. Figure 36 shows the orientation of the main body for the same climb. While the angle peaks as high as 8 degrees, it is still acceptable. The small spikes in the commanded position are artifacts of the planning algorithm.

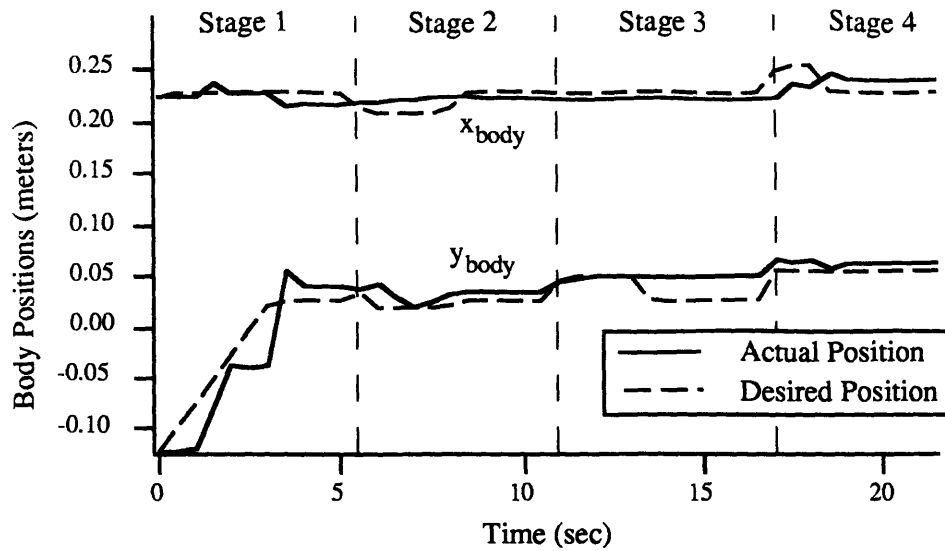


Fig. 35: Body movements for one gait cycle

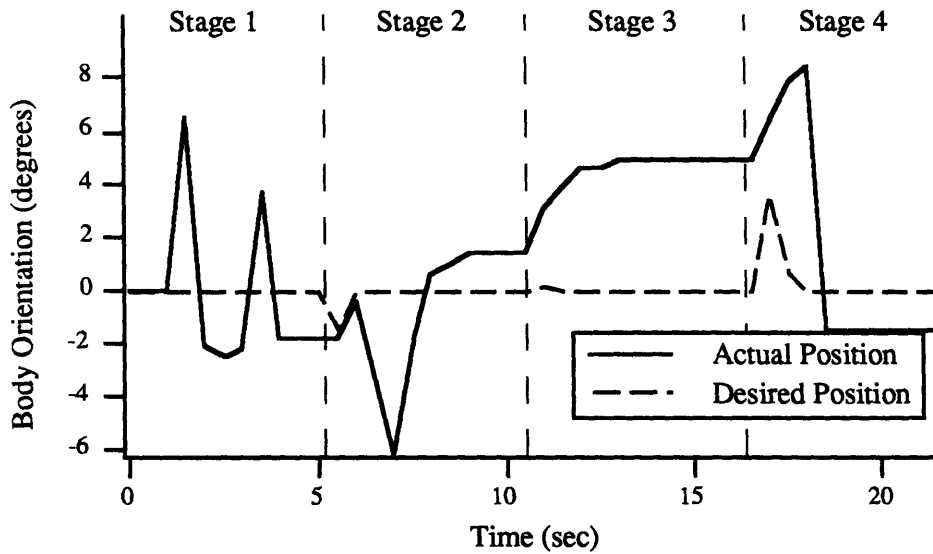


Fig. 36: Body orientations for one gait cycle

Figures 37 and 38 show the x and y positions of all the feet during the climb. The movements for the individual feet are given later in Figures 39 through 41. In Figure 37, the ladder step is located at $x=0.45\text{m}$. Even when the foot is pressing against the ladder, it still appears to move due to the backlash in the actuators and the compliance of the wheels. The commanded positions above 0.45 m indicate that forces are being commanded that are proportional to the error signal. In Figure 38, the steps are located at -0.135m , 0.0m and $+0.135\text{m}$. As can be clearly seen, the tracking for both the x and y of the feet is generally very accurate.

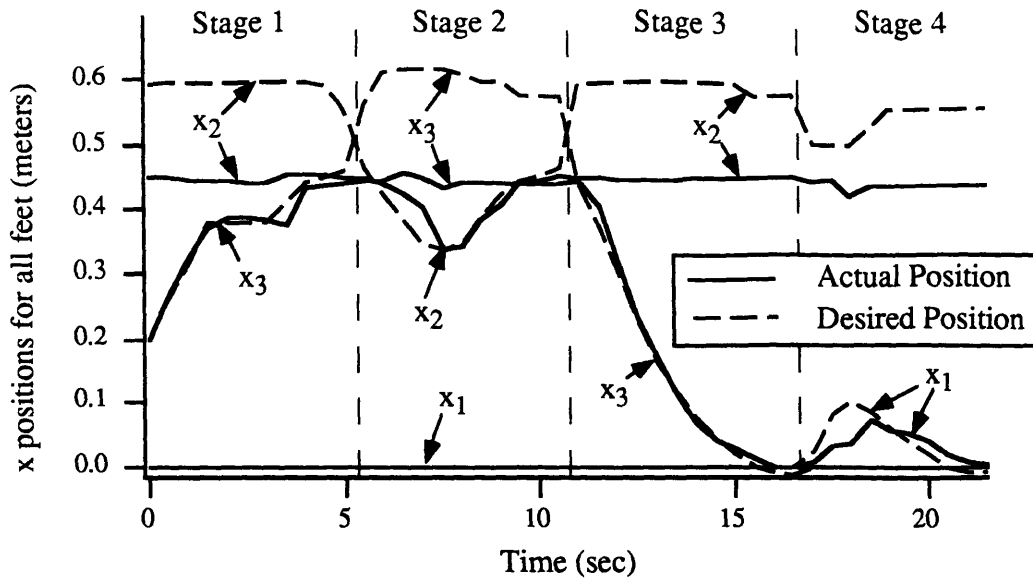


Fig. 37: x positions for all the feet for one gait cycle

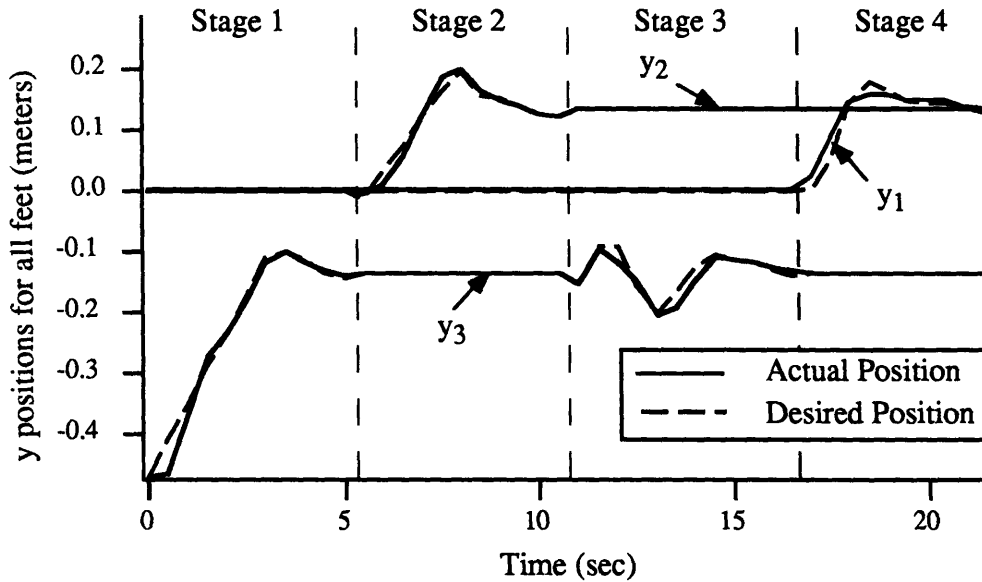


Fig. 38: y positions for all the feet for one gait cycle

Figure 39 shows the position data for foot 1. The majority of the time it sits on one rung, and only moves in Stage Four. Again, note the region where joint 1 was at its limit of -117° , and the commanded movement was unreachable. Even though it was unable to follow the x direction trajectory, it still continued to closely track the y direction trajectory.

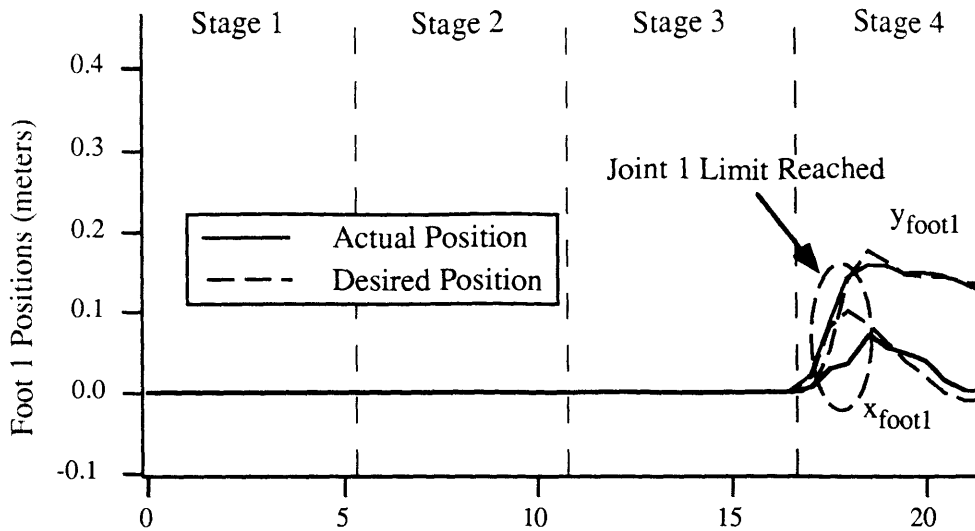


Fig. 39: Foot 1 position vs. time for one gait cycle

Figure 40 shows the position data for foot 2. In Stages 1,3 and 4, it is applying a force in the x-direction against the rungs that is equal to 100 N/m times the error signal. The rungs are located at $x = 0.45 \text{ m}$, and $y = 0$ and $y = 0.13 \text{ m}$. The small variations in the x position of the foot while it is pressed against the rungs are due to backlash in the gears and compliance in the environment. Note the region in Stage 2 where joint 4 was at its limit of -117° , and the commanded movement was unreachable. Like foot 1, even though foot 2 was unable to follow the x direction trajectory, it still continued to closely track the y direction trajectory.

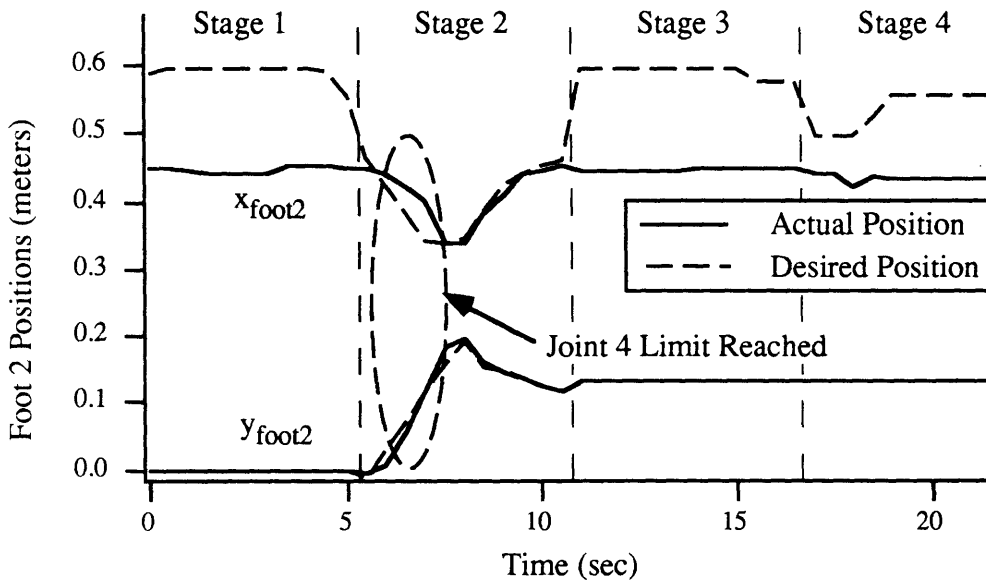


Fig. 40: Foot 2 position vs. time for one gait cycle

Figure 41 shows the position data for foot 3. In Stage 2 it is applying a controlled force in the x-direction against the rung that is equal to 100 N/m times the error signal. The rung is located at $x = 0.45 \text{ m}$ and $y = -0.13 \text{ m}$. The small variations in the x position of the foot while it is pressed against the rungs are due to backlash in the gears and compliance in the environment. In Stage 4 it is resting on a rung located at $x = 0.0 \text{ m}$ and $y = -0.13 \text{ m}$. At all times, foot 3 closely tracks the desired trajectory.

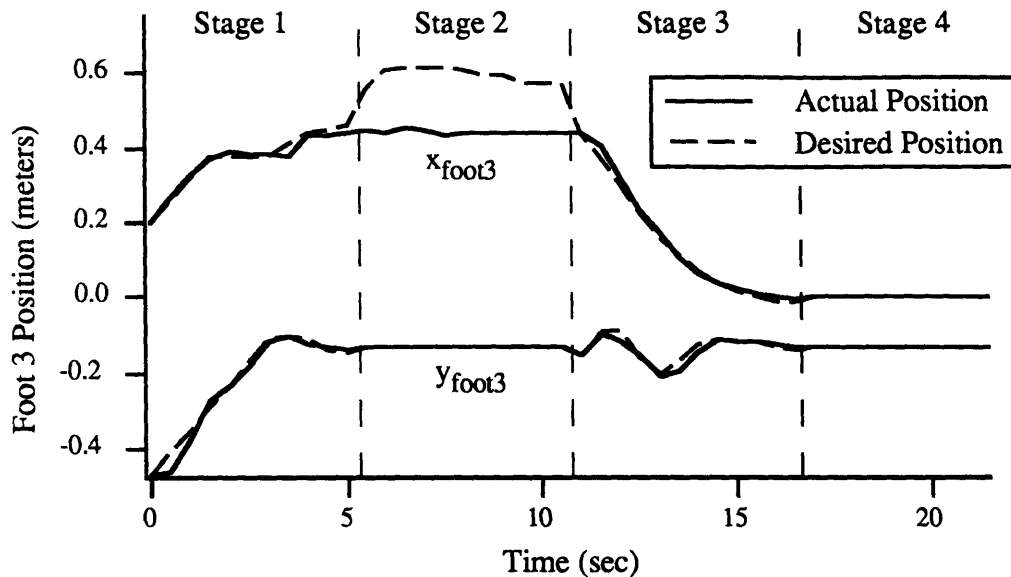


Fig. 41: Foot 3 position vs. time for one gait cycle

Looking at the data for a full climb, it is clear that the controller performed well, tracking the commanded trajectory. Even when joint limits were reached, the controller still continued to function and track the trajectories of control variables that it was physically capable of following. Even though force data was not collected it is assumed that the force was also well controlled.

5: Summary and Conclusions

The Coordinated Jacobian Transpose Control proposed is a viable method for controlling multiple control variables for both position and force of multilimbed robotic systems in a unified and coordinated manner. One of its advantages is that it is relatively easy to implement and can be interfaced with higher level planners and controllers in a straightforward manner. Also, it is computationally inexpensive and can be run on low capability processors. The control variables that can be controlled using CJTC are not restricted to positions of the system. They may be other differentiable functions of the joint variables, giving the system the ability to control important functions of the system in a simple fashion. Both mobility and manipulation can be controlled in this fashion. A methodology called the Extended Mobility Analysis provides a method for choosing an admissible set of control variables that will not overconstrain the system. Linear analysis and experimental studies of a three legged climbing robot show that the approach provides a stable and effective control strategy for both mobility and manipulation for some mobile multilimbed systems. Good performance was demonstrated experimentally even though only kinematics and gravity forces were taken into account.

6: References

- ¹Argaez, D.A., *An Analytical and Experimental Study of the Simultaneous Control of Motion and Force of a Climbing Robot*, M.S. Thesis, ME Dept., MIT, May 1993.
- ²Gradetsky, V., Rachkov, M., Uljanov, S., Nandi, G., "Robots for Cleaning and Decontamination of Building Construction," *8th International Symposium on Automation and Robotics in Construction*, Stuttgart, Germany, 3-5 June 1991.
- ³Meieran, H., "Frequent Incidents Increase Robot Potential," *HAZMAT World*, 2(9), September 1989, pp. 70-73.
- ⁴Nandi, G., Dwivedi, S., Lyons, D., "Climbing Robots for Decontamination of Nuclear Energy Producing Sites," *FAIM 1993 Conference*, Ireland, June 28-30 1993
- ⁵Potemkin, E., Astafurov, P., Osipov, A., Malenkov, M., Mishkinyuk, V., Sologub, P., "Remote Controlled Robots for Repair and Recovery in the Zones of High Radiation Levels," *Proceedings of the 1992 IEEE International Conference on Robotics and Automation*, Nice, France, May 1992, pp. 80-82
- ⁶Shaffer, G., Stentz, A., "A Robotic System for Underground Coal Mining," *Proceedings of the 1992 IEEE International Conference on Robotics and Automation*, Nice, France, May 1992, pp. 633-638
- ⁷Stone, H., Edmonds, G., "Hazbot: A Hazardous Materials Emergency Response Mobile Robot," *Proceedings of the 1992 IEEE International Conference on Robotics and Automation*, Nice, France, May 1992 pp. 67-73
- ⁸Woodbury, R., "Exploring the Ocean's Frontiers: Robots and Miniature Submarines take Oil Drillers to New Depths," *Time*, December 17, 1990.
- ⁹Harmon, S., "A Report on the NATO Workshop on Mobile Robot Implementation," *Proceedings of the 1988 IEEE International Conference on Robotics and Automation*, Philadelphia, PA, April 1988, pp. 604-610
- ¹⁰Meieran, H., Gelhaus, F., "Mobile Robots Designed for Hazardous Environments," *Robotics Engineering*, Vol. 8, March 1986, pp. 10-16

¹¹ Raibert, M., Brown, H., Chepponis, M., "Experiments in Balance with a 3D One-Legged Hopping Machine," *The International Journal of Robotics Research*, Vol. 3, No. 2, 1986, pp. 75-92

¹²Brooks, R. A. and Flynn, A. M., "Rover on a Chip," *Aerospace America*, Vol. 27, No. 10 Oct 1989, pp. 27-36

¹³ Pugh, D., Ribble, E., Vohnout, V., Bihari, T., Walliser, T., Patterson, M., Waldron, K., "Technical Description of the Adaptive Suspension Vehicle," *The International Journal of Robotics Research*, Vol. 9, No. 2, April 1990, pp 24-42.

¹⁴Saito, F.; Fukuda, T.; Fumihito, A., "Swing and Locomotion Control for a Two-Link Brachiation Robot," *Control Systems*, Vol. 14, No. 1, February 1994, pp. 5-12

¹⁵Puttré, M., "Undaunted Dante readies for Inferno," *Mechanical Engineering*, December 1993, pp. 58-59

¹⁶Bares, J.; Hebert, M.; Kanade, T.; "AMBLER, an Autonomous Rover for Planetary Exploration," *Computer*, Vol. 22, June 1989, pp. 18-26

¹⁷S.M. Song and K.J. Waldron, *Machines that Walk: The Adaptive Suspension Vehicle*, MIT Press, October 1988.

¹⁸Gorinevsky, D., Shneider, A., "Force Control in Locomotion of Legged Vehicles over Rigid and Soft Surfaces," *The International Journal of Robotics Research*, Vol. 9, No. 2, April 1990, pp. 4-23

¹⁹McGhee, R., Iswandhi, G., "Adaptive Locomotion of a Multilegged Robot over Rough Terrain," *IEEE Transactions on Systems. Man Cybernetics*, Vol. 9, No. 4, pp 176-182

²⁰Sutherland, I., Ullner, M., "Footprints in the Asphalt," *The International Journal of Robotics Research*, Vol. 3, No. 2, 1984, pp. 29-36

²¹Brooks, R., "A Robot that Walks : Emergent Behaviors from a Carefully Evolved Network," *Proceedings of the 1989 IEEE International Conference on Robotics and Automation*, Scottsdale, USA, May 1989, pp. 692

-
- ²²Lee, T., Shih, C., "Real Time Computer Control of a Quadruped Walking Robot," *Journal of Dynamic Systems, Measurement, and Control*, Vol. 108, December 1986, pp. 346-354
- ²³Hirose, S., Masui, T., Kikuchi, H., "Titan III: A Quadruped Walking Vehicle," *Proceedings of the 2nd ISSR Symposium*, Tokyo, Japan, 1984, pp. 247-253
- ²⁴Luk, B., Collie, A., Bingsley, J., "Robug II: An Intelligent Wall Climbing Robot," *Proceedings of the 1991 IEEE International Conference on Robotics and Automation*, Sacramento, CA, April 1991, pp. 2342-2347
- ²⁵Neubauer, W., "Locomotion with Articulated Legs in Pipes or Ducts," *Robotics and Autonomous Systems*, Vol. 11, 1993, pp. 163-169
- ²⁶Gradetsky, V. and Rachkov, M., "Wall Climbing Robot and Its Applications for Building Construction," *Mechanical Systems Engineering*, 1990, pp. 225-231
- ²⁷Nagakuba, A. and Hirose, S., "Walking and Running of the Quadruped Wall-Climbing Robot," *Proceedings of the 1994 IEEE International Conference on Robotics and Automation*, San Diego, Vol. 2, May, 1994, pp. 1005-1013
- ²⁸Byrd, J.S., and De Vries, K.R., "Six-legged Telerobot for Nuclear Applications Development," *The International Journal of Robotics Research*, Vol. 9, No. 2, April 1990, pp. 43-52
- ²⁹Foster-Miller, Inc., 350 Second Ave., Waltham, Massachusetts, 02154-1196
- ³⁰Klein, C. A.; Olson, K. M. and Pugh, D. R., "Use of Force and Attitude Sensors for Locomotion of a Legged Vehicle", *International Journal of Robotics Research*, Vol. 2, No. 2, 1983, pp. 3-17
- ³¹Gardner, J., Srinivasan, K., Waldron, K., "Closed Loop Trajectory Control of Walking Machines," *Robotica*, Vol. 8, 1990, pp. 13-22
- ³²Gardner, J., "Force Distribution in Walking Machines over Rough Terrain," *Journal of Dynamic Systems, Measurement, and Control*, Vol. 113, December 1991, pp. 754-758

-
- ³³Gardner, J., Srinivasan, K., Waldron, K., "A Solution for the Force Distribution Problem in Redundantly Actuated Closed Kinematic Chains," *Journal of Dynamic Systems, Measurement, and Control*, Vol. 112, September 1990, pp. 523-526
- ³⁴Khatib, O., "Motion/Force Redundancy of Manipulators," *American Symposium on Flexible Automation*, Kyoto, Japan, 1990
- ³⁵Raibert, M.H. and Craig, J. J., "Hybrid Position/Force Control of Manipulators", *Journal of Dynamic Systems, Measurement and Control*, June 1981, pp. 126-133
- ³⁶Yoshikawa, T. and Zheng, X., "Coordinated Dynamic Hybrid Position/Force Control for Multiple Robot Manipulators Handling One Constrained Object," *The International Journal of Robotics Research*, Vol. 12, No. 3, MIT, 1993, pp. 219-230
- ³⁷Asada, H and Slotine, J.-J. E., *Robot Analysis and Control*, Wiley-Interscience, 1986
- ³⁸Hogan, N., "Impedance Control: An Approach to Manipulation: Part I--Theory, Part II--Implementation, Part III--Applications," *Journal of Dynamic Systems, Measurement and Controls*, March 1985, pp. 1-24
- ³⁹Hogan, N., "Impedance Control of Robots with Harmonic Drive Systems," *Proceedings of the 1991 American Control Conference*, Boston, MA, June 1991
- ⁴⁰Schneider, S.A. and Cannon, R. H. Jr., "Object Manipulation Control for Cooperative Manipulation: Theory and Experimental Results," *IEEE International Conference on Robotics and Automation*, Vol. 8, No. 3, June 1992, pp. 383-394
- ⁴¹Schneider, S.A. and Cannon, R. H. Jr.; "Experimental Object-Level Strategic Control with Cooperating Manipulators," *International Journal of Robotics Research*, Vol. 12, No. 4, August 1993, pp 338-350
- ⁴²Mills, J., Lokhorst, D., "Stability and Control of Robotic Manipulators During Contact/Noncontact Task Transition," *IEEE Transactions on Robotics and Automation*, Vol. 9, No. 3, June 1993, pp. 335-345
- ⁴³Papadopoulos E. and Dubowsky S., "On the Nature of Control Algorithms for Free-Floating Space Manipulators," *IEEE Transactions on Robotics and Automation*, Vol. 7, No. 6, December 1991, pp. 750-758

⁴⁴Hootsman, N.A.M., *Motion Control of Manipulators on Mobile Vehicles*, Ph.D. Thesis, ME Dept., MIT, January 1992

⁴⁵ Hootsmans, N. A. M. and Dubowsky, S., "Control of Mobile Manipulators Including Vehicle Dynamic Characteristics," *Proceedings of the Fourth Topical Meeting on Robotics and Remote Systems*, February 24-28, 1991.

⁴⁶Seraji, H., "Configuration Control of Redundant Manipulators: Theory and Implementation," *IEEE Transactions on Robotics and Automation*, Vol. 5, No. 4, August 1989, pp. 472-490

⁴⁷Seraji, H., "An On-line Approach to Coordinated Mobility and Manipulation," *Proceedings of the 1993 International Conference on Robotics and Automation*, pp 28-33

⁴⁸Lim, D.; Lee, T. and Seraji, H., "A Real-Time Control System for a Mobile Dexterous 7 DOF Arm," *Proceedings of the 1994 IEEE International Conference on Robotics and Automation*, San Diego, Vol. 2, May, 1994, pp. 1188-1193

⁴⁹Papadopoulos, E. and Dubowsky, S., "Failure Recovery Control For Space Robotic Systems," *Proceedings of the 1991 American Control Conference*, Boston, MA, June 26-28, 1991. Invited.

⁵⁰Craig, J. J., *Introduction to Robotics Mechanics and Control, second edition*, Addison Wesley, 1989

⁵¹Morel, G., *Programmation et adaptation de l'impédance de manipulateurs au contact*, Ph.D. Thesis, L'Universite Pierre et Marie Curie, June 1994

⁵²Duffy, J., *Analysis of Mechanisms and Robot Manipulators*, Edwards Arnold Ltd., London, Great Britain, 1980

⁵³Sandor, G.; Erdman, A., *Advanced Mechanism Design: Analysis and Synthesis, Volume 2*, Prentice-Hall, Inc., New Jersey, 1984

⁵⁴Escap Motion Systems Catalog, 1991. Portescap US Inc., 36 Central Ave., Hauppauge, NY, 11788

⁵⁵Delta Tau Data Systems, Inc., 21119 Osborne St., Canoga Park, CA, 91304

Appendix A: LIBRA Jacobian Equations

Derivation of the Jacobian for the LIBRA

$$x_{body} = 2L \cdot \cos(\phi) + 2L \cdot \cos(\phi + \theta_1) + r \cdot \cos(\phi + \theta_1 + \theta_2 - \frac{\pi}{6})$$

$$y_{body} = 2L \cdot \sin(\phi) + 2L \cdot \sin(\phi + \theta_1) + r \cdot \sin(\phi + \theta_1 + \theta_2 - \frac{\pi}{6})$$

$$\theta_{body} = \phi + \theta_1 + \theta_2$$

$$x_{foot} = 2L[\cos(\phi) + \cos(\phi + \theta_1) + \cos(\phi + \theta_1 + \theta_2) + \cos(\phi + \theta_1 + \theta_2 + \theta_3 + \theta_4)] + N \cos(\phi + \theta_1 + \theta_2)$$

$$x_{free} = x_{body} + r \cdot \sin(\phi + \theta_1 + \theta_2) + 2L \cdot \sin(\phi + \theta_1 + \theta_2 + \theta_5) + 2L \cdot \sin(\phi + \theta_1 + \theta_2 + \theta_5)$$

$$y_{free} = y_{body} - r \cdot \cos(\phi + \theta_1 + \theta_2) - 2L \cdot \cos(\phi + \theta_1 + \theta_2 + \theta_5) - 2L \cdot \cos(\phi + \theta_1 + \theta_2 + \theta_5)$$

to derive phi using the y position constraint on foot 2:

$$y = \sin(\phi)[2L + 2L \cdot c_1 + 2L \cdot c_{123} + 2L \cdot c_{1234} + N \cdot c_{12}] + \cos(\phi)[2L \cdot s_1 + 2L \cdot s_{123} + 2L \cdot s_{1234} + N \cdot s_{12}]$$

$$\text{let } k_1 = 2L + 2L \cdot c_1 + 2L \cdot c_{123} + 2L \cdot c_{1234} + N \cdot c_{12}$$

$$k_2 = 2L \cdot s_1 + 2L \cdot s_{123} + 2L \cdot s_{1234} + N \cdot s_{12}$$

$$y = \sin(\phi) \cdot k_1 + \cos(\phi) \cdot k_2 = \frac{2u}{1+u^2} \cdot k_1 + \frac{1-u^2}{1+u^2} \cdot k_2$$

$$u = \frac{k_1 + \sqrt{k_1^2 + k_2^2 - y^2}}{y + k_2}$$

$$\phi = 2 \cdot \tan^{-1} \left(\frac{k_1 + \sqrt{k_1^2 + k_2^2 - y^2}}{y + k_2} \right)$$

let :

$$U = \begin{bmatrix} x_{body} \\ y_{body} \\ \theta_{body} \\ x_{foot} \\ x_{free} \\ y_{free} \end{bmatrix} \quad \Theta = \begin{bmatrix} \theta_1 \\ \theta_2 \\ \theta_3 \\ \theta_4 \\ \theta_5 \\ \theta_6 \end{bmatrix} \quad T = \begin{bmatrix} \tau_1 \\ \tau_2 \\ \tau_3 \\ \tau_4 \\ \tau_5 \\ \tau_6 \end{bmatrix}$$

$$Jacobian = \frac{\delta U}{\delta \Theta}, \quad T = J^T F_{imp}$$

Terms of the Jacobian:

$$J_{11} = \frac{\delta x_{body}}{\delta \theta_1} = (-2L \cdot s_\phi - 2L \cdot s_{\phi 1} - r \cdot s_{\phi 12 - \pi/6}) \left(1 + \frac{d\phi}{d\theta_1} \right) + 2L \cdot s_\phi$$

$$J_{12} = \frac{\delta x_{body}}{\delta \theta_2} = (-2L \cdot s_\phi - 2L \cdot s_{\phi 1} - r \cdot s_{\phi 12 - \pi/6}) \left(\frac{d\phi}{d\theta_2} \right) - r \cdot s_{\phi 12 - \pi/6}$$

$$J_{13} = \frac{\delta x_{body}}{\delta \theta_3} = (-2L \cdot s_\phi - 2L \cdot s_{\phi 1} - r \cdot s_{\phi 12 - \pi/6}) \left(\frac{d\phi}{d\theta_3} \right)$$

$$J_{14} = \frac{\delta x_{body}}{\delta \theta_4} = (-2L \cdot s_\phi - 2L \cdot s_{\phi 1} - r \cdot s_{\phi 12 - \pi/6}) \left(\frac{d\phi}{d\theta_4} \right)$$

$$J_{15} = 0$$

$$J_{16} = 0$$

$$J_{21} = \frac{\delta y_{body}}{\delta \theta_1} = (2L \cdot c_\phi + 2L \cdot c_{\phi 1} + r \cdot c_{\phi 12 - \pi/6}) \left(1 + \frac{d\phi}{d\theta_1} \right) - 2L \cdot c_\phi$$

$$J_{22} = \frac{\delta y_{body}}{\delta \theta_2} = (2L \cdot c_\phi + 2L \cdot c_{\phi 1} + r \cdot c_{\phi 12 - \pi/6}) \left(\frac{d\phi}{d\theta_2} \right) + r \cdot c_{\phi 12 - \pi/6}$$

$$J_{23} = \frac{\delta y_{body}}{\delta \theta_3} = (2L \cdot c_\phi + 2L \cdot c_{\phi 1} + r \cdot c_{\phi 12 - \pi/6}) \left(\frac{d\phi}{d\theta_3} \right)$$

$$J_{24} = \frac{\delta y_{body}}{\delta \theta_4} = (2L \cdot c_\phi + 2L \cdot c_{\phi 1} + r \cdot c_{\phi 12 - \pi/6}) \left(\frac{d\phi}{d\theta_4} \right)$$

$$J_{25} = 0$$

$$J_{26} = 0$$

$$J_{31} = \frac{\delta\theta_{body}}{\delta\theta_1} = 1 + \frac{d\phi}{d\theta_1}$$

$$J_{32} = \frac{\delta\theta_{body}}{\delta\theta_2} = 1 + \frac{d\phi}{d\theta_2}$$

$$J_{33} = \frac{\delta\theta_{body}}{\delta\theta_3} = \frac{d\phi}{d\theta_3}$$

$$J_{34} = \frac{\delta\theta_{body}}{\delta\theta_4} = \frac{d\phi}{d\theta_4}$$

$$J_{35} = \frac{\delta\theta_{body}}{\delta\theta_5} = 0$$

$$J_{36} = \frac{\delta\theta_{body}}{\delta\theta_6} = 0$$

$$J_{41} = \frac{\delta x_{foot}}{\delta\theta_1} = \left(-2L \cdot s_\phi - 2L \cdot s_{\phi_1} - 2L \cdot s_{\phi_{123}} - 2L \cdot s_{\phi_{1234}} - N \cdot s_{\phi_{12}}\right) \left(1 + \frac{d\phi}{d\theta_1}\right) + 2L \cdot s_\phi$$

$$J_{42} = \frac{\delta x_{foot}}{\delta\theta_2} = \left(-2L \cdot s_\phi - 2L \cdot s_{\phi_1} - 2L \cdot s_{\phi_{123}} - 2L \cdot s_{\phi_{1234}} - N \cdot s_{\phi_{12}}\right) \left(1 + \frac{d\phi}{d\theta_2}\right) + 2L \cdot s_\phi +$$

$$J_{43} = \frac{\delta x_{foot}}{\delta\theta_3} = \left(-2L \cdot s_\phi - 2L \cdot s_{\phi_1} - 2L \cdot s_{\phi_{123}} - 2L \cdot s_{\phi_{1234}} - N \cdot s_{\phi_{12}}\right) \left(\frac{d\phi}{d\theta_3}\right) - 2L \cdot s_{\phi_{123}} -$$

$$J_{44} = \frac{\delta x_{foot}}{\delta\theta_4} = \left(-2L \cdot s_\phi - 2L \cdot s_{\phi_1} - 2L \cdot s_{\phi_{123}} - 2L \cdot s_{\phi_{1234}} - N \cdot s_{\phi_{12}}\right) \left(\frac{d\phi}{d\theta_4}\right) - 2L \cdot s_{\phi_{1234}}$$

$$J_{45} = 0$$

$$J_{46} = 0$$

$$J_{51} = \frac{\delta x_{free}}{\delta \theta_1} = J_{11} + (r \cdot c_{\phi 12} + 2L \cdot c_{\phi 125} + 2L \cdot c_{\phi 1256}) \left(1 + \frac{d\phi}{d\theta_1} \right)$$

$$J_{52} = \frac{\delta x_{free}}{\delta \theta_2} = J_{12} + (r \cdot c_{\phi 12} + 2L \cdot c_{\phi 125} + 2L \cdot c_{\phi 1256}) \left(1 + \frac{d\phi}{d\theta_2} \right)$$

$$J_{53} = \frac{\delta x_{free}}{\delta \theta_3} = J_{13} + (r \cdot c_{\phi 12} + 2L \cdot c_{\phi 125} + 2L \cdot c_{\phi 1256}) \left(\frac{d\phi}{d\theta_3} \right)$$

$$J_{54} = \frac{\delta x_{free}}{\delta \theta_4} = J_{14} + (r \cdot c_{\phi 12} + 2L \cdot c_{\phi 125} + 2L \cdot c_{\phi 1256}) \left(\frac{d\phi}{d\theta_4} \right)$$

$$J_{55} = \frac{\delta x_{free}}{\delta \theta_5} = 2L \cdot c_{\phi 125} + 2L \cdot c_{\phi 1256}$$

$$J_{56} = \frac{\delta x_{free}}{\delta \theta_6} = 2L \cdot c_{\phi 1256}$$

$$J_{61} = \frac{\delta y_{free}}{\delta \theta_1} = J_{21} + (r \cdot s_{\phi 12} + 2L \cdot s_{\phi 125} + 2L \cdot s_{\phi 1256}) \left(1 + \frac{d\phi}{d\theta_1} \right)$$

$$J_{62} = \frac{\delta y_{free}}{\delta \theta_2} = J_{22} + (r \cdot s_{\phi 12} + 2L \cdot s_{\phi 125} + 2L \cdot s_{\phi 1256}) \left(1 + \frac{d\phi}{d\theta_2} \right)$$

$$J_{63} = \frac{\delta y_{free}}{\delta \theta_3} = J_{23} + (r \cdot s_{\phi 12} + 2L \cdot s_{\phi 125} + 2L \cdot s_{\phi 1256}) \left(\frac{d\phi}{d\theta_3} \right)$$

$$J_{64} = \frac{\delta y_{free}}{\delta \theta_4} = J_{24} + (r \cdot s_{\phi 12} + 2L \cdot s_{\phi 125} + 2L \cdot s_{\phi 1256}) \left(\frac{d\phi}{d\theta_4} \right)$$

$$J_{65} = \frac{\delta y_{free}}{\delta \theta_5} = 2L \cdot s_{\phi 125} + 2L \cdot s_{\phi 1256}$$

$$J_{66} = \frac{\delta y_{free}}{\delta \theta_6} = 2L \cdot s_{\phi 1256}$$

$$\frac{d\phi}{d\theta_i} = \frac{2(y + k_2)}{(y + k_2)^2 + \left(k_1 + \sqrt{k_1^2 + k_2^2 - y^2} \right)^2} \cdot \left(\frac{dk_1}{d\theta_i} + \frac{k_1 \frac{dk_1}{d\theta_i} + k_2 \frac{dk_2}{d\theta_i}}{\sqrt{k_1^2 + k_2^2 - y^2}} - \frac{\left(k_1 + \sqrt{k_1^2 + k_2^2 - y^2} \right)}{(y + k_2)} \right)$$

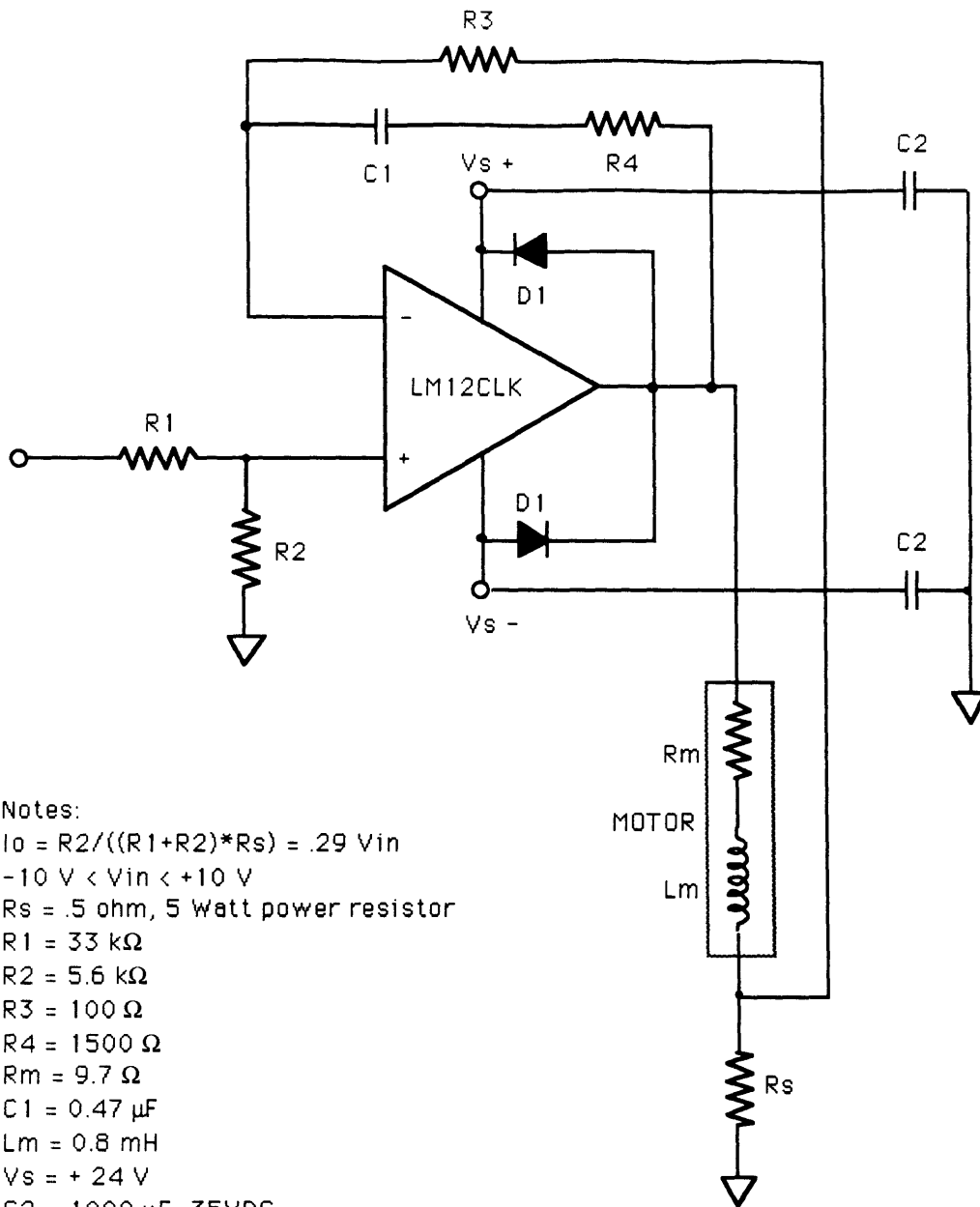
Appendix B: Power Amplifiers

Voltage to current amplifiers were custom built for the LIBRA project. They are powered by two Zytex 24 volt power supplies ¹ hooked in parallel to provide a driving voltage range from - 24 volts to + 24 volts, and an amperage of up to 6 amps, continuous. The hearts of the amplifiers are LM12CLK linear power operational amplifiers, manufactured by National Semiconductor ². Linear amplifiers, rather than pulse width modulated amplifiers are used for their simplicity, even though PWM amplifiers would be much more power efficient. Trimpots are used to tune the amplifiers to a uniform gain. The voltage offset is adjusted from the PMAC. Unfortunately, the PMAC tends to drift in its output signal, requiring periodic testing and adjustment every month.

Voltage to current amplifiers are used to make the motors behave as torque servos. The characteristic equation of the amplifier-motor circuit shown in Figure B1 is:

$$\frac{i_m}{V_{in}} = \frac{(2 \cdot R_s + R_3 + R_4) \cdot s + \frac{1}{C_1}}{(R_3 + R_s) \cdot L_m \cdot s^2 + [R_s \cdot (R_4 + R_m - R_3) + R_m \cdot R_3] \cdot s + \frac{R_s}{C_1}}$$

Using the appropriate values for the various elements, the time constant of the amplifier-motor system is 1.52 microseconds, resulting in a bandwidth of 656 Hz. Since this is much higher than the bandwidth of the controller, for the purposes of this thesis the amplifier-motor system can be considered to be an ideal torque servo system. It is important to note that this does not include the damping effects of the friction in the motor gearheads.



Notes:

$$I_o = R_2 / ((R_1 + R_2) * R_s) = .29 V_{in}$$

$$-10 V < V_{in} < +10 V$$

$R_s = .5 \text{ ohm}$, 5 Watt power resistor

$R_1 = 33 \text{ k}\Omega$

$R_2 = 5.6 \text{ k}\Omega$

$R_3 = 100 \Omega$

$R_4 = 1500 \Omega$

$R_m = 9.7 \Omega$

$C_1 = 0.47 \mu\text{F}$

$L_m = 0.8 \text{ mH}$

$V_s = +24 \text{ V}$

$C_2 = 1000 \mu\text{F}$, 35VDC

D1 = Harris A15A rectifiers

Heat sinks required

Fig. B1: Power amplifier schematic

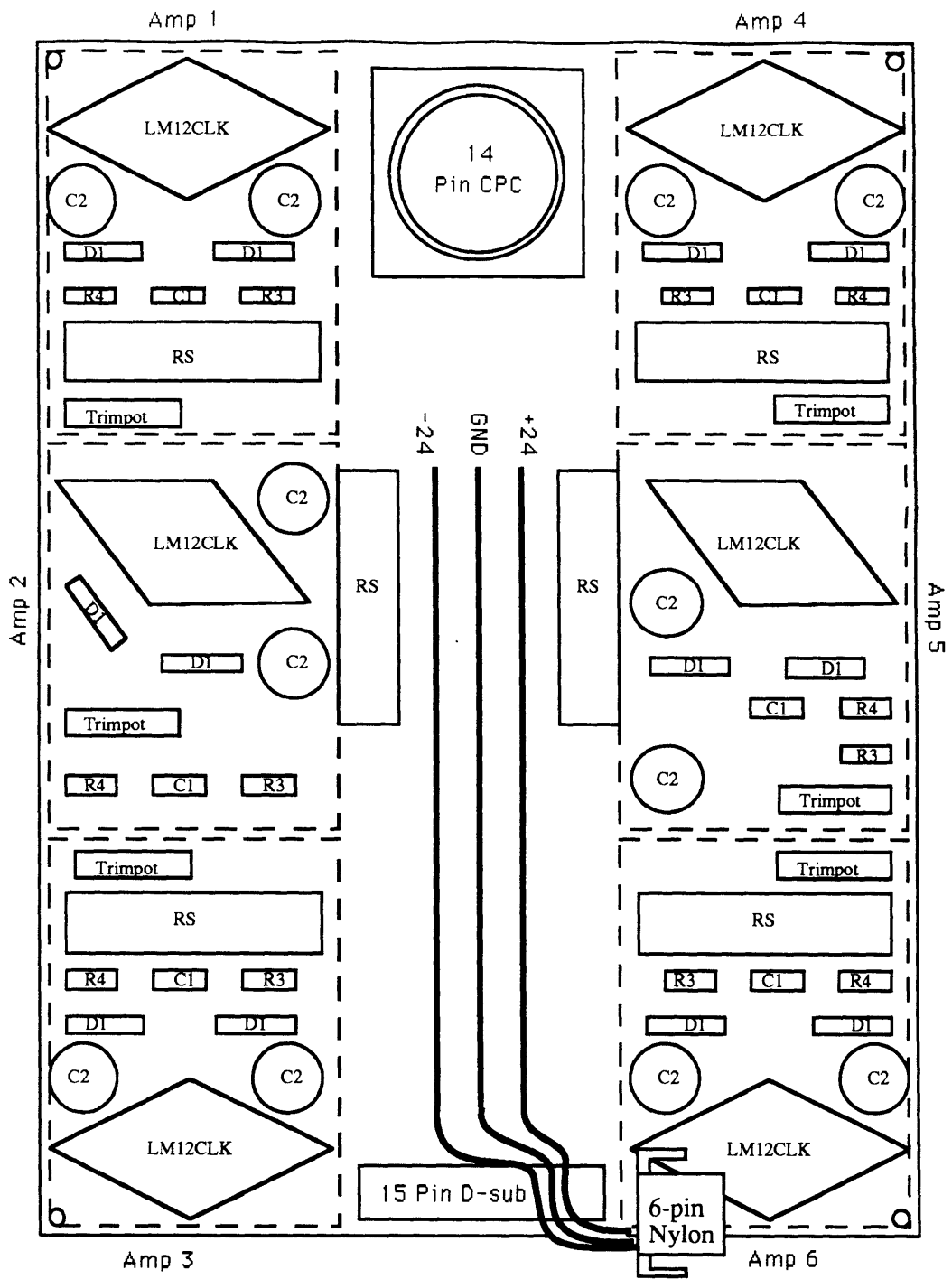


Fig. B2: Power Amplifier Card Layout

The parts list for the power amplifiers is included, in case another set of power amplifiers needs to be built or repairs effected on the current power amplifiers. The sources for the parts are C&H ¹, Gerber Electronics ³, Newark Electronics ⁴, Allied Electronics ⁵, the MIT Office of Lab Supplies and Radio Shack.

LIBRA Electronics Parts List

<u>Part No.</u>	<u>Quantity</u>	<u>Item</u>	<u>Price</u>	<u>Cost</u>
-----------------	-----------------	-------------	--------------	-------------

Power Supplies:

C&H - #PS8902	2	ZYTEC pwr sup.	51.50	103.00
---------------	---	----------------	-------	--------

Servo amp components:

Gerber

Clarostat VC-10-F 0.5 W	8	.5 W Power Res	2.21	17.68
National Semiconductor LM12CLK	7	Power Op Amp	25.40	177.80
Thermalloy 6016B	6	Heat Sinks	1.23	7.38
Harris A15A	14	Rectifier	0.60	8.40

Office of Lab Supplies

511116		Precision Res, 1/4W		
	10	5.6 kW	0.11	1.10
	10	33 KW	0.11	1.10
511115	10	100 W	0.16	1.60
504200	10	Cap, 0.47 mF, Tant.	0.48	4.80

Radio Shack

272-1018	15	1000mF bypass cap	1.59	23.85
276-1396	1	Perfboard	2.99	2.99

276-147	1	PC Board	3.79	3.79
271-343	9	10K trimmers	1.49	13.41

Connection components:

(1): 29 encoder lines from Ascender to the junction panel.

37 pin D-sub connectors, connected by a 37 line flat ribbon cable.

2 male ribbon connectors and 2 female receptacles required. A wire wrap rec. will be used on the junction panel, but the connector for the LIBRA has yet to be finalized.

Newark:

Stock No. 81F5186	2 req'd	rec	14.45	28.90
Stock No. 81F5025	3 req'd	ribbon plugs	6.73	20.19

(2): 12 motor lines from junction panel to ascender.

1 12 line cable, using reverse sex circular plastic connectors.

2 plugs are required for the cable, and 1 receptacle each for the junction panel and the Ascender. 14 pin connectors will be used.

Allied:

Stock No. 512-1172	3 req'd	plug	2.28	11.40
Stock No. 512-1173	4 req'd	rec	1.85	11.10
Stock No. 512-1210	1 req'd	100 pins	19.00	19.57
Stock No. 512-1215	1 req'd	100 sockets	22.00	22.94

(3): 3 power lines from junction panel to servo amps.

Heavy-duty nylon interlocking connectors.

Radio Shack:

274-152	1 req'd	male	1.69	1.69
274-155	1 req'd	female	1.69	1.69

(4): 6 PMAC control lines from junction panel to servo amps.

1 line, 15 pin D-sub connectors.

The cable will only need 1 connector, as the end coming from the junction panel will come directly off of the 50 pin PMAC connector. The other end of the cable will

terminate in a wire wrap 15 pin plug. A 15 pin wire wrap D-sub rec will be used on the servo mount board. Strain relief will be provided with a hood on the plug, and another hood on the 50 pin D-sub from the PMAC.

Newark:

Stock No. 81F5181	2 req'd	15 pin plug	7.24	14.48
Stock No. 81F5184	2 req'd	15 pin recep	8.51	17.02
Stock No. 46F2345	1 req'd	15 pin hood	3.38	3.38
Stock No. 46F2345	1 req'd	50 pin hood	6.11	6.11

(5): 12 motor lines from servo amps to junction panel.

1 12 line cable, using reverse sex circular plastic connectors.

1 plug is required for the cable, and 1 receptacle for the junction panel. The other side will be connected through terminal blocks. 14 pin connectors will be used.

Allied:

Stock No. 512-1172	2 req'd	plug	2.28	4.56
Stock No. 512-1173	2 req'd	rec	1.85	3.70

(6): 3 power lines from power supplies.

2 cables - one from each power supply.

The mate for the current connector in the power supply is very difficult to procure, and the connector will be replaced for ease of connection. Microphone connectors will be used.

Newark:

Stock No. 46F8554	5 req'd	Male	3.45	17.25
Stock No. 46F8556	5 req'd	Female	3.64	18.20

(7): PMAC to junction panel.

1 line using a 50 pin wire wrap D-sub will be used.

The connector and ribbon cable is in hand.

(8): Breakout Box to Motors.

6 2-pin nylon interlocking connectors will be used.

Radio Shack:

274-151	7 req'd	Pair	0.99	6.93
---------	---------	------	------	------

(9): Breakout Box to Encoders.

10-pin DIP connectors will be used

Newark:

Stock No. 46F730	12 req'd	male	2.96	35.52
------------------	----------	------	------	-------

CABLING:

100 Feet of 24AWG 12 wire cable

Newark:

Stock No. 44F3506WA	100 ft	6-pair cable	62.62	62.62
---------------------	--------	--------------	-------	-------

100 Feet of 37 line ribbon cable

Newark:

Stock No. 36F661WA	100 ft		80.38	80.38
--------------------	--------	--	-------	-------

20 Feet of 16AWG stranded 2 wire cable

Radio Shack:

278-1105	30 ft		4.99	4.99
----------	-------	--	------	------

1 AC power plug for power supplies (1 already in hand)

Radio Shack:

278-1257	1 req'd	6 foot cable	3.99	3.99
----------	---------	--------------	------	------

Total Cost:

=====
\$763.51

Appendix C: Gain Selection

The dynamic model was derived using Lagrange's equations. The equations are linearized about various positions, with the velocity equal to zero. This allows simplification of the equations. The friction in the gearheads, which is difficult to characterize, is not included in the dynamic model. This means that the analysis will show less damping than the actual experimental system.

The LIBRA system is analyzed using the model shown in Figure 24. The figure is repeated here for convenience:

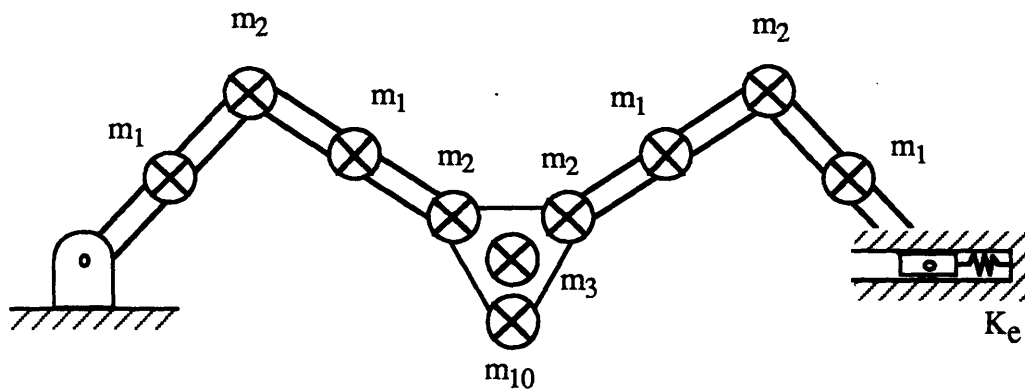


Fig. C1: Model of the LIBRA

The masses used are given as:

$$m_1 = 0.1960 \text{ kg}$$

$$m_2 = 0.3466 \text{ kg}$$

$$m_3 = 1.00 \text{ kg}$$

$$m_{10} = 1.09 \text{ kg}$$

$$K_e = 5837 \text{ N/m}$$

The length of each link is given as $2 \cdot L$, where L is specified as:

$$L = 0.078 \text{ m}$$

The distance from a motor mounted on the body to the center of body is given as:

$$r = 0.048 \text{ m}$$

The distance from a motor mounted on the body to another motor mounted on the body is given as:

$$N = 0.083 \text{ m}$$

The LIBRA positions (x_b , y_b , θ_b , x_2) are given by:

$$x_b = 2 \cdot L \cdot (\cos(\phi) + \cos(\phi + \theta_1)) + r \cdot \cos(\phi + \theta_1 + \theta_2 - \pi/6)$$

$$y_b = 2 \cdot L \cdot (\sin(\phi) + \sin(\phi + \theta_1)) + r \cdot \sin(\phi + \theta_1 + \theta_2 - \pi/6)$$

$$\theta_b = \phi + \theta_1 + \theta_2$$

$$x_2 = 2 \cdot L \cdot (\cos(\phi + \theta_1) + \cos(\phi + \theta_1) + \cos(\phi + \theta_1 + \theta_2 + \theta_3) + \cos(\phi + \theta_1 + \theta_2 + \theta_3 + \theta_4)) + N \cdot \cos(\phi + \theta_1 + \theta_2)$$

Define the inertia matrix M as:

$$M = \begin{bmatrix} c0 & c1 & c2 & c3 & c4 \\ d0 & d1 & d2 & d3 & d4 \\ e0 & e1 & e2 & e3 & e4 \\ f0 & f1 & f2 & f3 & f4 \\ g0 & g1 & g2 & g3 & g4 \end{bmatrix}$$

where:

$$c0 = 24 \cdot m_1 \cdot L^2 + 26 \cdot m_2 \cdot L^2 + 6 \cdot (m_3 + m_{10}) \cdot L^2 + m_3 \cdot r^2 + 2 \cdot (m_1 + m_2) \cdot N^2 + m_{10} \cdot N^2$$

$$c0 = c0 + L^2 \cdot \cos(2 \cdot \phi + \theta_1) \cdot (10 \cdot m_1 + 12 \cdot m_2 + 4 \cdot m_3 + 4 \cdot m_{10})$$

$$c0 = c0 + 2 \cdot m_3 \cdot L \cdot r \cdot (\cos(2 \cdot \phi + \theta_1 + \theta_2 - \pi/6) + \cos(2 \cdot \phi + 2 \cdot \theta_1 + \theta_2 - \pi/6))$$

$$c0 = c0 + 2 \cdot m_{10} \cdot L \cdot N \cdot (\cos(2 \cdot \phi + \theta_1 + \theta_2 - \pi/3) + \cos(2 \cdot \phi + 2 \cdot \theta_1 + \theta_2 - \pi/3))$$

$$c0 = c0 + 4 \cdot (m_1 + m_2) \cdot L \cdot N \cdot (\cos(2 \cdot \phi + \theta_1 + \theta_2) + \cos(2 \cdot \phi + 2 \cdot \theta_1 + \theta_2))$$

$$c0 = c0 + (6 \cdot m_1 + 4 \cdot m_2) \cdot L^2 \cdot (\cos(2 \cdot \phi + \theta_1 + \theta_2 + \theta_3) + \cos(2 \cdot \phi + 2 \cdot \theta_1 + \theta_2 + \theta_3))$$

$$c0 = c0 + (3 \cdot m_1 + 2 \cdot m_2) \cdot L \cdot N \cdot (\cos(2 \cdot \phi + 2 \cdot \theta_1 + 2 \cdot \theta_2 + \theta_3))$$

$$c0 = c0 + 2 \cdot m_1 \cdot L^2 \cdot (\cos(2 \cdot \phi + \theta_1 + \theta_2 + \theta_3 + \theta_4) + \cos(2 \cdot \phi + 2 \cdot \theta_1 + \theta_2 + \theta_3 + \theta_4) + \cos(2 \cdot \phi + 2 \cdot \theta_1 + 2 \cdot \theta_2 + 2 \cdot \theta_3 + \theta_4))$$

$$c0 = c0 + m_1 \cdot L \cdot N \cdot \cos(2 \cdot \phi + 2 \cdot \theta_1 + 2 \cdot \theta_2 + \theta_3 + \theta_4)$$

$$\begin{aligned}
c1 &= 15 \cdot m_1 \cdot L^2 + 16 \cdot m_2 \cdot L^2 + 4 \cdot (m_3 + m_{10}) \cdot L^2 + \\
&\quad (5 \cdot m_1 + 6 \cdot m_2 + 2 \cdot m_3 + 2 \cdot m_{10}) \cdot L^2 \cdot \cos(2\phi + \theta_1) \\
c1 &= c1 + m_3 \cdot r^2 + m_3 \cdot L \cdot r \cdot (\cos(2\phi + \theta_1 + \theta_2 - \pi/6) + 2 \cdot \cos(2\phi + 2\theta_1 + \theta_2 - \pi/6)) \\
c1 &= c1 + m_{10} \cdot N^2 + m_{10} \cdot L \cdot N \cdot (\cos(2\phi + \theta_1 + \theta_2 - \pi/3) + 2 \cdot \cos(2\phi + 2\theta_1 + \theta_2 - \pi/3)) \\
c1 &= c1 + 2 \cdot (m_1 + m_2) \cdot N^2 + 2 \cdot (m_1 + m_2) \cdot L \cdot N \cdot (\cos(2\phi + \theta_1 + \theta_2) + 2 \cdot \cos(2\phi + 2\theta_1 + \theta_2)) \\
c1 &= c1 + (3 \cdot m_1 + 2 \cdot m_2) \cdot L^2 \cdot (\cos(2\phi + \theta_1 + \theta_2 + \theta_3) + 2 \cdot \cos(2\phi + 2\theta_1 + \theta_2 + \theta_3)) \\
c1 &= c1 + (3 \cdot m_1 + 2 \cdot m_2) \cdot L \cdot N \cdot \cos(2\phi + 2\theta_1 + 2\theta_2 + \theta_3) \\
c1 &= c1 + m_1 \cdot L^2 \cdot (\cos(2\phi + \theta_1 + \theta_2 + \theta_3 + \theta_4) + 2 \cdot \cos(2\phi + 2\theta_1 + \theta_2 + \theta_3 + \theta_4) + \\
&\quad 2 \cdot \cos(2\phi + 2\theta_1 + 2\theta_2 + 2\theta_3 + \theta_4)) \\
c1 &= c1 + m_1 \cdot L \cdot N \cdot \cos(2\phi + 2\theta_1 + 2\theta_2 + \theta_3 + \theta_4) \\
\\
c2 &= 6 \cdot m_1 \cdot L^2 + 4 \cdot m_2 \cdot L^2 + m_3 \cdot r^2 + m_{10} \cdot N^2 + 2 \cdot (m_1 + m_2) \cdot N^2 \\
c2 &= c2 + m_3 \cdot L \cdot r \cdot (\cos(2\phi + \theta_1 + \theta_2 - \pi/6) + \cos(2\phi + 2\theta_1 + \theta_2 - \pi/6)) \\
c2 &= c2 + m_{10} \cdot L \cdot N \cdot (\cos(2\phi + \theta_1 + \theta_2 - \pi/3) + \cos(2\phi + 2\theta_1 + \theta_2 - \pi/3)) \\
c2 &= c2 + 2 \cdot (m_1 + m_2) \cdot L \cdot N \cdot (\cos(2\phi + \theta_1 + \theta_2) + \cos(2\phi + 2\theta_1 + \theta_2)) \\
c2 &= c2 + (3 \cdot m_1 + 2 \cdot m_2) \cdot L^2 \cdot (\cos(2\phi + \theta_1 + \theta_2 + \theta_3) + \cos(2\phi + 2\theta_1 + \theta_2 + \theta_3)) \\
c2 &= c2 + (3 \cdot m_1 + 2 \cdot m_2) \cdot L \cdot N \cdot \cos(2\phi + 2\theta_1 + 2\theta_2 + \theta_3) \\
c2 &= c2 + m_1 \cdot L^2 \cdot (\cos(2\phi + \theta_1 + \theta_2 + \theta_3 + \theta_4) + \cos(2\phi + 2\theta_1 + \theta_2 + \theta_3 + \theta_4) + \\
&\quad 2 \cdot \cos(2\phi + 2\theta_1 + 2\theta_2 + 2\theta_3 + \theta_4)) \\
c2 &= c2 + m_1 \cdot L \cdot N \cdot \cos(2\phi + 2\theta_1 + 2\theta_2 + \theta_3 + \theta_4) \\
\\
c3 &= 4 \cdot m_2 \cdot L^2 + 6 \cdot m_1 \cdot L^2 + (3 \cdot m_1 + 2 \cdot m_2) \cdot L^2 \cdot (\cos(2\phi + \theta_1 + \theta_2 + \theta_3) + \\
&\quad \cos(2\phi + 2\theta_1 + \theta_2 + \theta_3)) \\
c3 &= c3 + (1/2) \cdot (3 \cdot m_1 + 2 \cdot m_2) \cdot L \cdot N \cdot \cos(2\phi + 2\theta_1 + 2\theta_2 + \theta_3) \\
c3 &= c3 + m_1 \cdot L^2 \cdot (\cos(2\phi + \theta_1 + \theta_2 + \theta_3 + \theta_4) + \cos(2\phi + 2\theta_1 + \theta_2 + \theta_3 + \theta_4) + \\
&\quad 2 \cdot \cos(2\phi + 2\theta_1 + 2\theta_2 + 2\theta_3 + \theta_4)) \\
c3 &= c3 + (1/2) \cdot m_1 \cdot L \cdot N \cdot \cos(2\phi + 2\theta_1 + 2\theta_2 + \theta_3 + \theta_4) \\
\\
c4 &= m_1 \cdot L^2 \cdot (1 + \cos(2\phi + \theta_1 + \theta_2 + \theta_3 + \theta_4) + \cos(2\phi + 2\theta_1 + \theta_2 + \theta_3 + \theta_4) + \\
&\quad \cos(2\phi + 2\theta_1 + 2\theta_2 + 2\theta_3 + \theta_4)) \\
c4 &= c4 + (1/2) \cdot m_1 \cdot L \cdot N \cdot \cos(2\phi + 2\theta_1 + 2\theta_2 + \theta_3 + \theta_4) \\
\\
d0 &= 15 \cdot m_1 \cdot L^2 + 5 \cdot m_1 \cdot L^2 \cdot \cos(2\phi + \theta_1) + (8 \cdot m_2 + 2 \cdot m_3 + 2 \cdot m_{10}) \cdot L^2 \cdot (2 + \cos(2\phi + \theta_1)) + \\
&\quad m_3 \cdot r^2 \\
d0 &= d0 + m_{10} \cdot N^2 + 2 \cdot (m_1 + m_2) \cdot N^2 + m_3 \cdot L \cdot r \cdot (\cos(2\phi + \theta_1 + \theta_2 - \pi/6) + \\
&\quad 2 \cdot \cos(2\phi + 2\theta_1 + \theta_2 - \pi/6)) \\
d0 &= d0 + m_{10} \cdot L \cdot N \cdot (\cos(2\phi + \theta_1 + \theta_2 - \pi/3) + 2 \cdot \cos(2\phi + 2\theta_1 + \theta_2 - \pi/3))
\end{aligned}$$

$$\begin{aligned}
e1 &= m_3 \cdot r^2 + m_{10} \cdot N^2 + 2 \cdot (m_1 + m_2) \cdot N^2 + 6 \cdot m_1 \cdot L^2 + 4 \cdot m_2 \cdot L^2 \\
e1 &= e1 + m_3 \cdot L \cdot r \cdot \cos(2 \cdot \phi + 2 \cdot \theta_1 + \theta_2 - \pi/6) + m_{10} \cdot L \cdot N \cdot \cos(2 \cdot \phi + 2 \cdot \theta_1 + \theta_2 - \pi/3) \\
e1 &= e1 + 2 \cdot (m_1 + m_2) \cdot L \cdot N \cdot \cos(2 \cdot \phi + 2 \cdot \theta_1 + \theta_2) \\
e1 &= e1 + (3 \cdot m_1 + 2 \cdot m_2) \cdot (L^2 \cdot \cos(2 \cdot \phi + 2 \cdot \theta_1 + \theta_2 + \theta_3) + L \cdot N \cdot \cos(2 \cdot \phi + 2 \cdot \theta_1 + 2 \cdot \theta_2 + \theta_3)) \\
e1 &= e1 + m_1 \cdot L \cdot (L \cdot \cos(2 \cdot \phi + 2 \cdot \theta_1 + \theta_2 + \theta_3 + \theta_4) + N \cdot \cos(2 \cdot \phi + 2 \cdot \theta_1 + 2 \cdot \theta_2 + \theta_3 + \theta_4) + \\
&\quad 2 \cdot L \cdot \cos(2 \cdot \phi + 2 \cdot \theta_1 + 2 \cdot \theta_2 + 2 \cdot \theta_3 + \theta_4))
\end{aligned}$$

$$\begin{aligned}
e2 &= m_3 \cdot r^2 + m_{10} \cdot N^2 + 2 \cdot (m_1 + m_2) \cdot N^2 + 6 \cdot m_1 \cdot L^2 + 4 \cdot m_2 \cdot L^2 \\
e2 &= e2 + (3 \cdot m_1 + 2 \cdot m_2) \cdot L \cdot N \cdot \cos(2 \cdot \phi + 2 \cdot \theta_1 + 2 \cdot \theta_2 + \theta_3) \\
e2 &= e2 + m_1 \cdot (L \cdot N \cdot \cos(2 \cdot \phi + 2 \cdot \theta_1 + 2 \cdot \theta_2 + \theta_3 + \theta_4) + 2 \cdot L^2 \cdot \cos(2 \cdot \phi + 2 \cdot \theta_1 + 2 \cdot \theta_2 + 2 \cdot \theta_3 + \theta_4))
\end{aligned}$$

$$\begin{aligned}
e3 &= (1/2) \cdot (3 \cdot m_1 + 2 \cdot m_2) \cdot L \cdot N \cdot \cos(2 \cdot \phi + 2 \cdot \theta_1 + 2 \cdot \theta_2 + \theta_3) + 6 \cdot m_1 \cdot L^2 + 4 \cdot m_2 \cdot L^2 \\
e3 &= e3 + (1/2) \cdot m_1 \cdot (L \cdot N \cdot \cos(2 \cdot \phi + 2 \cdot \theta_1 + 2 \cdot \theta_2 + \theta_3 + \theta_4) + \\
&\quad 4 \cdot L^2 \cdot \cos(2 \cdot \phi + 2 \cdot \theta_1 + 2 \cdot \theta_2 + 2 \cdot \theta_3 + \theta_4))
\end{aligned}$$

$$\begin{aligned}
e4 &= m_1 \cdot L^2 + (1/2) \cdot m_1 \cdot (L \cdot N \cdot \cos(2 \cdot \phi + 2 \cdot \theta_1 + 2 \cdot \theta_2 + \theta_3 + \theta_4) + \\
&\quad 2 \cdot L^2 \cdot \cos(2 \cdot \phi + 2 \cdot \theta_1 + 2 \cdot \theta_2 + 2 \cdot \theta_3 + \theta_4))
\end{aligned}$$

$$\begin{aligned}
f0 &= 6 \cdot m_1 \cdot L^2 + 4 \cdot m_2 \cdot L^2 + (1/2) \cdot (3 \cdot m_1 + 2 \cdot m_2) \cdot L \cdot N \cdot \cos(2 \cdot \phi + 2 \cdot \theta_1 + 2 \cdot \theta_2 + \theta_3) \\
f0 &= f0 + (3 \cdot m_1 + 2 \cdot m_2) \cdot L^2 \cdot (\cos(2 \cdot \phi + \theta_1 + \theta_2 + \theta_3) + \cos(2 \cdot \phi + 2 \cdot \theta_1 + \theta_2 + \theta_3)) \\
f0 &= f0 + m_1 \cdot L^2 \cdot (\cos(2 \cdot \phi + \theta_1 + \theta_2 + \theta_3 + \theta_4) + \cos(2 \cdot \phi + 2 \cdot \theta_1 + \theta_2 + \theta_3 + \theta_4) + \\
&\quad 2 \cdot \cos(2 \cdot \phi + 2 \cdot \theta_1 + 2 \cdot \theta_2 + 2 \cdot \theta_3 + \theta_4)) \\
f0 &= f0 + (1/2) \cdot m_1 \cdot L \cdot N \cdot \cos(2 \cdot \phi + 2 \cdot \theta_1 + 2 \cdot \theta_2 + \theta_3 + \theta_4)
\end{aligned}$$

$$\begin{aligned}
f1 &= 6 \cdot m_1 \cdot L^2 + 4 \cdot m_2 \cdot L^2 + (1/2) \cdot (3 \cdot m_1 + 2 \cdot m_2) \cdot (2 \cdot L^2 \cdot \cos(2 \cdot \phi + 2 \cdot \theta_1 + \theta_2 + \theta_3) + \\
&\quad L \cdot N \cdot \cos(2 \cdot \phi + 2 \cdot \theta_1 + 2 \cdot \theta_2 + \theta_3)) \\
f1 &= f1 + m_1 \cdot L^2 \cdot (\cos(2 \cdot \phi + 2 \cdot \theta_1 + \theta_2 + \theta_3 + \theta_4) + 2 \cdot \cos(2 \cdot \phi + 2 \cdot \theta_1 + 2 \cdot \theta_2 + 2 \cdot \theta_3 + \theta_4)) \\
f1 &= f1 + (1/2) \cdot m_1 \cdot L \cdot N \cdot \cos(2 \cdot \phi + 2 \cdot \theta_1 + 2 \cdot \theta_2 + \theta_3 + \theta_4)
\end{aligned}$$

$$\begin{aligned}
f2 &= 6 \cdot m_1 \cdot L^2 + 4 \cdot m_2 \cdot L^2 + (1/2) \cdot (3 \cdot m_1 + 2 \cdot m_2) \cdot L \cdot N \cdot \cos(2 \cdot \phi + 2 \cdot \theta_1 + 2 \cdot \theta_2 + \theta_3) \\
f2 &= f2 + (1/2) \cdot m_1 \cdot (L \cdot N \cdot \cos(2 \cdot \phi + 2 \cdot \theta_1 + 2 \cdot \theta_2 + \theta_3 + \theta_4) + 4 \cdot L^2 \cdot \cos(2 \cdot \phi + 2 \cdot \theta_1 + 2 \cdot \theta_2 + 2 \cdot \theta_3 + \theta_4))
\end{aligned}$$

$$f3 = 6 \cdot m_1 \cdot L^2 + 4 \cdot m_2 \cdot L^2 + 2 \cdot m_1 \cdot L^2 \cdot \cos(2 \cdot \phi + 2 \cdot \theta_1 + 2 \cdot \theta_2 + 2 \cdot \theta_3 + \theta_4)$$

$$f4 = m_1 \cdot L^2 + m_1 \cdot L^2 \cdot \cos(2 \cdot \phi + 2 \cdot \theta_1 + 2 \cdot \theta_2 + 2 \cdot \theta_3 + \theta_4)$$

$$g0 = m_1 \cdot L^2 \cdot (1 + \cos(2 \cdot \phi + \theta_1 + \theta_2 + \theta_3 + \theta_4) + \cos(2 \cdot \phi + 2 \cdot \theta_1 + \theta_2 + \theta_3 + \theta_4) + \cos(2 \cdot \phi + 2 \cdot \theta_1 + 2 \cdot \theta_2 + 2 \cdot \theta_3 + \theta_4))$$

$$g0 = g0 + (1/2) \cdot m_1 \cdot L \cdot N \cdot \cos(2 \cdot \phi + 2 \cdot \theta_1 + 2 \cdot \theta_2 + \theta_3 + \theta_4)$$

$$g1 = m_1 \cdot L \cdot (L + L \cdot \cos(2 \cdot \phi + 2 \cdot \theta_1 + \theta_2 + \theta_3 + \theta_4) + (1/2) \cdot N \cdot \cos(2 \cdot \phi + 2 \cdot \theta_1 + 2 \cdot \theta_2 + \theta_3 + \theta_4) + L \cdot \cos(2 \cdot \phi + 2 \cdot \theta_1 + 2 \cdot \theta_2 + 2 \cdot \theta_3 + \theta_4))$$

$$g2 = m_1 \cdot L \cdot (L + (1/2) \cdot N \cdot \cos(2 \cdot \phi + 2 \cdot \theta_1 + 2 \cdot \theta_2 + \theta_3 + \theta_4) + L \cdot \cos(2 \cdot \phi + 2 \cdot \theta_1 + 2 \cdot \theta_2 + 2 \cdot \theta_3 + \theta_4))$$

$$g3 = m_1 \cdot L^2 + m_1 \cdot L^2 \cdot \cos(2 \cdot \phi + 2 \cdot \theta_1 + 2 \cdot \theta_2 + 2 \cdot \theta_3 + \theta_4)$$

$$g4 = m_1 \cdot L^2$$

The angle ϕ , which has been used to define the inertia matrix, needs to be eliminated through the use of the constraint equation on the y position of foot 2:

$$y_2 = 2 \cdot L \cdot \sin(\phi) + 2 \cdot L \cdot \sin(\phi + \theta_1) + N \cdot \sin(\phi + \theta_1 + \theta_2) + 2 \cdot L \cdot \sin(\phi + \theta_1 + \theta_2 + \theta_3) + 2 \cdot L \cdot \sin(\phi + \theta_1 + \theta_2 + \theta_3 + \theta_4)$$

This is used to set up a transformation matrix T which transforms the over specified angle set including ϕ to the joint vector q. This matrix is given by:

$$\begin{bmatrix} \delta\phi \\ \delta\theta_1 \\ \delta\theta_2 \\ \delta\theta_3 \\ \delta\theta_4 \end{bmatrix} = [T] \begin{bmatrix} \delta\theta_1 \\ \delta\theta_2 \\ \delta\theta_3 \\ \delta\theta_4 \end{bmatrix} = \begin{bmatrix} \frac{-a_1}{b_1} & \frac{-a_2}{b_1} & \frac{-a_3}{b_1} & \frac{-a_4}{b_1} \\ 1 & 0 & 0 & 0 \\ 0 & 1 & 0 & 0 \\ 0 & 0 & 1 & 0 \\ 0 & 0 & 0 & 1 \end{bmatrix} \begin{bmatrix} \delta\theta_1 \\ \delta\theta_2 \\ \delta\theta_3 \\ \delta\theta_4 \end{bmatrix}$$

where:

$$a1 = 2 \cdot L \cdot \cos(\phi + \theta_1) + N \cdot \cos(\phi + \theta_1 + \theta_2) + 2 \cdot L \cdot \cos(\phi + \theta_1 + \theta_2 + \theta_3) + 2 \cdot L \cdot \cos(\phi + \theta_1 + \theta_2 + \theta_3 + \theta_4)$$

$$a2 = N \cdot \cos(\phi + \theta_1 + \theta_2) + 2 \cdot L \cdot \cos(\phi + \theta_1 + \theta_2 + \theta_3) + 2 \cdot L \cdot \cos(\phi + \theta_1 + \theta_2 + \theta_3 + \theta_4)$$

$$a3 = 2 \cdot L \cdot \cos(\phi + \theta_1 + \theta_2 + \theta_3) + 2 \cdot L \cdot \cos(\phi + \theta_1 + \theta_2 + \theta_3 + \theta_4)$$

$$a4 = 2 \cdot L \cdot \cos(\phi + \theta_1 + \theta_2 + \theta_3 + \theta_4)$$

$$b1 = 2 \cdot L \cdot (\cos(\phi) + \cos(\phi + \theta_1) + \cos(\phi + \theta_1 + \theta_2 + \theta_3) + \cos(\phi + \theta_1 + \theta_2 + \theta_3 + \theta_4)) + N \cdot \cos(\phi + \theta_1 + \theta_2)$$

For convenience, the Jacobian matrix is redefined in terms of the over specified angle vector. It is defined to be:

$$J = \begin{bmatrix} j11 & j12 & j13 & j14 & j15 \\ j21 & j22 & j23 & j24 & j25 \\ j31 & j32 & j33 & j34 & j35 \\ j41 & j42 & j43 & j44 & j45 \end{bmatrix}$$

where:

$$j11 = -2 \cdot L \cdot \sin(\phi) - 2 \cdot L \cdot \sin(\phi + \theta_1) - r \cdot \sin(\phi + \theta_1 + \theta_2 - \pi/6)$$

$$j12 = -2 \cdot L \cdot \sin(\phi + \theta_1) - r \cdot \sin(\phi + \theta_1 + \theta_2 - \pi/6)$$

$$j13 = -r \cdot \sin(\phi + \theta_1 + \theta_2 - \pi/6)$$

$$j14 = 0$$

$$j15 = 0$$

$$j21 = 2 \cdot L \cdot \cos(\phi) + 2 \cdot L \cdot \cos(\phi + \theta_1) + r \cdot \cos(\phi + \theta_1 + \theta_2 - \pi/6)$$

$$j22 = 2 \cdot L \cdot \cos(\phi + \theta_1) + r \cdot \cos(\phi + \theta_1 + \theta_2 - \pi/6)$$

$$j23 = r \cdot \cos(\phi + \theta_1 + \theta_2 - \pi/6)$$

$$j24 = 0$$

$$j25 = 0$$

$$j31 = 1$$

$$j32 = 1$$

$$j33 = 1$$

$$j34 = 0$$

$$j35 = 0$$

$$j41 = -2 \cdot L \cdot (\sin(\phi) + \sin(\phi + \theta_1) + \sin(\phi + \theta_1 + \theta_2 + \theta_3) + \sin(\phi + \theta_1 + \theta_2 + \theta_3 + \theta_4)) - N \cdot \sin(\phi + \theta_1 + \theta_2)$$

$$j42 = -2 \cdot L \cdot (\sin(\phi + \theta_1) + \sin(\phi + \theta_1 + \theta_2 + \theta_3) + \sin(\phi + \theta_1 + \theta_2 + \theta_3 + \theta_4)) - N \cdot \sin(\phi + \theta_1 + \theta_2)$$

$$j43 = -2 \cdot L \cdot (\sin(\phi + \theta_1 + \theta_2 + \theta_3) + \sin(\phi + \theta_1 + \theta_2 + \theta_3 + \theta_4)) - N \cdot \sin(\phi + \theta_1 + \theta_2)$$

$$j44 = -2 \cdot L \cdot (\sin(\phi + \theta_1 + \theta_2 + \theta_3) + \sin(\phi + \theta_1 + \theta_2 + \theta_3 + \theta_4))$$

$$j45 = -2 \cdot L \cdot \sin(\phi + \theta_1 + \theta_2 + \theta_3 + \theta_4)$$

It is important to note that the over specified Jacobian matrix, multiplied by the transformation matrix T, is equivalent to the Jacobian matrix given in Appendix A. That is:

$$J(4 \times 5) \cdot T = J(4 \times 4)$$

The potential energy term added by the environmental contact at the end of foot 2 is given by:

$$\delta V = K_e \cdot \begin{bmatrix} 0 & 0 & 0 & 0 & 0 \\ 0 & 0 & 0 & 0 & 0 \\ 0 & 0 & 0 & 0 & 0 \\ j_{41} & j_{42} & j_{43} & j_{44} & j_{45} \end{bmatrix}$$

Let H^{-1} be the inverse transformed inertia matrix:

$$H^{-1} = (T^T \cdot M \cdot T)^{-1}$$

The state space equations are:

$$\dot{x} = A \cdot x + B \cdot u$$

$$y = C \cdot x + D \cdot u$$

where:

$$x = [x_{body} \ y_{body} \ \theta_{body} \ x_2]$$

$$u = [x_{bcmd} \ y_{bcmd} \ \theta_{bcmd} \ x_{2cmd}]$$

$$A = \begin{bmatrix} J \cdot T \cdot H^{-1} \cdot T^T \cdot J^T \cdot K_d & J \cdot T \cdot H^{-1} \cdot T^T \cdot (J^T \cdot K_p - \delta V) \\ I(4 \times 4) & 0(4 \times 4) \end{bmatrix}$$

$$B = - \begin{bmatrix} J \cdot T \cdot H^{-1} \cdot T^T \cdot J^T \cdot K_d & J \cdot T \cdot H^{-1} \cdot T^T \cdot J^T \cdot K_p \\ 0(4 \times 4) & 0(4 \times 4) \end{bmatrix}$$

$$C = \begin{bmatrix} 0 & 0 & 0 & 0 & 1 & 0 & 0 & 0 \\ 0 & 0 & 0 & 0 & 0 & 1 & 0 & 0 \\ 0 & 0 & 0 & 0 & 0 & 0 & 1 & 0 \\ 0 & 0 & 0 & 0 & 0 & 0 & 0 & 1 \end{bmatrix}$$

$$D = \begin{bmatrix} 0 & 0 & 0 & 0 & 0 & 0 & 0 & 0 \\ 0 & 0 & 0 & 0 & 0 & 0 & 0 & 0 \\ 0 & 0 & 0 & 0 & 0 & 0 & 0 & 0 \\ 0 & 0 & 0 & 0 & 0 & 0 & 0 & 0 \end{bmatrix}$$

As can plainly be seen from these equations, the response of the system will vary as a function of the configuration dependent effective inertia matrix. The gains chosen after experimental testing are $k_p = [1000, 500, 8, 100]$ and $k_d = [100, 50, 8, 10]$.

The analytical response of the LIBRA with these gains is shown in two domains: plots of the roots of the characteristic equation for the various representative configurations, and as bode plots for one configuration at $y_{body} = 0$. The eighteen configurations chosen for testing are:

$x_{body} = 9$ cm, $\theta_{body} = 0$, $x_2 = 18$ cm, $y_{body} = 0.14, 0.12, 0.10, 0.08, 0.06, 0.04, 0.02, 0.00, -0.02, -0.04, -0.06, -0.08, -0.10, -0.12, -0.14, -0.18, \text{ and } -0.20$

The roots for these configurations are shown in Figure C2. However, as the scale is so large it is difficult to extract meaningful information. A figure of the dominant poles is given in Figure C3. As can be seen in Figure C3, some of the configurations appear to be under damped. However, since the significant damping in the motor gearheads is not included in the analysis, the actual system will respond in a more damped manner.

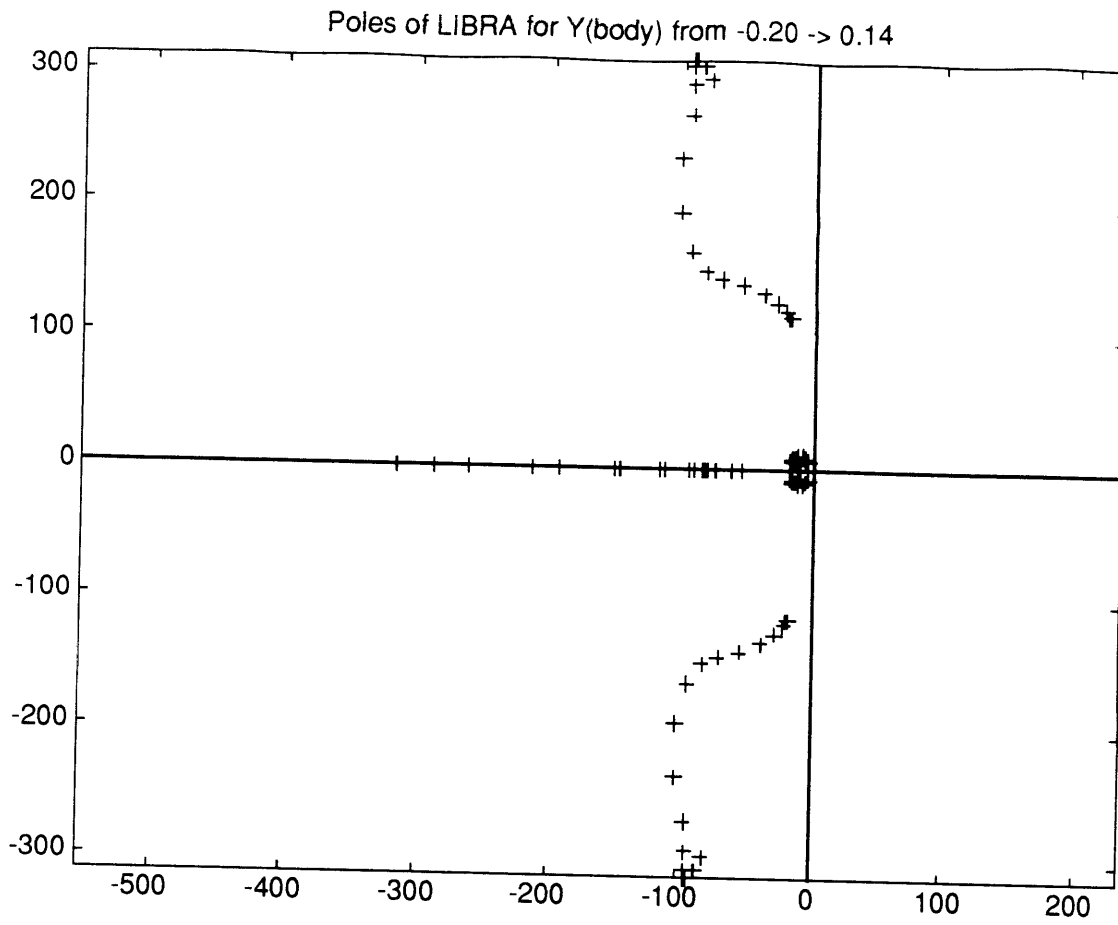


Fig. C2: Poles of the LIBRA for y_{body} from -0.20m \rightarrow 0.14m

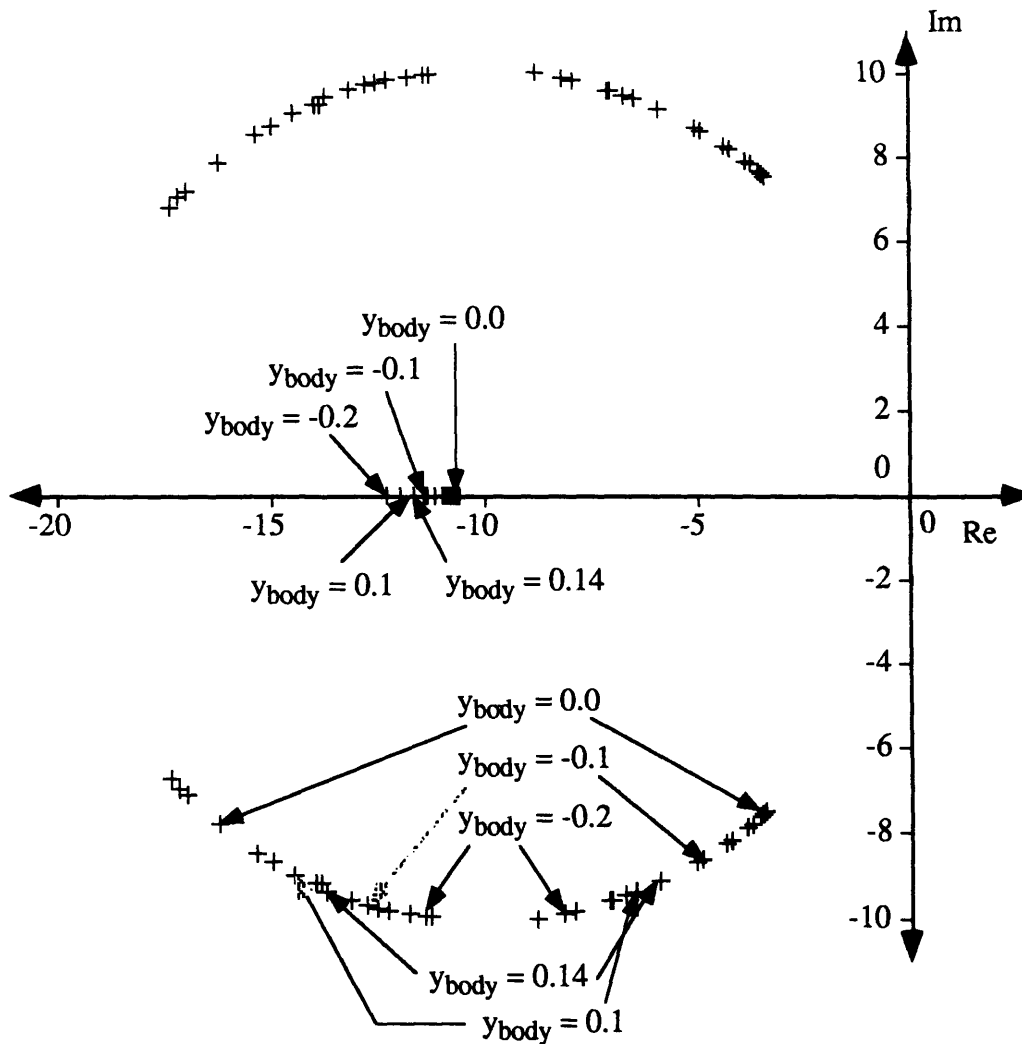


Fig. C3: Dominant poles of the LIBRA for y_{body} from -0.20m to 0.14m

The dominant Bode plots of the system for the chosen configuration of $y_{\text{body}} = 0$ are given in Figures C4 through C6. The design goal is for the system to have a bandwidth of 6 Hz. For our system, it is desirable for the three free control variables (x_{body} , y_{body} and θ_{body}) to have close to the same bandwidth, and for the constrained control variable (x_{foot}) to have a much lower bandwidth. The only input variable to output variable loops with magnitudes above -3dB are the loops for the x_{body} position variables, y_{body} position variables and θ_{body} position variables. This is expected, since the x_{body} , y_{body} and θ_{body} position variables have the highest control gains by a considerable amount. The x_{foot} position loop has very low magnitudes, since it is largely constrained by the environment.

If excessive coupling were found between one of these input variables and a different output variable, that control loop would also have high magnitude gains. Since no such loops are found, the coupling is not excessive in this configuration.

As can be seen in Figure C4, the analysis of the x_{body} position loop yielded a bandwidth of 5.2 Hz. This is slightly lower than desired, but still very acceptable. Both the gain margin and phase margin are large, indicating good stability.

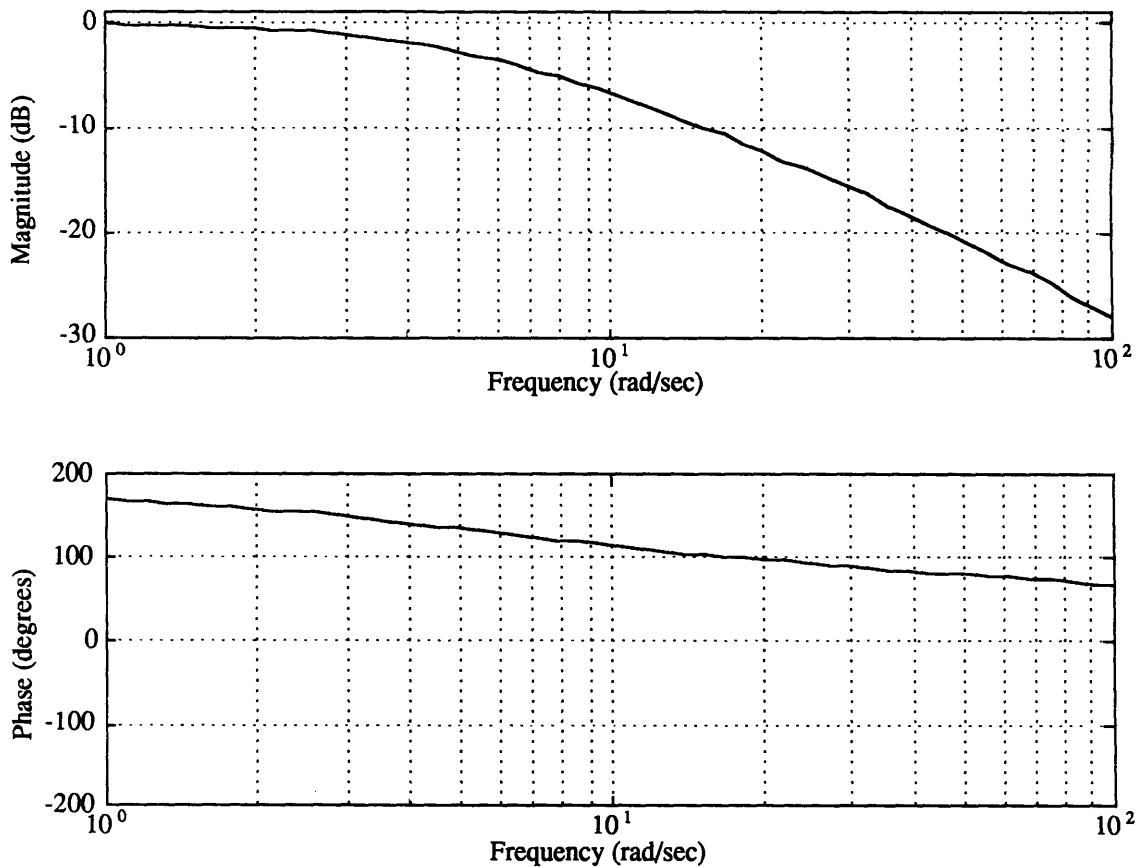


Fig. C4: Bode plot for the x_{body} position variable

Figure C5 shows the y_{body} position control loop. The bandwidth of this loop is even higher than that of the x_{body} position control loop, being close to 7 Hz. Even though this is over the desired bandwidth of 6 Hz, it is still acceptable. The additional damping of the actuators that is not modeled will lower the bandwidth of the actual system. Once again, the phase margin and gain margins are large, indicating good stability.

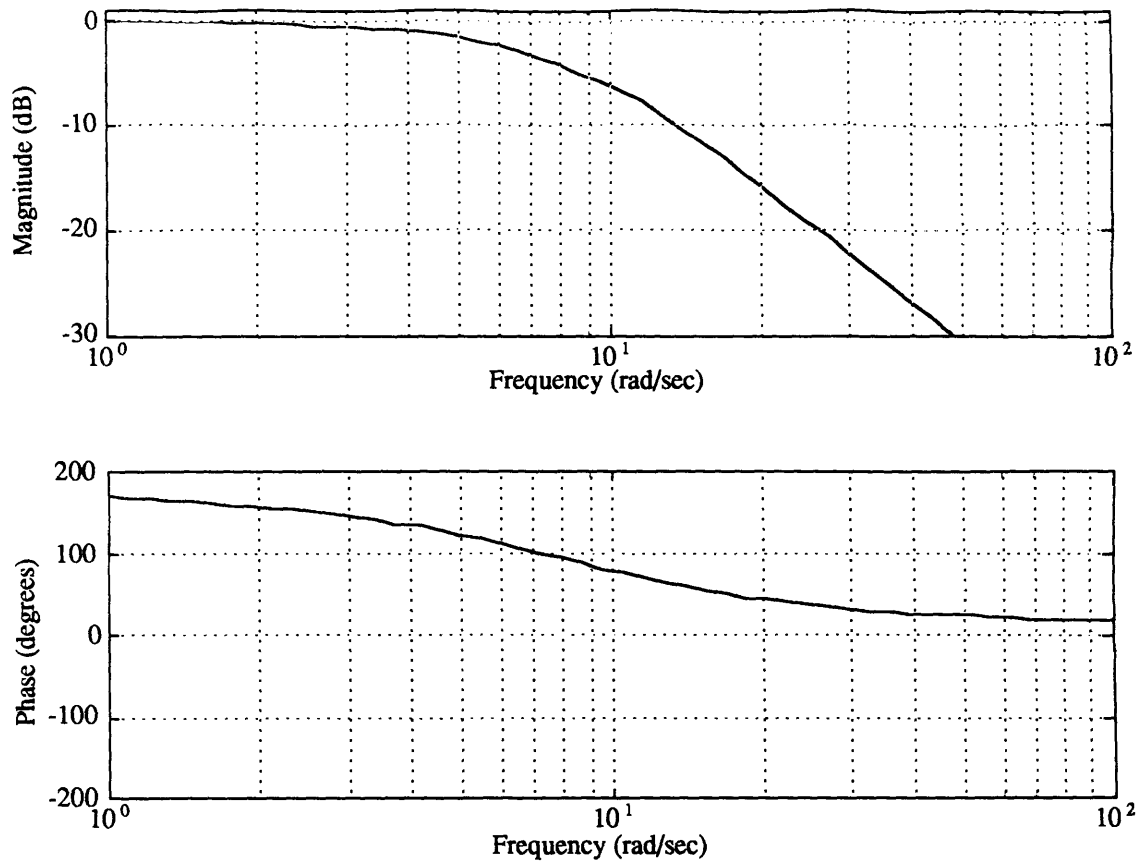


Fig. C5: Bode plot for the y_{body} position variable

Figure C6 shows the control loop for the θ_{body} position. Its bandwidth is near 5.6 Hz, which is still acceptable. Like the other two loops, the control loop for θ_{body} shows good stability.

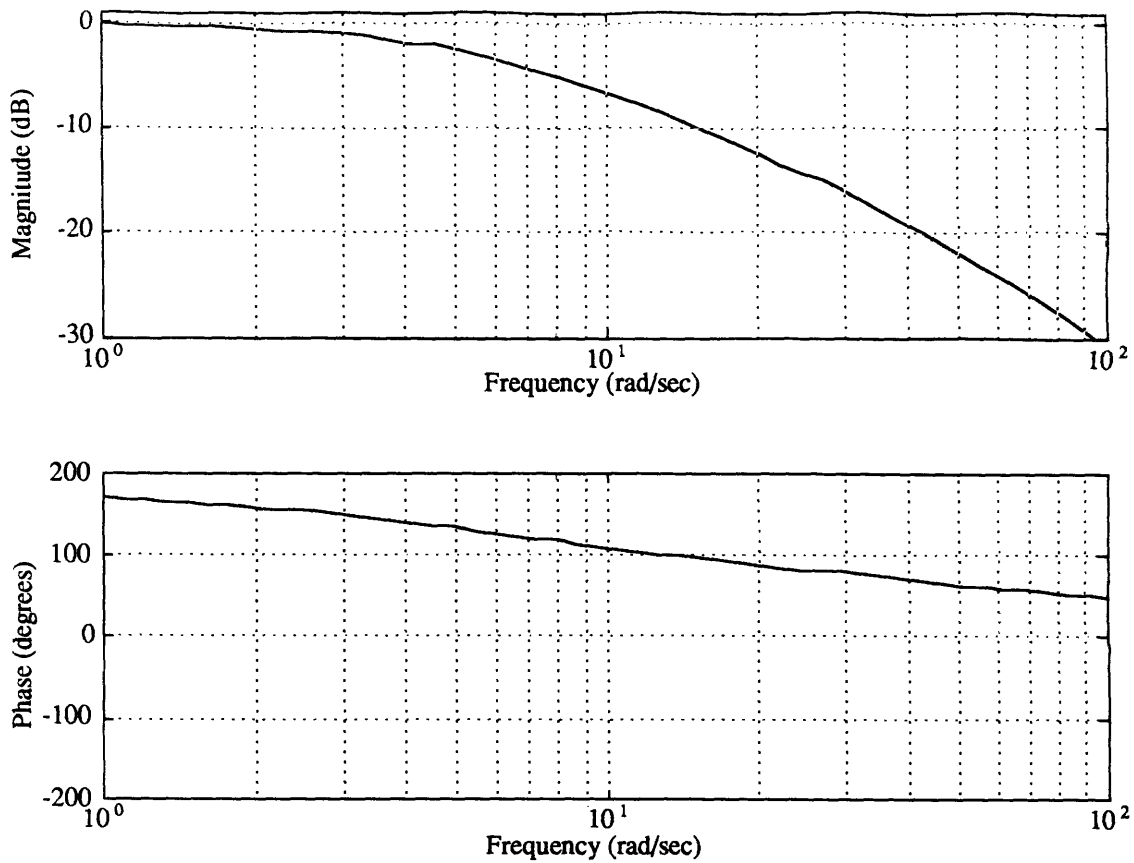


Fig. C6: Bode plot for the θ_{body} position variable

While the dynamic model yields bandwidths that are near the desired in this configuration, the unmodeled damping in the actuators lowers the bandwidth of the actual system. The bandwidths are all close to each other as desired, and little coupling between control variables is seen. Thus the linear analysis of the system using gains chosen experimentally shows that the system still meets the design goals for the gains.

Appendices References

- ¹C and H sales Co.
P.O. Box 5356, 2176 East Colorado Blvd.,
Pasadena, CA, 91107
- ²National Semiconductor
2900 Semiconductor Drive, P.O. Box 58090
Santa Clara, CA, 95052-8090
- ³Gerber Electronics
128 Carnegie Row
Norwood, MA, 02062
- ⁴Newark Electronics
248 Pleasant St.
Methuen, MA, 01844-7195
- ⁵Allied Electronics, Inc., 1-800-433-5700